

SINGH, JAGJEET, Ph.D. A Model System for Understanding Cellular Signaling of The Cannabinoid CB₂ receptor via The Inhibitory G_i Protein. (2014)
Directed by Dr. Patricia H. Reggio 104pp.

One key signaling pathway in the cellular signaling involving G protein coupled receptors (GPCR) is via heterotrimeric G proteins. The first step in GPCR/G protein signaling is the activation of a GPCR by the ligand binding and the next step is the activation of the G protein. Understanding the molecular mechanism behind the GPCR/G protein interactions will help in characterizing this important signaling pathway and should ultimately lead to the design of functionally selective ligands for this larger class of receptors. Earlier, the Reggio group used molecular dynamics simulations to study the activation of the cannabinoid CB₂ receptor, a class A GPCR, by its endogenous ligand, 2-arachidonoylglycerol (2-AG) via the lipid bilayer. The goal of the current project was to study the next step in the G-protein mediated signal transduction, when an agonist activated CB₂ receptor forms a complex with G_i protein and catalyzes the activation of G_i protein, releasing the guanosine diphosphate (GDP) bound between the ras-like (also known as GTPase domain) and helical domains of the G_α protein. To this end, we report here the CB₂ / G_αi1β1γ2 complex formation using our 2-AG activated CB₂ receptor model. For G protein activation (dissociation of GDP), we hypothesized that GDP release from the ras-like and helical domains of G_α_i would be triggered by the hydration of GDP. We probed the role of the CB₂ receptor interactions with the G_α_i protein and the resultant progression of GDP hydration. We have seen the number of waters surrounding GDP increase from 16 (t= 0 ns) to 28 waters (t=5 μs). Two important interactions between the receptor and G-protein appear to lead to the increased hydration of GDP. (1)

A hydrophobic interaction occurred between CB₂ IC2 loop residue P139 and the G α i hydrophobic pocket residues: V34 (N terminus); L194 (β 1 sheet); F196 (β 2 sheet); and, F336, T340, I343, I344 (α 5 helix) multiple times in our 5 μ s long trajectory. Each time this interaction occurred, an increase in GDP hydration was observed in our simulation.

2) We also observed an IC3 loop interaction with the G α i α 4 helix between 1.4 to 1.6 μ s, in which the IC3 loop residue R229 reached to interact with E297 and E298. Taken together, our results show that the intracellular loops play a critical role in the hydration of GDP that should lead to G protein activation.

GPCRs exist as dimers also and there is not much known concerning CB₂ receptor dimerization. We investigated the dimer interface for the cannabinoid CB₂ receptor; two residues on TMH6 A6.60C and H6.57C were identified to be part of the CB₂ homodimer interface by our collaborator, Dr. Zhao-Hui Song using substituted cysteine accessibility method (SCAM). Our molecular dynamics studies of 2 independent trajectories (500 ns each) confirm the involvement of the residues A6.60 (270) and H6.57 (267) in the formation of the CB₂ active/ inactive homodimer interface.

A MODEL SYSTEM FOR UNDERSTANDING CELLULAR SIGNALING OF THE
CANNABINOID CB₂ RECEPTOR VIA THE INHIBITORY G_i PROTEIN

by

Jagjeet Singh

A Dissertation Submitted to
the Faculty of The Graduate School at
The University of North Carolina at Greensboro
in Partial Fulfillment
of the Requirements for the Degree
Doctor of Philosophy

Greensboro
2014

Approved by

Dr. Patricia Reggio
Committee Chair

APPROVAL PAGE

This dissertation written by Jagjeet Singh has been approved by the following committee of the Faculty of The Graduate School at The University of North Carolina at Greensboro.

Committee Chair _____

Patricia Reggio

Committee Members _____

Ethan Taylor

Nadja Cech

Greogry Raner

Date of Acceptance by Committee

Date of Final Oral Examination

TABLE OF CONTENTS

	Page
LIST OF TABLES	iv
LIST OF FIGURES	v
CHAPTER	
I. STRUCTURAL BASIS OF G PROTEIN-COUPLED RECEPTOR- Gi PROTEIN INTERACTION: FORMATION OF THE CANNABINOID CB2 RECEPTOR / Gi PROTEIN COMPLEX	1
Abstract	2
Introduction.....	3
Methods.....	4
Results.....	12
Discussion.....	36
Conclusions.....	42
II. ROLE OF THE INTRACELLULAR LOOPS OF THE CANNABINOID CB2 RECEPTOR IN THE ACTIVATION OF THE Gi PROTEIN.....	44
Abstract	44
Introduction.....	45
Methods.....	46
Results.....	48
Discussion.....	63
Conclusions.....	67
III. HOMODIMER FORMATION OF THE CANNABINOID CB2 RECEPTOR	68
Abstract	68
Introduction.....	69
Methods.....	72
Results.....	76
Discussion.....	90
Conclusions.....	93
REFERENCES	94

LIST OF TABLES

	Page
Table 1. Interaction Energy of CB2 Homodimer	80
Table 2. Interaction Energy of CXCR4 Homodimer	81

LIST OF FIGURES

	Page
Figure 1. MS Spectrums of CB2 and $G\alpha_i$ Crosslinks	15
Figure 2. CB2 R* / $G\alpha i1\beta 1\gamma 2$ Protein Complex.....	16
Figure 3. Crosslinked Residues on CB2 R* / $G\alpha i1$ Protein.....	18
Figure 4. CB2 R* / $G\alpha i1\beta 1\gamma 2$ Protein Complex in Lipid Bilayer	19
Figure 5. Change in the $G\alpha i1\beta 1\gamma 2$ Protein Relative to CB2 Receptor	21
Figure 6. Change in the C-Terminal $\alpha 5$ Helix of $G\alpha i1$	23
Figure 7. IC-2 Proline 139 Interaction with $G\alpha i1\beta 1\gamma 2$ Protein	25
Figure 8. Solvent Accessible Surface Area and Interaction Energy of Proline 139	26
Figure 9. Shape of the C-Terminal $\alpha 5$ Helix of $G\alpha i1$	28
Figure 10. TMH3 and C-Terminal $\alpha 5$ Helix Interaction.....	30
Figure 11. Outward Movement of TMH5 - TMH6.....	31
Figure 12. Movement of Intracellular Loop 3 (IC3).....	32
Figure 13. Distances Between the Crosslinked Residue Pairs.....	35
Figure 14. The Orientation of CB2 Intracellular Loops Relative to $G\alpha i1$ Protein	48
Figure 15. CB2 IC-1 Loop Interactions with the $G\alpha i1$ N-terminal Helix.....	50
Figure 16. CB2 IC-2 Loop / $G\alpha i1\beta 1\gamma 2$ Interaction.....	51
Figure 17. IC-2 Loop P139 Interaction with $G\alpha i1$ Protein.....	53
Figure 18. IC-3 Loop R229 Interaction with $G\alpha i1$ $\alpha 4$ Helix Residue E308.....	54

Figure 19. Interaction Between CB2 TMH7/Hx8 Elbow Region and Gai C-Terminus.....	55
Figure 20. Plot of N – O Distance Between CB ₂ TMH7/Hx8 Elbow Residue R7.56 and Gai C-Terminus Residue D350 (i-4) as a Function of Time.....	56
Figure 21. GDP Hydration.....	57
Figure 22. Solvent Accessible Surface Area of GDP.....	59
Figure 23. GDP Hydrogen Bonding.....	60
Figure 24. CB2 Intracellular Loops Contacting Gai Protein and GDP Hydration.....	62
Figure 25. IC-2 Loop P138 Interaction with Gai Protein.....	65
Figure 26. IC-3 Loop Residue R229 Interaction with Gai α 4 Helix Residues Q304.....	66
Figure 27. CB2 R/ R* Homodimer.....	77
Figure 28. TMH5-TMH6 Dimer Interface Residues.....	78
Figure 29. Hydrogen Bond Between A6.60 - T271.....	79
Figure 30. CB2 Homodimer/ Gai1 β 1 γ 2 Complex.....	82
Figure 31. Relative Location of TMH6 Residue A6.60 in CB2 R/ R* Homodimer.....	85
Figure 32. Relative Location of TMH6 Residue H6.57 in CB2 R/ R* Homodimer.....	86
Figure 33. Plots of Distance versus Simulation Time for the TMH6 Dimer Interface.....	87
Figure 34. TMH5 Dimer Interface Interaction Energy.....	88
Figure 35. Change in the Orientation of Gai1 β 1 γ 2 Protein.....	90

CHAPTER I

STRUCTURAL BASIS OF G PROTEIN-COUPLED RECEPTOR- Gi PROTEIN INTERACTION: FORMATION OF THE CANNABINOID CB2 RECEPTOR / Gi PROTEIN COMPLEX

Jagjeet Singh¹, Zhuanhong Qiao², Jian Cai², Diane L. Lynch¹, Alan Grossfield³, Nicholas Leioatts³, Dow P. Hurst¹, Michael C. Pitman^{1,4}, Zhao-Hui Song² and Patricia H. Reggio¹
The Journal of Biological Chemistry, 2014, 289, 20259-20272.

¹Department of Chemistry and Biochemistry, University of North Carolina, Greensboro, NC 27402

²Department of Pharmacology and Toxicology, University of Louisville School of Medicine, Louisville, KY 40292

³Department of Biochemistry and Biophysics, University of Rochester Medical Center, Rochester, NY 14642

⁴Computational Biology Center, IBM Thomas J. Watson Research Center, Yorktown Heights, New York, NY 10598

Abbreviations: GPCR – G protein-coupled receptor, CB₂ – Cannabinoid Receptor Sub-type 2, R – Inactive receptor, R* - Activated receptor, 2AG – sn-2-arachidonoylglycerol, POPC– 1-palmitoyl-2-oleoyl-phosphatidylcholine, β₂-AR – beta-2-adrenergic receptor, MD – Molecular Dynamics, EC – Extracellular, IC – Intracellular, TMH – Transmembrane helix, DSS – Disuccinimidyl Suberate, MS – Mass Spectrometry, LCMS – Liquid Chromatography- Mass Spectrometry

Abstract

In this study, we applied a comprehensive G protein-coupled receptor - $G\alpha_i$ protein chemical cross-linking strategy to map the cannabinoid receptor subtype 2 (CB_2) - $G\alpha_i$ interface and then used molecular dynamics simulations to explore the dynamics of complex formation. Three crosslink sites were identified using LC MS/MS and electrospray ionization (ESI)-MS/MS as follows: (1) a sulfhydryl crosslink between C3.53 (134) in TMH3 and the $G\alpha_i$ C-terminal i-3 residue, C351; (2) a lysine crosslink between K6.35 (245) in TMH6 and the $G\alpha_i$ C-terminal i-5 residue, K349; and (3) a lysine crosslink between K5.64 (215) in TMH5 and the $G\alpha_i \alpha_4\beta_6$ loop residue, K317.

To investigate the dynamics and nature of the conformational changes involved in CB_2 - G_i complex formation, we carried out microsecond-timescale molecular dynamics (MD) simulations of the CB_2 R*/ $G\alpha_{i1}\beta_1\gamma_2$ complex embedded in a 1-palmitoyl-2-oleoyl-phosphatidylcholine (POPC) bilayer, using crosslinking information as validation. Our results show that although MD simulations started with the G protein orientation in the β_2 -AR*/ $G\alpha_s\beta_1\gamma_2$ complex crystal structure, the $G\alpha_{i1}\beta_1\gamma_2$ protein re-oriented itself within 300 ns. Two major changes occurred: (1) The $G\alpha_{i1} \alpha_5$ helix tilt changed due to the outward movement of TMH5 in CB_2 R*. (2) A 25° clockwise rotation of $G\alpha_{i1}\beta_1\gamma_2$ underneath CB_2 R* occurred, with rotation ceasing when P139 (IC2 loop) anchors in a hydrophobic pocket on $G\alpha_{i1}$ (V34, L194, F196, F336, T340, I343 and I344). In this complex, all three experimentally identified crosslinks can occur. These findings should be relevant for other Class A GPCRs that couple to G_i proteins.

Introduction

G protein coupled receptors (GPCRs) represent excellent drug targets because they are involved in regulating nearly all known physiological functions (1,2). Class A GPCRs are thought to have a common topology that includes an extracellular N-terminus, a transmembrane core formed by a bundle of seven transmembrane α -helices (TMH1–7), three extracellular (EC) and three intracellular (IC) loops that connect these helices, and, an intracellular C-terminus that begins with a short amphipathic helix lying parallel to the membrane (3-6). Physiologically, GPCRs are activated by ligands (extracellular and membrane based) that enable the receptors to interact with and activate distinct sets of heterotrimeric G proteins ($G\alpha\beta\gamma$), as well as β -arrestins (7,8). Specifically, ligand-activated GPCRs catalyze the exchange of GDP for GTP on the $G\alpha$ subunit. GTP binding to $G\alpha$ is predicted to trigger the dissociation of the heterotrimeric G protein into $G\alpha$ -GTP and free $\beta\gamma$, which are then able to modulate the activity of a multitude of downstream effectors including adenylate cyclase and ion channels, such as G protein gated inwardly-rectifying potassium (GIRK2, GIRK4) channels, phospholipase $C\beta$ and plasma membrane Ca^{2+} pumps (9-12).

The CB_2 receptor belongs to Class A of the GPCRs and is mainly expressed in T cells of the immune system (13) and the gastrointestinal system (14,15). CB_2 has also been reported to play an important role in central immune responses during neuropathic pain in mice (16). We have previously performed microseconds long MD simulations of the CB_2 endogenous ligand, sn-2-arachidonoylglycerol (2-AG), entering and activating

CB₂ via the lipid bilayer (17). Activation of CB₂ has been shown experimentally to produce coupling to G_{α_i} inhibitory protein (18-20). Although a significant amount of information is available for GPCR catalyzed activation of G proteins (21), many atomic level details concerning complex formation and signal transduction remain unanswered.

In this work, we studied the formation of a CB₂R*/ G protein complex both experimentally and computationally. Systematic cross-linking experiments were performed using HgCl₂ and a short bi-functional, irreversible chemical crosslinker disuccinimidyl suberate (DSS). These studies yielded three specific contact sites between CB₂ and G_{α_{i1}} protein, providing new insights into the molecular architecture of the CB₂ and G_{α_{i1}} interaction. Then, in order to place these crosslinks in a structural perspective and also to explore the dynamical formation of the CB₂R*/ G_{α_{i1}}β₁γ₂ complex, we undertook two independent microsecond-long molecular dynamics simulations of the CB₂R*/ G_{α_{i1}}β₁γ₂ complex in a POPC bilayer. These studies revealed a stepwise formation of the complex that brings all crosslinked pairs into spatial proximity.

Methods

Cell Transfection and Culture

Human Embryonic Kidney 293 (HEK293) cells were maintained in Dulbecco's Modified Eagle Medium (DMEM) containing 10% fetal bovine serum, 2 mM glutamine, 100 units/ml penicillin, and 100 μg/ml streptomycin in a humidified atmosphere consisting of 5% CO₂, at 37°C. Expression plasmids containing the N-terminal FLAG peptide (DYKDDDDK) tagged human CB₂ cannabinoid receptors were stably transfected

into HEK293 cells using Lipofectamine, according to manufacturer's instructions. Stably transfected cells were selected in culture medium containing 800 $\mu\text{g/ml}$ geneticin. Having established cell lines stably expressing FLAG-CB₂ receptors, the cells were maintained in growth medium containing 400 $\mu\text{g/ml}$ of geneticin until needed for experiments.

Crosslinking Reactions and Purification of the Crosslinked Protein Complex

The CB₂ receptor has been shown to exhibit high constitutive activity (19). For this reason, crosslinking experiments were conducted in the absence of exogenous agonist. For each crosslinker, the crosslinking reactions were performed according to manufacturer's instructions. Briefly, cells expressing FLAG-CB₂ receptors were collected and cell membranes were prepared as previously described (22) in 20 mM HEPES buffer containing 150 mM NaCl. After adding cross linkers at a final concentration of 2 mM, the cell membranes were incubated on ice for 2 hours. At the end of incubation, the cross linking reactions were terminated by adding quench solutions. Subsequently, Triton-X100 was added to a final concentration of 1% and the membrane suspension was incubated at 4 °C for 2 hours by end-to-end gentle rotations. The suspension was then centrifuged at 100,000g for 1 hour at 4 °C to remove unsolubilized particles. For anti-FLAG M2 affinity chromatography, the solubilized suspension was incubated with 0.5 ml of anti-FLAG M2 agarose affinity gel at 4 °C for 2 hours with gentle rocking. After extensive washing with 20 mM HEPES containing 150 mM NaCl and 1% Triton X-100, the bound CB₂ was eluted with 8-column volumes of 0.1 mM glycine HCl, pH2.5 containing 1% Triton X-100.

In-gel Digestion

The purified CB₂ complex was resolved by SDS-PAGE and then subjected to Western blot and Coomassie Blue staining. Both anti-CB₂ antibody and anti-G protein antibody was used to identify the band corresponding to the CB₂-G protein complex. The CB₂-G protein complex band was then excised from Coomassie blue stained gel and subjected to enzymatic digestions according to a published protocol (22,23) with slight modifications. Briefly, the bands were cut into small pieces, destained with 50 mM NH₄HCO₃/acetonitrile (1:1, v/v), and digested with 10 ng/μl pepsin overnight.

ESI-MS/MS

Peptides from the enzymatic digests were analyzed by ESI-MS/MS as described previously (22). Briefly, peptides from the enzymatic digests were condensed to 1–2 μl with a Speedvac, diluted with 5 μl of 0.2% trifluoroacetic acid (TFA), and analyzed by a Waters CapLC coupled to a Q-TOF API-US mass spectrometer (Waters, Milford, MA). The samples (5 μl) were injected onto a 300 μM × 5 mm PepMap C18 precolumn (LC Packing, Sunnyvale, CA), washed with 5% ACN in 0.1% formic acid at 30 μl/min for 3 min, eluted onto and separated with a 75 μM × 150 mm Atlantis dC18 analytical column (Waters, Milford, MA). Separation was started with a 5 min isocratic elution with 95% solvent A (5% ACN with 0.1% formic acid) and 5% solvent B (95% ACN with 0.1% formic acid) and followed by a linear gradient from 5% solvent B to 40% solvent B over 115 min and then from 40% solvent B to 60% solvent B in 30 min. The flow rate on the column was about 200 nL/min. The eluted peptides were directed to a Q-TOF API-US

mass spectrometer with a nanoflow source and MS and MS/MS spectra were acquired by Data Dependent Scan.

Data analyses were performed with the aid of on-line server MS3D (24,25). First, the precursor peptide ions from LC-MS/MS were screened by the “Links” program from MS3D. Links calculates the theoretical crosslinking possibilities for CB₂-G protein complex, with information provided about the crosslinkers and protease used and the expected amino acid modifications. The Links program then gives us putative assignments within a defined mass error threshold for a list of input mass (MH⁺) values. Once the candidates of CB₂-G protein crosslinked peptides were obtained, each candidate peptide was further analyzed by the “MS2Links” program from MS3D. MS2Links is a program for assigning tandem MS peak lists generated from the fragmentation of crosslinked, modified or unmodified peptides. MS2Links calculates the theoretical MS/MS fragment library given information about the identity of the base ion, crosslinkers, desired ion types, and amino acid modifications. MS2Links then returns assignments within a defined mass error threshold for the list of input mass (MH⁺) values.

CB₂ Receptor Model

The CB₂ model employed here was taken from our previous microsecond-long simulation of the activation of the CB₂ receptor by the endogenous ligand, 2-AG, via the lipid bilayer (17). In this simulation, the ionic lock at the IC ends of TMH3-TMH6 (R3.55-D6.30) was broken within 3 ns of 2-AG head group entry between TMH6 and

TMH7 from the lipid bilayer (POPC). To represent the CB₂ activated state, we chose coordinates corresponding to time point 184.138 ns from trajectory E in which the salt bridge between TMH3 and TMH6 is broken (17). The α -carbon distance between R3.55 (136) and D6.30 (240) was 15.2 Å and the heteroatom distance N (R3.55 (136)) – O (D6.30 (240)) was 12.7 Å (17). In this bundle, the C-terminus contains the palmitoylation site at C320 and was truncated after G322.

G Protein Modeling

For this study, the crystal structure of G $\alpha_{i1}\beta_1\gamma_2$ (26) was used to dock with CB₂ R*. The extreme G α_{i1} C-terminus is unresolved in this structure, so the undecapeptide NMR structure (27) of this region in G α_t was grafted onto the backbone of residues K345, N346 and N347 (see Discussion section). The C-terminus of G γ_2 is also unresolved in the G $\alpha_{i1}\beta_1\gamma_2$ structure. This region was built by homology modeling using the NMR structure of G γ_1 (28) as template and the Maestro module from Schrodinger, LLC, New York, NY.

Lipidation Sites

Palmitic acid was attached to the N-terminus of G α_{i1} at Cys3 (29). Myristic acid was attached to Gly2 of G α_{i1} (30) and a geranylgeranyl group was attached to Cys 68 in the G γ_2 C-terminus (31).

CB₂/G_i-Protein Complex

The relative orientations of CB₂ R* and G $\alpha_{i1}\beta_1\gamma_2$ were based on the β_2 -AR / G $\alpha_s\beta_1\gamma_2$ complex crystal structure (32). To get relative receptor position, first the

activated CB₂ receptor was superimposed on the α carbon atoms of the residues N1.50, D2.50, R3.50 and W4.50 on the β 2-AR receptor from the β 2-AR / G $\alpha_s\beta_1\gamma_2$ complex. To obtain the relative orientation of G $\alpha_i\beta_1\gamma_2$ heterotrimer with the CB₂ receptor, G β_1 of G $\alpha_i\beta_1\gamma_2$ was superimposed on the α carbon atoms of residues from 51 to 340 of G β_1 in the G $\alpha_s\beta_1\gamma_2$ protein from the β 2-AR / G $\alpha_s\beta_1\gamma_2$ complex. To relieve steric clashes between CB₂ and G α_i , the whole G $\alpha_i\beta_1\gamma_2$ heterotrimer was translated in the z-direction.

Construction of CB₂/G $\alpha_i\beta_1\gamma_2$ Complex in POPC Bilayer

The CB₂ R*/G protein complex was aligned such that the transmembrane region of the CB₂ receptor was centered at the middle of the POPC lipid bilayer and the amphipathic helix 8 was oriented parallel to the plane of the membrane at approximately the lipid/water interface. The model membrane simulation cell was constructed with the replacement method, using scripts derived from CHARMM-GUI (33). The CHARMM22 protein force field with CMAP corrections (34,35) and the CHARMM 36 lipid force field (36) were used in this study. Parameters for GDP were obtained by analogy to ADP using the nucleic acid force field (37) and those for 2AG were derived from the lipid force field (17, 36). The lipidation sites are covalent modifications of their respective amino acids. The parameters for the palmitoylation sites were taken from our earlier simulations (17). Parameters for the myristoylation of G α_i and prenylation of the G γ_2 covalent linkages were taken by analogy with existing CHARMM force field parameters. Given that the primary role for these lipidation sites in these simulations is to anchor their respective proteins to the lipid matrix, no further optimization was performed. Charge neutrality was

enforced with addition of chloride counter ions and an overall ionic strength of 0.1M was obtained by adding NaCl. The final system contained 451 POPC lipid molecules, the protein complex, ions, and solvating water molecules with a simulation cell size of 130.0 Å x 130.0 Å x 170.6 Å.

Initial Minimization and Equilibration

To relieve poor initial contacts, 500 steps of steepest descent minimization was performed using CHARMM (38), with all heavy atoms of the protein complex fixed. This was followed by 20,000 steps of conjugate gradient minimization using NAMD (39). The fully minimized system was heated in 10 K increments to 310 K with restraints on the protein (force constant of 10 kcal/mol/Å² / 5.0 kcal/mol/Å² for the backbone/sidechains and ligands respectively), on the POPC phosphates (force constant of 5.0 kcal/mol/Å²), and a harmonic dihedral restraint on the POPC cis double bond and the glycerol c2 chiral center (force constant of 500 kcal/mol/rad²). At each increment, 500 steps of minimization were performed followed by 20 ps of dynamics at the higher temperature. Equilibration was continued for 100 ps of molecular dynamics and then the restraints were released in 6 steps over 1.5 ns.

Details of Molecular Dynamics Simulations

For all production runs, NAMD (39) was used. Long range electrostatics were included using PME (40) with a 10 Å short range cutoff and van der Waals interactions were treated with a switching function and a 10 Å cutoff. The NPT ensemble, as implemented in NAMD, was used to maintain temperature (T=310 K, damping

coefficient of 2 ps^{-1}) and pressure ($P=1.01325 \text{ bar}$, piston period/decay of 100/50 fs). High frequency bonds to hydrogen were restrained using the shake method implemented in NAMD allowing a 2 fs integration time step. Production dynamics was performed on a Blue Gene supercomputer (41) located at the Thomas J. Watson Research Center and on the BSBC cluster at UNC Greensboro (<http://bsbc.uncg.edu/index.html>). Two separate trajectories were run for this complex. Results from these trajectories each at 1 μs in length are reported here. All analysis were performed using visual molecular dynamics (42) and LOOS (43).

Measuring the Angle of Rotation for $G\alpha_i\beta_1\gamma_2$ Relative to the CB_2 Bundle

To measure the rotation of the G protein under the CB_2 receptor throughout the trajectories, the CB_2 receptor TMH bundle for each nanosecond of Trajectory 1 and Trajectory 2 was superimposed on the transmembrane region of the CB_2 receptor starting structure ($t=0 \text{ ns}$). The atoms used for the superposition were K1.32 (33) to S1.59 (60), P2.38 (68) to N2.63 (93), A3.23 (104) to R3.55 (136), R4.39 (147) to M4.62 (170), D5.38 (189) to K5.64 (215), L6.33 (243) to A6.60 (270) and K7.33 (279) to R7.56 (302). Two centers of mass were calculated: (1) the center of mass of $G\alpha$ ras-like domain (GTPase domain) backbone atoms E33 to G60 and T181 to D328 (this excludes the C-terminal α_5 helix and the N-terminal helix); and (2) the center of mass of the $G\beta$ subunit, D38 to N340 (this excludes the N-terminal helix). The vector between these two centers of mass was calculated for the starting structure ($t=0 \text{ ns}$) and for each 1 ns frame of each

trajectory. The angle between the starting structure vector and that of each trajectory time point was projected into the x-y plane and measured.

Results

Mass Spectrometry Identification of CB₂ and G α _i Crosslinks

To identify contacts between CB₂ and G α _i, the CB₂ receptor and G α _i were crosslinked with either disuccinimidyl suberate (DSS) (Lys-Lys) or HgCl₂ (Cys-Cys). Protein complexes were then purified by an M-2 anti-FLAG affinity column. Following SDS-PAGE separation, bands of the cross-linked CB₂/G_i complexes were excised and subjected to enzymatic digestion with pepsin. We used the nonspecific enzyme pepsin to digest the crosslinked CB₂-G_i protein complex, because there are very few trypsin digestion sites in the CB₂ regions in which we were interested. The peptide mixtures resulting from *in-gel* digestions were analyzed by LC-MS/MS mass spectrometry. Data analysis was performed with the aid of the on-line server MS3D (24). The MS/MS spectrum of each candidate peptide was then manually checked to see whether it is a validated CB₂-G protein crosslinked peptide. Several important guidelines were used for identification of crosslinked peptide, including: (1) The main MS/MS peaks should match fragment ions; (2) Fragment ions from each of the two peptides that are crosslinked should be found; (3) Fragments that contain both peptides and linker should be found.

The ESI-MS/MS spectrum of crosslinked peptides between CB₂ and G α _i are shown in Figure 1 (A-C). The fragment ions corresponding to two crosslinked peptides are designated with either the α (peptide from CB₂) or β (peptide from G α _i) subscript to

indicate the peptide of origin. In Figure 1A, the spectrum can be assigned to two peptides: peptide α from CB₂ with a sequence of RYLCLRY and peptide β from G α_i with a sequence of KNNLKDCGL. The only cysteines in these two sequences that would have been available for crosslinking are Cys-134 in CB₂ and Cys-351 in G α_i . Close inspection revealed the presence of three ions that originate from cleavage reactions involving both peptide chains, i.e., $b7\alpha/y6\beta$, $a4\alpha/b7\beta$, and $b4\alpha/b7\beta$.

In Figure 1B, the spectrum can be assigned to two peptides: peptide α from CB₂ with a sequence of LAKTL and peptide β from G α_i with a sequence of LKDCG. The only lysines in these two sequences that would have been available for crosslinking are Lys-245 in CB₂ and Lys-349 in G α_i . The spectrum was closely examined for the possible presence of fragment ions originating from cleavages involving both peptide chains. There are five ions that originate from cleavage reactions involving both peptide chains. For example, $y3\alpha/b3\beta$ demonstrates clearly the crosslink between Lys-245 in CB₂ and Lys-349 in G α_i .

In Figure 1C, the spectrum can be assigned to two peptides: peptide α from CB₂ with a sequence of HVLWKA and peptide β from G α_i with a sequence of KDTKE. There are eight ions that originate from cleavage reactions involving both peptide chains. Among these, $y2\alpha-H_2O/y2\beta$ demonstrates directly the crosslink between Lys-215 in CB₂ and Lys-317 in G α_i .

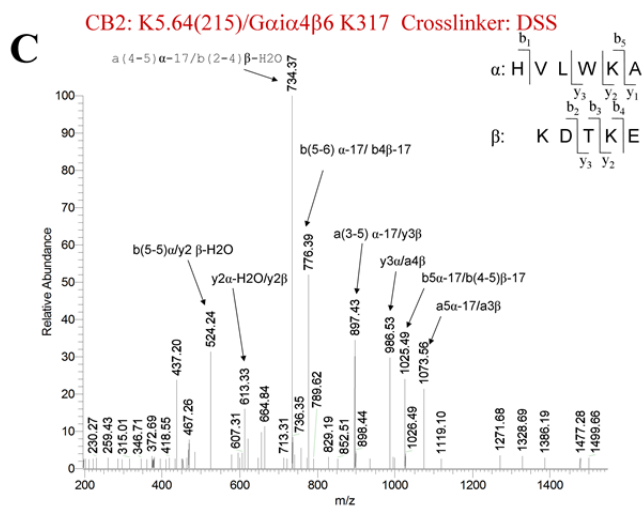


Figure 1. (C) The ESI-MS/MS spectrum of a crosslinked peptide between CB₂ and Gα_i is presented here. The [M+2H]²⁺ peak at *m/z* 755.89 (M = 2264.67) was selected as the precursor ion with a collision energy of 35 eV. The peptide α from CB₂ and the peptide β from Gα_i crosslinked between Lys-215 and Lys-317.

Figure 1. MS Spectrums of CB₂ and Gα_i Crosslinks

Orientation of Gα_iβ₁γ₂ Protein in the Initial CB₂ R* / Gα_iβ₁γ₂ Protein Dock

Our initial dock of CB₂ R* with Gα_iβ₁γ₂ protein (Figure 2) was based on the crystal structure of the β₂ adrenergic receptor in complex with G_s protein (32). In this structure, the C terminal α₅ helix of Gα_s is inserted between TMH3, TMH5 and TMH6, pointing towards the TMH7/Hx8 “elbow” region. TMH5 is packed closely with the C terminal α₅ helix. This orientation of Gα_s places the N terminus of Gα_s below TMH3 and TMH4, while the receptor IC2 loop fits in the region between the C terminus and N terminus of Gα_s.

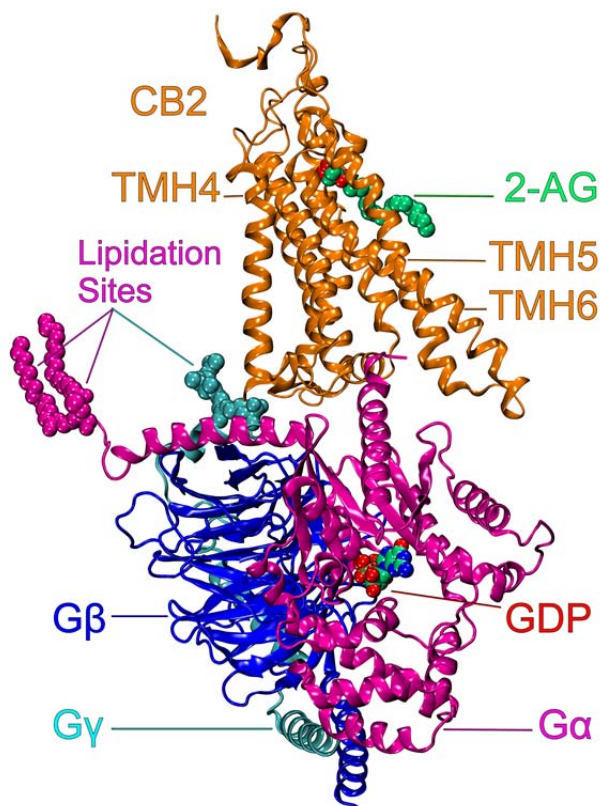


Figure 2. CB₂ R* / G α i1 β 1 γ 2 Protein Complex

The CB₂ receptor is shown in orange bound to 2-AG (VdW green carbons and red oxygens). The G α _{i1} subunit of the G α _{i1} β 1 γ 2 heterotrimer, is in magenta, G β ₁ is in blue and G γ ₂ is in cyan. The palmitic and myristic acids attached to G α _{i1} are shown in VdW colored magenta. The geranylgeranyl group attached to G γ ₂ is shown in VdW and colored cyan. GDP is bound between the helical and ras-like domains of G α _{i1}. Here, GDP is shown in VdW display with carbons, nitrogens and oxygens colored green, blue and red respectively.

Cysteine Crosslink Between TMH3 and G α _{i1} C-Terminal α 5 helix

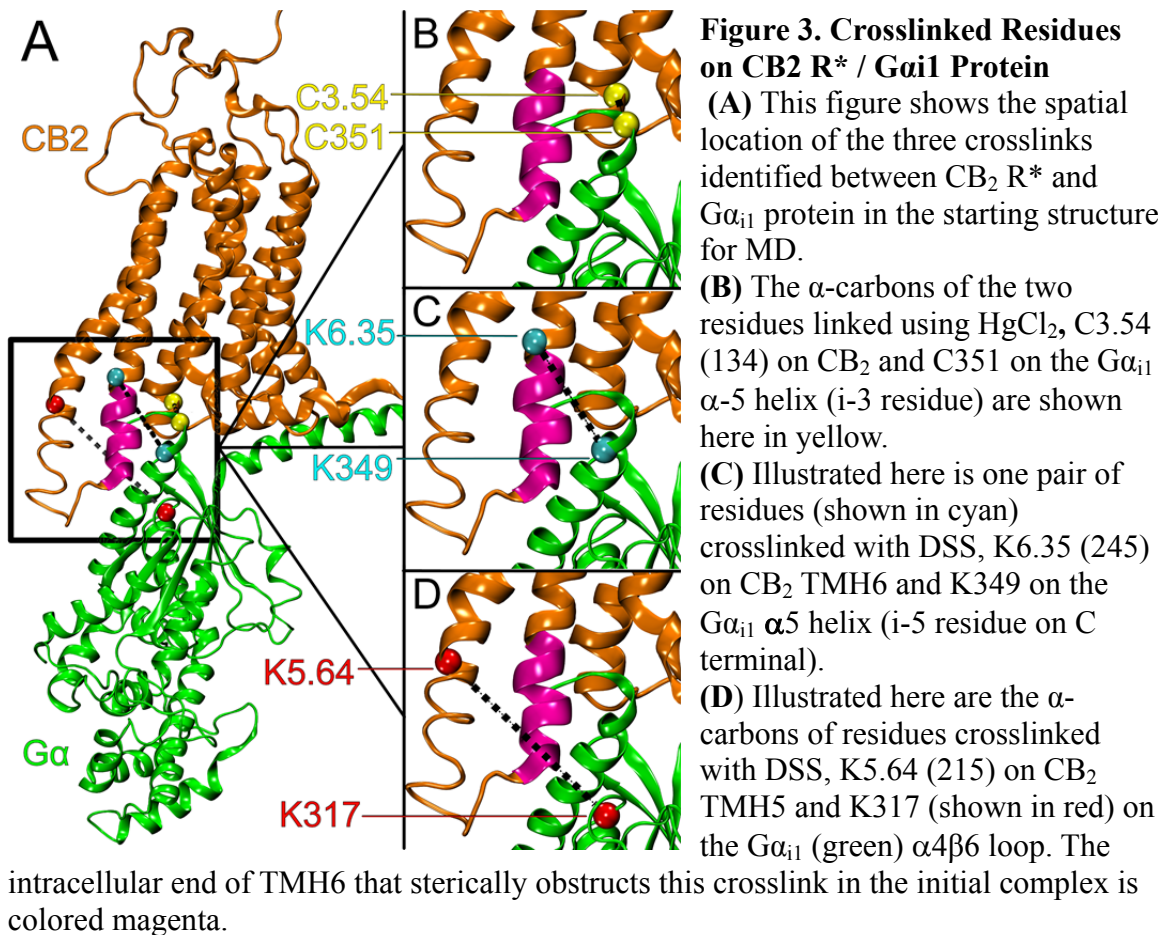
The C α - C α distance range for formation of a cysteine crosslink using HgCl₂ is 7 to 10 Å (44,45). The cysteine crosslink identified by LC/MS/MS analysis from the HgCl₂ (Cys-Cys) crosslinking study was found to be between C3.54 (134) and C351 on the G α _{i1} α -5 helix (i-3 residue). The C α - C α distance between these two residues in the initial CB₂/G α _{i1} β 1 γ 2 complex was found to be 10.6Å, which is just 0.6 Å outside the range for a cysteine crosslink formation using HgCl₂. The C α positions of the crosslinked residues (colored yellow) at t=0 ns in the context of the whole complex is shown in Figure 3A. Figure 3B presents a close-up view.

Lys-Lys Crosslinks

The spacer arm length, N-N distance reported for disuccinimidyl suberate (DSS) is 11.4 Å (46). L-lysine measures 6.4 Å from α carbon to nitrogen (47). This makes 24.2 Å the maximum $C\alpha$ - $C\alpha$ distance for formation of a Lys-Lys crosslink. The first lysine crosslink identified by LC/MS/MS analysis was between K6.35 (245) on TMH6 and K349 on the $G\alpha_{i1}$ $\alpha 5$ helix (i-5 residue on C terminal). In the initial $CB_2/G\alpha_{i1}\beta_1\gamma_2$ complex, these residues were 17 Å apart ($C\alpha$ - $C\alpha$), which is within the range for formation of the DSS (Lys-Lys) crosslink. In addition, the space between these two residues provides no steric obstruction to crosslink formation. The $C\alpha$ position of the crosslinked residues (colored cyan) at $t=0$ ns in the context of the whole complex is shown in Figure 3A. Figure 3C presents a close-up view.

The initial $C\alpha$ - $C\alpha$ distance for the second Lys-Lys crosslink between K5.34 (215) on TMH5 and K317 in the $\alpha 4\beta 6$ region of $G\alpha_{i1}$ was 24.5 Å. This distance is only 0.3 Å outside the range for the formation of these Lys-Lys crosslinks. However, it is not sterically possible to form this crosslink even if the distance was lower because the space between these two residues is blocked by the intracellular end of TMH6. This is illustrated in Figure 3C, where the intracellular extension of the TMH6 (shown in magenta) provides this steric obstruction ($t=0$ ns). In figure 3D the $C\alpha$ positions of K5.64 (215) and K317 are colored red. This suggests that during the dynamic interaction of the two proteins, this region may change conformation allowing these residues to be crosslinked. Our MD simulations of the $CB_2 R^*/ G\alpha_{i1}\beta_1\gamma_2$ protein complex embedded in a

POPC bilayer test this hypothesis. Figure 4 illustrates the full system for Trajectory 1 simulated over time, including the POPC bilayer (lipid acyl chains, cyan; phosphate atoms in phospholipid headgroup, open gold circles), the CB₂ receptor (orange) and G $\alpha_{i1}\beta_1\gamma_2$ protein (green) with the G α_{i1} $\alpha 5$ helix shown in yellow.



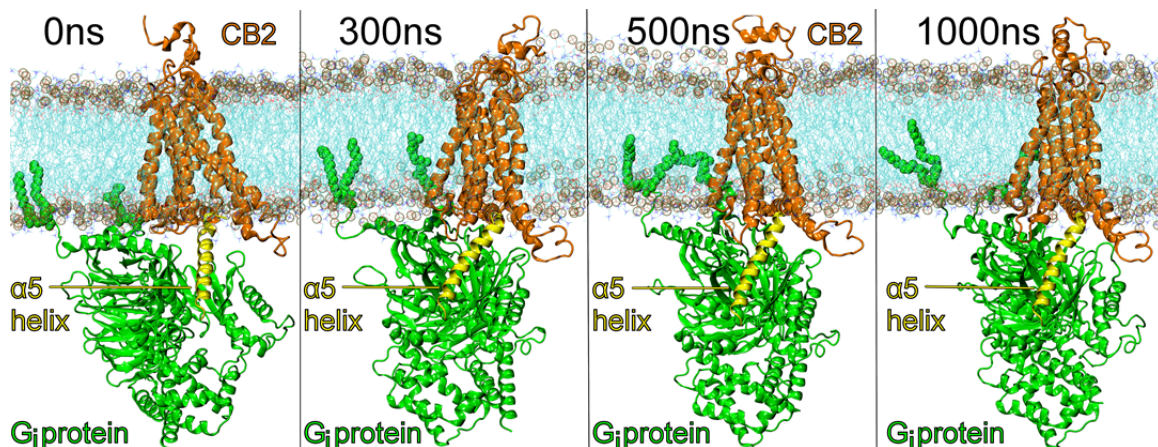


Figure 4. CB2 R* / G_{αi1}β₁γ₂ Protein Complex in Lipid Bilayer

This figure illustrates the full system for Trajectory 1 simulated over time here including the POPC bilayer (fatty acid acyl chains, cyan; phosphate atoms in phospholipid headgroup, open gold circles), the CB₂ receptor (orange) and G_{αi1}β₁γ₂ protein (green) with the G_{αi1} α5 helix shown in yellow.

Molecular Dynamics Simulations

Molecular dynamics (MD) calculations reported here used the results of crosslinking experiments to validate the receptor-G protein complex that emerged from our simulations. Crosslinking information was not used as a constraint for these simulations. It is also important to note that because of pepsin digestion, it is impossible to know whether all three crosslinks occurred in a single CB₂-G_{αi} complex, whether each crosslink was found in a different CB₂-G_{αi} complex or any other permutation between these two extremes. In other words, we do not know in advance if all three distance constraints implied by the cross-linking are ever met simultaneously. In the starting structure for the MD simulations, the Cys-Cys crosslink is just outside the range for crosslink formation. One of the Lys-Lys crosslinks is within range to form in the initial

CB₂-G_i protein complex similar to β₂-AR*/ Gα_sβ₁γ₂ complex. The second Lys-Lys crosslink, however, is not initially possible due to steric obstruction from the IC extension of TMH6. .

Results from our two independent 1 μs long trajectories suggest that conformational changes occur in both CB₂ and Gα_{i1}β₁γ₂ during the first 300-400 ns of the trajectories, as these proteins optimize their interaction with each other: Gα_{i1}β₁γ₂, re-orientes with respect to the receptor and uses a CB₂ IC-2 loop interaction to register the two proteins into new orientations, whereas TMH5 and TMH6 on CB₂ move outward, reorganizing the associated IC-3 loop. These changes are discussed in detail below.

Rotation of Gα_{i1}β₁γ₂ Relative to CB₂

Figure 5A illustrates the change about the z-axis in Gα_{i1}β₁γ₂ orientation relative to CB₂ that occurs within the first 300 ns in Trajectory 1. Here, the perspective is from the receptor interface toward the cytoplasm through the TMH bundle (the CB₂ receptor is omitted from the view for clarity). A clockwise rotation of ~25° can be clearly seen by considering the change in position of the N-terminal helix of Gα_{i1} (Figure 5A, shown in cylinder display: purple cylinder (t=0 ns) versus green cylinder (t=300 ns)). A similar rotation occurs in Trajectory 2 within the first 400 ns (not shown). Figure 5B shows the evolution of the rotation angle for Trajectory 1 (black) and Trajectory 2 (blue). The red and yellow lines in figure 5B represent the running averages. It is clear here that the distances plateau at about 300ns for Trajectory 1 and 400ns for Trajectory 2. Although the rotation angle for Trajectory 1 stabilizes to ~25°, the rotation for Trajectory 2 is ~35°.

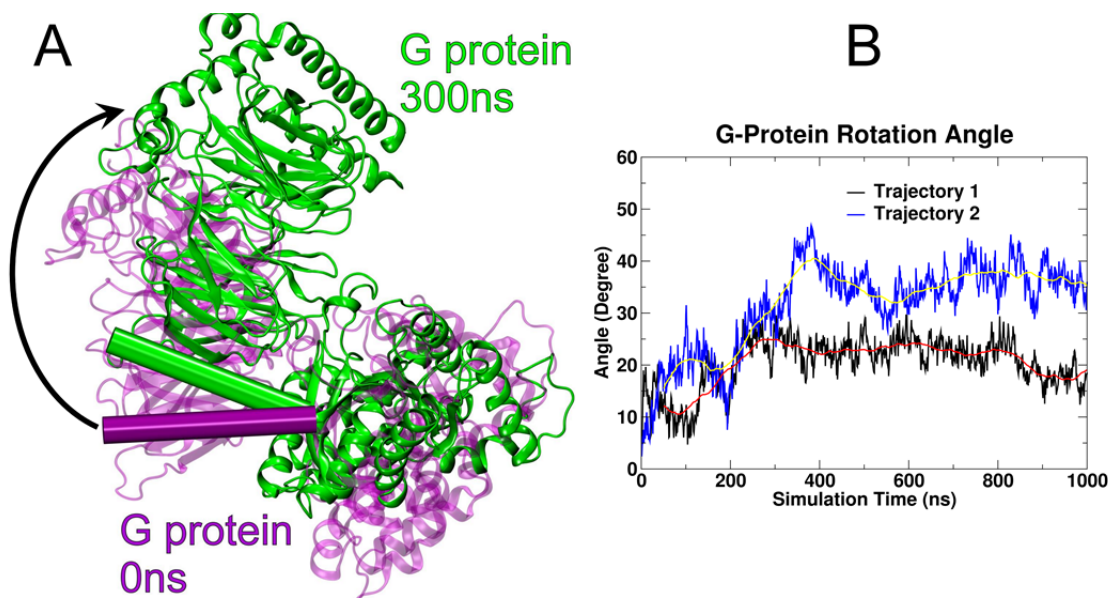


Figure 5. Change in the $G\alpha_i\beta_1\gamma_2$ Protein Relative to CB₂ Receptor

(A) This figure illustrates for Trajectory 1 that a rotation of the entire $G\alpha_i\beta_1\gamma_2$ protein ($t=0$ ns, purple; $t=300$ ns, green) relative to CB₂ occurs along the z-axis. Here the view is from the receptor interface toward the cytoplasm. The CB₂ TMH bundle has been turned off for clarity. A clockwise rotation of $\sim 25^\circ$ can be clearly seen by considering the change in position of the N-terminal helix of $G\alpha_{i1}$ (shown in cylinder display: purple cylinder ($t=0$ ns) versus green cylinder ($t=300$ ns)).

(B) This graph shows the evolution of the rotation angle for $G\alpha_i\beta_1\gamma_2$ relative to the CB₂ TMH bundle over time in Trajectory 1 (black line) and Trajectory 2 (blue line). The red and yellow lines represent the running average over 100 ns for Trajectory 1 and Trajectory 2 respectively.

Change in $G\alpha_{i1}$ C-Terminal α_5 Helix Tilt

Figure 6 illustrates that another important change in $G\alpha_i\beta_1\gamma_2$ orientation relative to CB₂ occurred during the MD runs. Here the intracellular ends of TMH5-6-7 and Hx8 are shown with TMH-1-2-3-4 omitted for clarity. The C-terminal α_5 helix of $G\alpha_{i1}$ is shown in cylinder display (Figure 6, green). In Trajectory 1 (Figure 6A), the C-terminal α_5 helix of $G\alpha_{i1}$ changed from a tilt towards the TMH7-Hx8 elbow (as seen in the crystal

structure of the β 2-AR(32)) to a tilt more aligned with the membrane normal, bringing the extreme C-terminus near the IC end of TMH6. This change occurred over the first 300 ns of the MD production run and was maintained through the rest of the trajectory ($t=300$ ns \rightarrow $t=1,000$ ns). Results were similar for Trajectory 2 (Figure 6B) except that the change in orientation happened over the first 400 ns. In both trajectories, the α 5 helix changes its orientation by pivoting about a point near the center of the α 5 helix in a rigid body motion. The helix does not also roll or undergo a face shift.

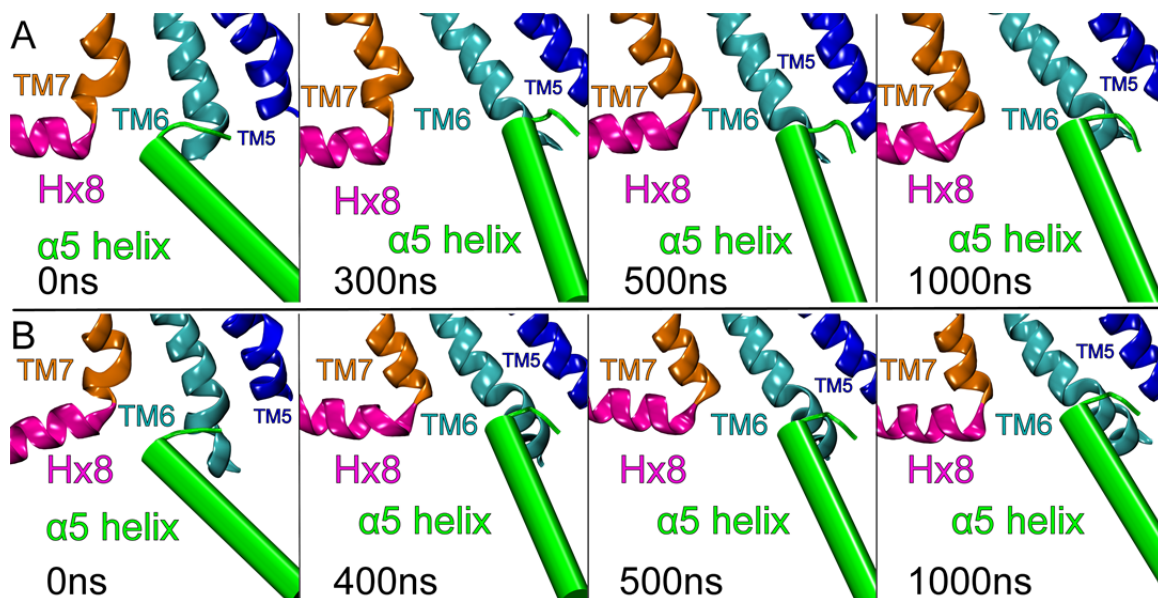


Figure 6. Change in the C-Terminal $\alpha 5$ Helix of $G\alpha_{i1}$

This figure illustrates an important change in $G\alpha_{i1}\beta_1\gamma_2$ orientation relative to CB_2 occurred during the MD runs. Here the intracellular ends of TMH5-6-7 and Hx8 are shown in blue, cyan, orange and magenta respectively. TMH-1-2-3-4 omitted for clarity and the C-terminal $\alpha 5$ helix of $G\alpha_{i1}$ is shown in green cylinder display.

(A) In Trajectory 1, the C-terminal $\alpha 5$ helix of $G\alpha_{i1}$ changed from a tilt towards the TMH7-Hx8 elbow (as seen in the crystal structure of the $\beta 2$ -AR (32)) to a tilt more aligned with the membrane normal, bringing the extreme C-terminus near the IC end of TMH6. This change occurred over the first 300 ns of the MD production run and was maintained through the rest of the trajectory ($t=300\text{ ns} \rightarrow t=1,000\text{ ns}$).

(B) Results were similar for Trajectory 2 except that the change in orientation happened over the first 400 ns of the MD production run and was maintained through the rest of the trajectory ($t=400\text{ ns} \rightarrow t=1,000\text{ ns}$).

IC-2 / $G\alpha_{i1}\beta_1\gamma_2$ “Registering” Interaction

The rotation of $G\alpha_{i1}\beta_1\gamma_2$ about the z-axis (illustrated in Figure 5) promotes an interaction between the IC-2 loop of CB_2 and a hydrophobic pocket on $G\alpha_{i1}$ (see Figure 7). This hydrophobic pocket is composed of residues immediately after the $G\alpha_{i1}$ N-terminus (V34), residues on the $G\alpha_{i1}$ $\beta 1$ and $\beta 2$ sheets (L194 and F196), as well as

residues on the $G\alpha_{i1}$ $\alpha 5$ helix (I344, I343, T340 and F336). In our initial CB_2 R*/ $G\alpha_{i1}\beta_1\gamma_2$ dock (based on the $\beta 2$ -AR/ $G\alpha_s\beta_1\gamma_2$ crystal structure), the IC-2 loop of CB_2 was located between the N-terminal helix and C-terminal helix of $G\alpha_{i1}$, on top of the loop connecting the $\beta 2$ and $\beta 3$ sheets. Figure 7 (t=0 ns) illustrates the hydrophobic pocket and the orientation of the receptor IC-2 loop relative to this pocket at the beginning of each trajectory. As the result of the rotation of $G\alpha_{i1}\beta_1\gamma_2$ about the z-axis discussed previously (see Figure 5), an IC-2 loop residue, P139, establishes a hydrophobic interaction with the hydrophobic pocket residues on $G\alpha_{i1}$ within the first 300 ns of the Trajectory 1 (Figure 7A) and 400ns of Trajectory 2 (Figure 7B). Over both 1 μ s trajectories, P139 entered and exited the hydrophobic pocket several times, but the rotation of $G\alpha_{i1}\beta_1\gamma_2$ about the y-axis ceased once this “registering” interaction was established around 300 ns for Trajectory 1 and 400ns for Trajectory 2.

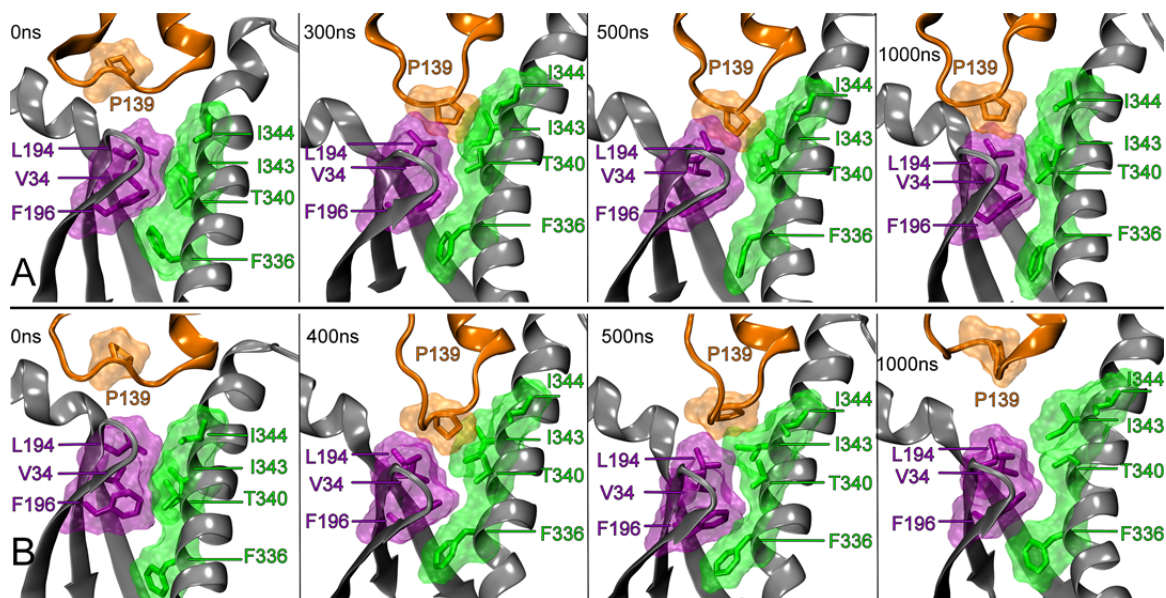


Figure 7. IC-2 Proline 139 Interaction with *Gai1*β1γ2 Protein

This figure shows the interaction between the CB₂ IC-2 loop residue (P139, colored orange) and a hydrophobic pocket on Gα_{i1}. This hydrophobic pocket is composed of residue(s) immediately after the Gα_{i1} N-terminus (V34, colored purple), residue(s) on the Gα_{i1} β1, and β2 sheets (L194 and F196, colored purple), as well as residues on the Gα_{i1} α5 helix (F336, T340, I343 and I344, colored green).

(A) This shows the interaction of P139 with the hydrophobic pocket at selected time points over 1 μs in Trajectory 1. The first interaction of P139 with the hydrophobic pocket occurred at t=300 ns.

(B) This shows the interaction of P139 with the hydrophobic pocket at selected time points over 1 μs in Trajectory 2. The first interaction with the hydrophobic pocket in Trajectory 2 occurred at t=400 ns.

The interaction of P139 with the hydrophobic pocket can also be followed by considering the solvent accessible surface area (SASA) of P139 over the course of each trajectory or the interaction energy of P139 with the hydrophobic pocket over the course of the trajectory. At the start of the Trajectory 1, the SASA of P139 was 200 Å² (t=0 ns), but decreased to 80 Å² during the period between 250 ns and 300 ns (black line in Figure 8A) and for Trajectory 2, the SASA of P139 was 200 Å² (t=0 ns), but decreased to 100 Å

during the period between 350 ns and 400 ns (blue line in Figure 8A). The interaction energy between P139 and the hydrophobic pocket was close to zero at the start of Trajectory 1, but dropped to -7 kcal/mol between 250 ns to 300 ns (black line Figure 8B). For Trajectory 2, the interaction energy dropped to -5 kcal/mol between 350 ns to 400 ns (blue line Figure 8B).

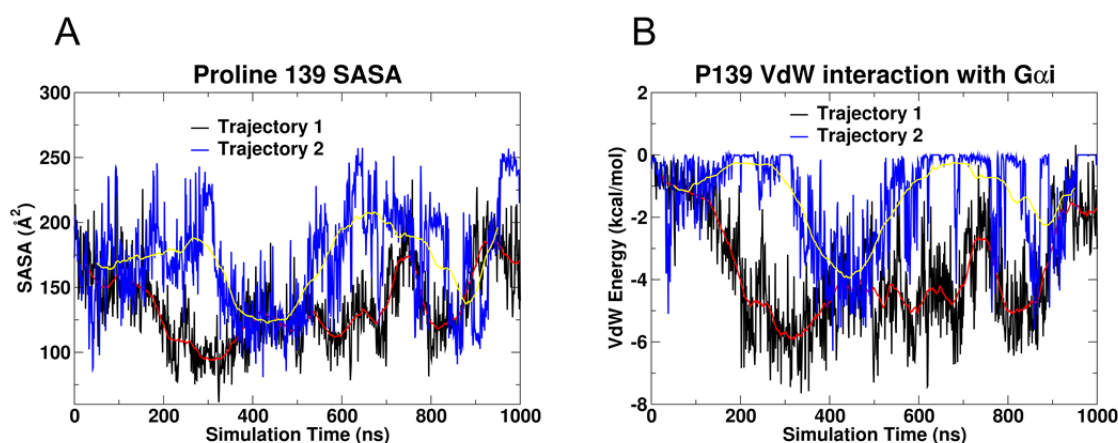


Figure 8. Solvent Accessible Surface Area and Interaction Energy of Proline 139

These plots (Trajectory 1, black; Trajectory 2, blue) show the change in the (A) Solvent accessible surface area and (B) Van der Waals interaction energy for the P139 (CB₂ IC-2 loop) interaction with the Gα_{i1} hydrophobic pocket. The red and yellow lines represent the running average over 100 ns for Trajectory 1 and Trajectory 2 respectively. Over the 1000 ns trajectory, P139 entered and exited the hydrophobic pocket several times, but the rotation of Gα_{i1}β₁γ₂ about the z-axis ceased once this anchoring interaction was first established at 300 ns for Trajectory 1 and 400ns for Trajectory 2. (see Figure 7 for further detail).

Shape of α5 Helix C-Terminal Portion

The crystal structure of Gα_{i1}β₁γ₂ is missing the last ten residues of the Gα_{i1} α5 helix. The three-dimensional structure of the transducin (Gt) α subunit C-terminal

undecapeptide $G\alpha_t$ 340 IKENLKDCGLF 350 was determined by Kisselev *et al.* using transferred nuclear Overhauser effect spectroscopy while it was bound to photoexcited rhodopsin (PDB 1AQG) (27). Light activation of rhodopsin caused a dramatic shift from a disordered conformation of $G\alpha_t$ (340–350) to a binding motif with a helical turn followed by an open reverse turn centered at Gly-348, with a helix-terminating C capping motif of an α L type. We used this NMR structure to complete the missing C-terminus of $G\alpha_{i1}$ in our initial model of the CB₂ G protein complex. Figure 9A shows a comparison of the $G\alpha_t$ (340–350) NMR structure (cyan) with the corresponding last ten residues of $G\alpha_{i1}$ at $t=400$ ns in each simulation (Trajectory 1, purple; Trajectory 2 green). It is clear that in both the trajectories the two segments have very similar shapes. We calculated the RMSD of the $C\alpha$'s of the last ten residues of $G\alpha_{i1}$ in our simulations versus the NMR structure. The RMSD plot in Figure 9B shows that this region of the C-terminus of $G\alpha_{i1}$ undergoes changes during the period ($t=0$ ns \rightarrow $t=300$ ns) for Trajectory 1 and ($t=0$ ns \rightarrow $t=400$ ns) for Trajectory 2 when the tilt of the $G\alpha_{i1}$ α 5 helix is changing, but the RMSD reaches a stable value by 300 ns for Trajectory 1 and 400 ns for Trajectory 2 and remains low thereafter.

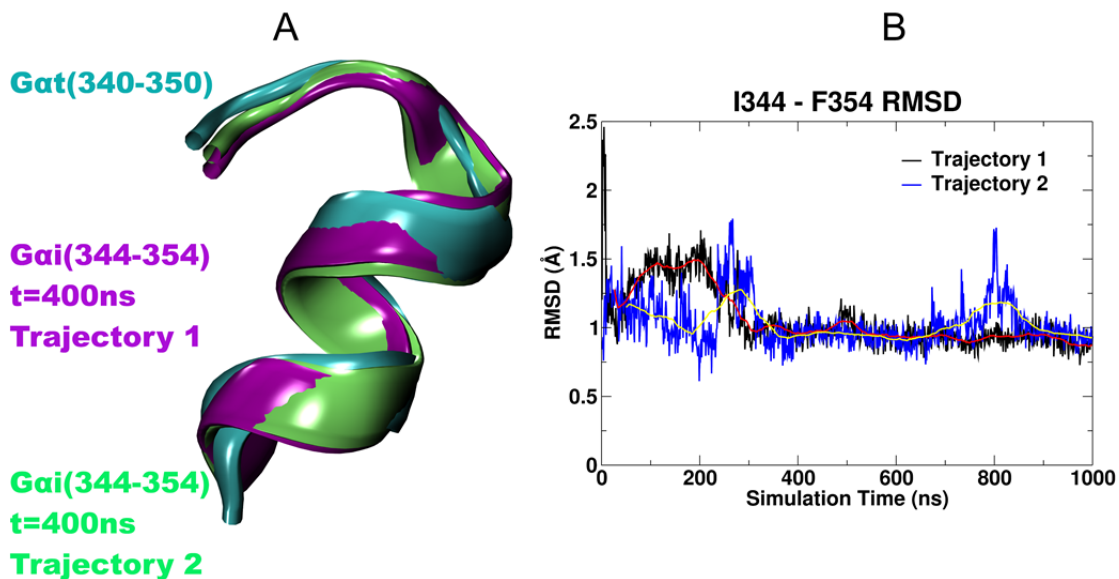


Figure 9. Shape of the C-Terminal $\alpha 5$ Helix of Gai

(A) This figure shows a comparison of the $G\alpha_i$ (340–350) NMR structure (27) (cyan) with the corresponding last ten residues of $G\alpha_{i1}$ at $t=400$ ns in Trajectory 1 (purple) and Trajectory 2 (green). It is clear that the two segments from both the trajectories have very similar shapes.

(B) The RMSD plot versus simulation time shows that I344 to F354 region of the C-terminus of $G\alpha_{i1}$ undergoes changes during the period ($t=0$ ns \rightarrow $t=300$ ns for Trajectory 1 (black line) and $t=0$ ns \rightarrow $t=400$ ns for Trajectory 2 (blue line)), but the RMSD reaches a stable value by 300 ns for Trajectory 1 and 400ns for Trajectory 2 and remains low thereafter. The red and yellow lines represent the running average over 100 ns for Trajectory 1 and Trajectory 2 respectively.

Why Does the $\alpha 5$ Helix Change Its Tilt?

There are two differences between the $CB_2/G\alpha_{i1}\beta_1\gamma_2$ and $\beta 2\text{-AR}/G\alpha_s\beta_1\gamma_2$ complexes that may contribute to the change in tilt of the $\alpha 5$ Helix. These are $G\alpha$ sequence differences and GPCR sequence differences.

1. Sequence Differences- $\alpha 5$ Helix

The reorientation of the $G\alpha_{i1}$ $\alpha 5$ helix illustrated in Figures 5 may be attributable in part to sequence differences between $G\alpha_s$ and $G\alpha_i$. The sequences of the last ten residues of the various isoforms of $G\alpha$ ($G\alpha_{i1}$, $G\alpha_{i2}$, $G\alpha_o$, $G\alpha_t$, $G\alpha_s$, $G\alpha_q$ etc.) have high homology; however, there is an important difference at the i-4 position. For the $G\alpha_i$ proteins, this position is occupied by a negatively charged residue (D in $G\alpha_{i1}$ and $G\alpha_{i2}$; E in $G\alpha_{i3}$). For $G\alpha_s$, however, this position is an uncharged residue (Q390 (i-4)). Figure 10 illustrates the difference in the interaction of the extreme C-terminus of $G\alpha_{i1}$ with the receptor that occurs partly as a consequence of this sequence difference. In the $\beta 2$ -AR (see Figure 10A), R3.50 has an aromatic stacking interaction with Y391 (i-3) on the $G\alpha_s$ $\alpha 5$ helix. Although our initial dock of $G\alpha_i$ with CB_2 R* mimicked this (see Figure 10B), during the initial 300-400 ns of the trajectories, the $\alpha 5$ helix changed its tilt angle to be more aligned with the membrane normal. This tilt change allows CB_2 R3.50 to now interact with D350 (i-4) on the $G\alpha_i$ $\alpha 5$ helix (see Figure 10C), while CB_2 R3.55 interacts with L353 (i-1) on the $G\alpha_i$ $\alpha 5$ helix. This latter interaction is a Van der Waals interaction.

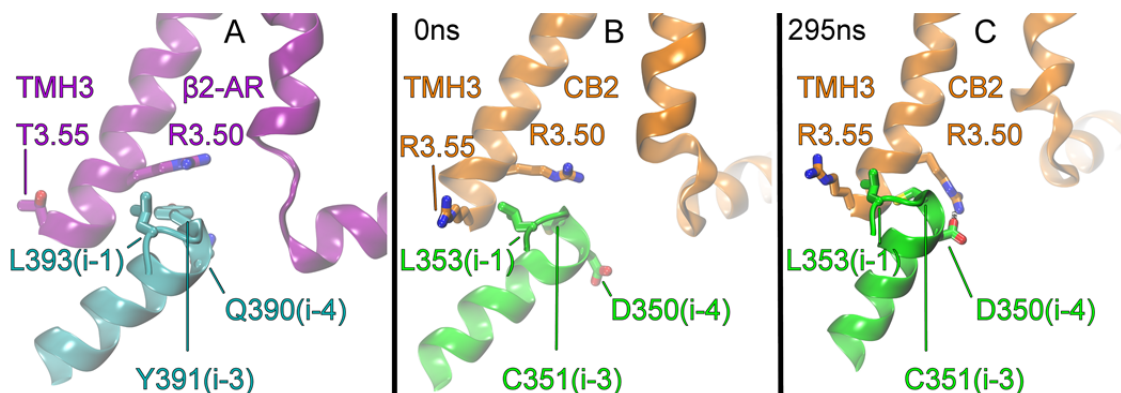


Figure 10. TMH3 and C-Terminal $\alpha 5$ Helix Interaction

This figure illustrates the interaction between receptor residues at the intracellular end of TMH3 with the three (i-1, i-3, i-4) residues of the C-terminal $\alpha 5$ helix of $G\alpha$.

(A) This figure shows that R3.50 of the $\beta 2$ -AR receptor interacts with Y391 (i-3) on $G\alpha_s$ (32). (B) This figure shows that in the initial $CB_2/G\alpha_{i1}\beta_1\gamma_2$ complex, R3.50 interacts with C351 (i-3) on $G\alpha_{i1}$ and R3.55 interacts with L353 (i-1). Here, the tilt of the $\alpha 5$ helix is very similar to that of $G\alpha_s$ in part A.

(C) However, after 295 ns in Trajectory 1, the tilt angle of the $G\alpha_{i1}$ $\alpha 5$ helix has changed permitting CB_2 R3.50 to form a salt bridge with D350 (i-4) on $G\alpha_{i1}$, while the hydrocarbon portion of R3.55 has a VdW interaction with L353 (i-1). Note here that in order to establish these interactions; the $\alpha 5$ helix changes its tilt angle to be more aligned with the membrane normal.

2. Sequence Differences-TMH5-TMH6 Movement

To accommodate the re-orientation of the $G\alpha_{i1}$ $\alpha 5$ helix and the rotation of $G\alpha_{i1}\beta_1\gamma_2$, CB_2 undergoes an outward movement of TMH5-TMH6 and the associated IC-3 loop moves away from the CB_2 TMH bundle. This is illustrated in Figure 11 for Trajectory 1. This is facilitated by the fact that both TMH5 and TMH6 have hinge points that allow these helices to move away from the TMH bundle when CB_2 is activated (17). TMH5 hinges at G5.53 (204), whereas the hinge point for TMH6 is at G6.38 (248). Figure 12 shows that the position of the CB_2 IC-3 loop relative to the $G\alpha_{i1}$ $\alpha 4\beta 6$ loop changes before 300 ns in the Trajectory 1. Here the G protein has clearly undergone a

rotation that places the $\alpha 4\beta 6$ loop of $G\alpha_{i1}$ near the IC-3 loop of CB_2 . This movement also removes the steric obstruction to the formation of the Lys-Lys crosslink between K5.34 (215) on TMH5 and K317 in the $\alpha 4\beta 6$ region of $G\alpha_{i1}$ that existed at the outset of the simulation (see Figure 3D). Similar results were obtained with Trajectory 2.

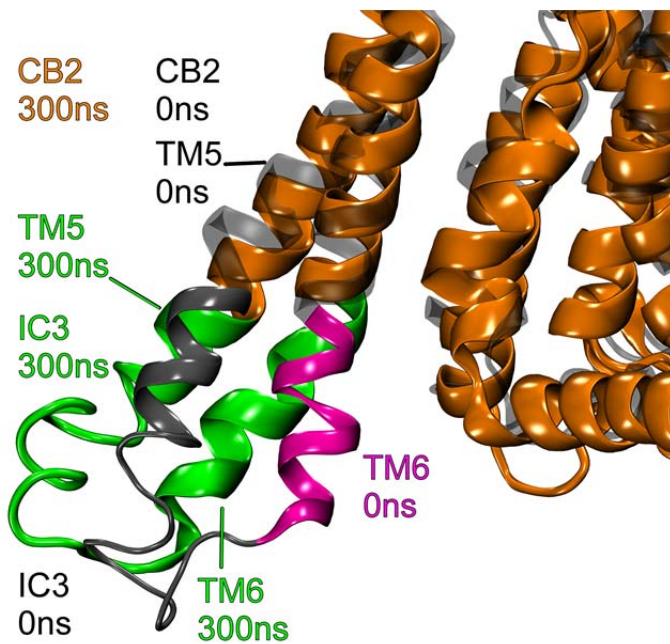


Figure 11. Outward Movement of TMH5 - TMH6

The CB_2 (shown partially) structure at $t=0$ ns is colored gray here, while the CB_2 structure at $t=300$ ns is colored orange for Trajectory 1 from the TMH6-7 perspective. Intracellular extension of TMH5-TMH6 including IC3 at $t=0$ ns is in gray and magenta while same at $t=300$ ns is colored green.

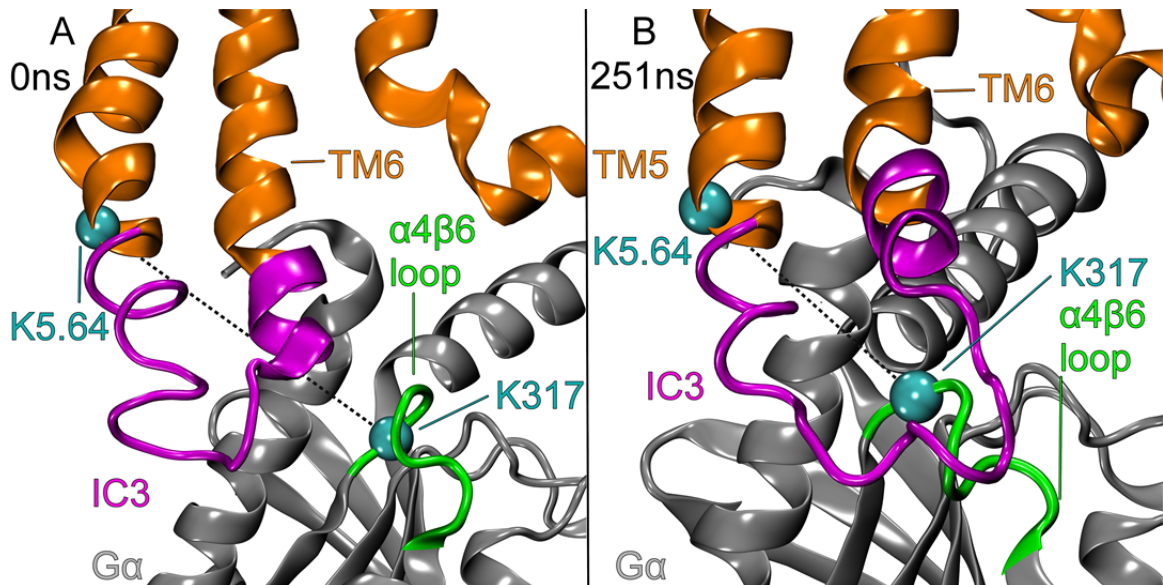


Figure 12. Movement of Intracellular Loop 3 (IC3)

This figure shows that the position of the CB₂ IC-3 loop (magenta) relative to the G α_{i1} α 4 β 6 loop (green) at

(A) t=0ns

(B) t=251ns

in the Trajectory 1. Here the G protein has clearly undergone a rotation that places the α 4 β 6 loop of G α_{i1} near the IC-3 loop of CB₂. This movement also removes the steric obstruction to the formation of the Lys-Lys crosslink between K5.34 (215) on TMH5 and K317 in the α 4 β 6 region of G α_{i1} that existed at the outset of the simulation (see Figure 3D). Similar results were obtained with Trajectory 2 (not shown).

Crosslink Correlations: Cysteine Crosslink between TMH3 and C-Terminal G α_{i1} α 5

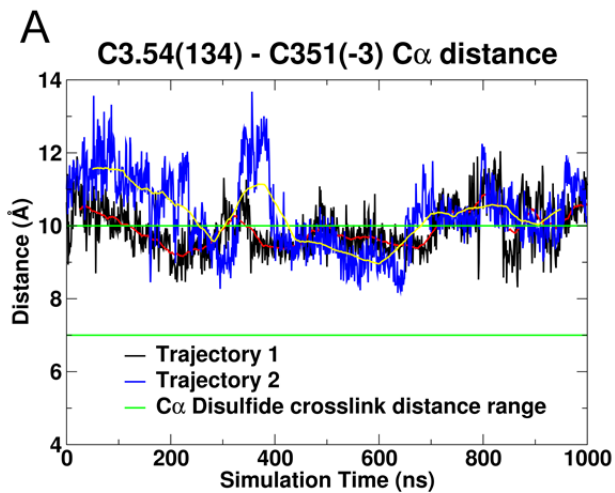
Helix

In order to test if experimentally obtained crosslinks were possible in Trajectories 1 and 2, we considered C α - C α distances for each pair of linked residues. We compared these distances to the range of C α - C α distances over which the crosslinking has been shown to form. In some trajectories this distance was below the cut-off distance for the entire trajectory. In others, there were only regions of the trajectory that were below the

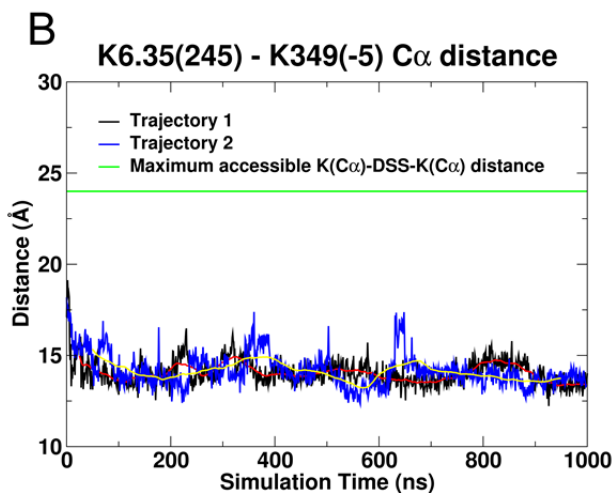
cut-off. We begin here by discussing each of the crosslinks individually. At the end of this section, we assess in what percentage of the trajectories is the C α - C α distance below the cut-off at the same time. Figure 13A shows a plot of the C α - C α distance between C3.54 (134) on CB₂ and C351 on the G α_{i1} $\alpha 5$ helix (i-3 residue on C terminal) for both trajectories. This plot has the distance range for cysteine crosslink formation indicated by the green lines. This distance was 10.6 Å in the starting structure, which was just 0.6 Å outside the crosslink range. The distance does decrease into the range of 7 - 10 Å, for multiple times in both trajectories. As a result, we conclude that our MD simulations suggest that the formation of a Cys-Cys crosslink is possible.

Crosslink between TMH6 and C-Terminal $\alpha 5$ Helix of G α_{i1}

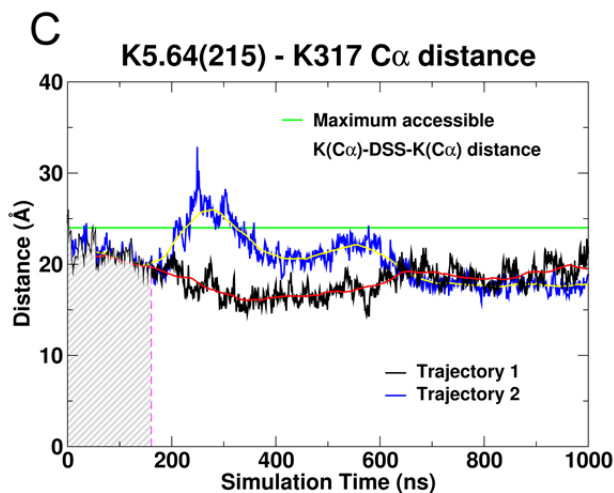
Figure 13B shows a plot of the C α - C α distance for the Lys-Lys crosslink between K6.35 (245) on CB₂ and K349 on the G α_{i1} $\alpha 5$ helix (i-5 residue on C terminal) for both the trajectories. The green line at 24.2Å indicates the distance below which a crosslink would be possible. The plot shows that this distance remained around 15 Å during the entire 1 μ s MD simulation for both the trajectories. In addition, there were no steric obstructions of this interaction present at any time in either trajectory. Therefore, we conclude that our MD simulations suggest that the formation of this Lys-Lys crosslink is possible.



(A) The C α - C α distance between C3.54 (134) and C351 on the G α_{i1} $\alpha 5$ helix (i-3 residue on C terminal) is shown here. The green lines at 7 Å and 10 Å correspond to the distance range for crosslink formation between two cysteines using HgCl₂.



(B) The C α - C α distance between K6.35 (245) and K349 on the G α_{i1} $\alpha 5$ helix (i-5 residue on C terminal) is shown here. The green line at 24.2 Å is the maximum C α distance to form a crosslink formation between two lysines using DSS.



(C) The $C\alpha$ - $C\alpha$ distance between K5.64 (215) and K317 on the $G\alpha_{i1}$ $\alpha4\beta6$ loop is shown here. The green line at 24.2 Å is the maximum $C\alpha$ distance to form a crosslink formation between two lysines using DSS. The hatched area before 200 ns represents that part of trajectory during for which the intracellular end of TMH6 sterically obstructs this crosslink. This corresponds to the section of TMH6 colored magenta in Figure 3D.

Figure 13. Distances Between the Crosslinked Residue Pairs

A plot of $C\alpha$ - $C\alpha$ distance as a function of simulation time is shown here for the three crosslinks reported here. Trajectory 1 is shown in black and Trajectory 2 is blue. The red and yellow lines represent the running average over 100 ns for Trajectory 1 and Trajectory 2 respectively.

Crosslink between TMH5 and the $G\alpha_{i1}$ $\alpha4\beta6$ Loop

We have indicated above that one consequence of the $G\alpha_{i1}\beta_1\gamma_2$ rotation relative to CB_2 is that TMH5-IC3-TMH6 moves away from the TMH bundle at the IC side in the first 300 ns for Trajectory 1 and 400 ns for Trajectory 2. Prior to this movement, it is structurally impossible to crosslink K5.34 (215) on TMH5 and K317 in the $\alpha4\beta6$ region of $G\alpha_{i1}$ even though the $C\alpha$ - $C\alpha$ distance between these residues is below the 24.2Å cutoff for crosslink formation. Figure 13C shows a plot of the $C\alpha$ - $C\alpha$ distance for this Lys-Lys crosslink for both trajectories. That section of the simulation for which the crosslink is structurally not possible is indicated by the hashed region. For Trajectory 1 (black line in figure 13C), once the structural interference is removed as TMH5-IC3-TMH6 moves

away from the bundle, the crosslink is possible at all other time points. Trajectory 2 (blue line in figure 13C) does have one region that goes above the allowed distance after the steric obstruction is cleared (200 - 375 ns). After this region, the C α - C α distance for Trajectory 2 remains below the cut-off. Therefore, our MD simulations suggest that the formation of this Lys-Lys crosslink is also possible.

Finally, we assessed at 1 ns intervals for both trajectories, those times for which all three sets of C α - C α distances were below the cut-off (and therefore possible) at the same time. We found that in Trajectory 1, this percentage was 60.8%, while for Trajectory 2, this percentage was 33.4%.

Discussion

High-resolution X-ray structures have been obtained for multiple class A (“rhodopsin-like”) GPCRs (3-6,48-56), various G protein heterotrimers (G $\alpha\beta\gamma$) (26,57,58) and isolated G α subunits in different functional states (59-61). Combined with biochemical and biophysical data, these structures reveal a surface on G α that is predicted to face the intracellular side of GPCRs. Information about the nature of this interface has been obtained via x-ray crystallography and chemical cross-linking studies. At present, there is only one crystal structure of a GPCR–G protein complex available (32), which shows the interaction of the β 2 adrenoreceptor (β 2-AR) with Gs protein after GDP has dissociated from the G α subunit. This structure represents an empty state that exists between the GDP bound and GTP bound G protein, artificially stabilized by a nanobody, insertion of which was necessary for crystallization (32).

Chemical crosslinking studies of protein-protein interactions can identify pairs of residues that come close enough to each other to form a respective crosslink. The identification of multiple crosslink sites can provide information about the relative orientation of the two interacting proteins.

In this paper, a comprehensive GPCR– $G\alpha_i$ protein chemical cross-linking strategy was applied with the goal of ascertaining the orientation of the CB_2 receptor relative to $G\alpha_{i1}$. These experiments revealed three crosslinks: (1) a cysteine crosslink between TMH3 residue C3.54 (134) and C351 on the $G\alpha_{i1}$ $\alpha 5$ helix (i-3 residue); (2) a lysine crosslink between TMH6 residue K6.35 (245) and K349 on the $G\alpha_{i1}$ $\alpha 5$ helix (i-5 residue); and (3) a lysine crosslink between TMH5 residue K5.64 (215) and K317 on the $G\alpha_{i1}$ $\alpha 4\beta 6$ loop. An examination of the initial complex we constructed to mimic the $\beta 2$ -AR*/ $G\alpha_s\beta_1\gamma_2$ x-ray crystal structure (32) revealed that one of these crosslinks (K6.35 (245) to K349) is possible in the initial complex. A second crosslink (C3.54 (134) to C351) is only 0.6 Å above the $C\alpha - C\alpha$ distance limit for crosslinking in the initial complex. But the third crosslink was sterically impossible in the initial complex. This suggested that either the orientation of the G protein with respect to a GPCR varies depending on the receptor and G protein to be complexed or that the orientation of $G\alpha_s\beta_1\gamma_2$ with respect to the $\beta 2$ -AR* in the crystal structure changes after GDP leaves the $G\alpha_s$ subunit, as has occurred in the $\beta 2$ -AR*/ $G\alpha_s\beta_1\gamma_2$ crystal structure.

To understand the origins of the experimental crosslinks between CB_2 and $G\alpha_i$ identified in this paper, we undertook microsecond timescale molecular dynamics

simulations of the CB₂ R*/ G α_{i1} $\beta_1\gamma_2$ complex in a POPC bilayer. We show here that when two MD runs of the CB₂ R*/ G α_{i1} $\beta_1\gamma_2$ complex in lipid are initiated using the same G protein orientation (including the angle of the G α_{i1} α_5 helix) as seen in the β_2 -AR*/ G $\alpha_s\beta_1\gamma_2$ crystal structure, rearrangements ensue fairly quickly in each. There is a gross clockwise rotation of the entire G protein underneath CB₂ R* during the first 300 ns (Trajectory 1) or 400 ns (Trajectory 2) of the production runs. This rotation ceases once an interaction is established between the IC-2 loop residue, P139 and a hydrophobic pocket on G α_{i1} formed by residues V34, L194, F196, F336, T340, I343 and I344. A change in the tilt of the G α_{i1} α_5 helix also occurs early in the trajectories facilitated by the outward movement of TMH6 and TMH5 at their IC ends. The change in tilt allows R3.50 on CB₂ to form a salt bridge with D350 (i-4) on the G α_{i1} α_5 helix.

Importance of the G α_{i1} α_5 Helix and the Change in Its Tilt Angle

In the present crosslinking study, a cysteine crosslink was formed between TMH3 residue C3.54 (134) and C351 on the G α_{i1} α_5 helix (i-3 residue). The extreme C terminus was one of the first regions within G α identified as being critical to receptor-promoted activation. Hamm and co-workers (62) first demonstrated that synthetic peptides corresponding to the C terminus of G α_t could block rhodopsin promoted activation, suggesting that the C terminus of G α is a critical receptor-binding site. Alanine-scanning experiments confirmed that the C terminus/ α_5 helix were essential for rhodopsin-promoted activation of G α_t (63). In many early G protein crystal structures, the extreme C-terminus of G α was unresolved. The first three-dimensional structure of

the transducin (G_t) α subunit C-terminal undecapeptide G α_t ³⁴⁰IKENLKDCGLF³⁵⁰ bound to photoexcited rhodopsin registered in the Protein Data Bank was determined by using transferred nuclear Overhauser effect spectroscopy (27). Light activation of rhodopsin caused a dramatic shift from a disordered conformation of G α_t (340–350) to a binding motif with a helical turn followed by an open reverse turn centered at G348, with a helix-terminating C capping motif of an α L type. Docking of the NMR structure to the GDP-bound x-ray structure of G_t reveals that photoexcited rhodopsin promotes the formation of a continuous helix over residues 325–346 terminated by the C-terminal helical cap with a unique cluster of crucial hydrophobic side chains. Subsequently, this C-terminal region has been resolved in three GPCR crystal structures: (1) the bovine Opsin*–G α -C terminal peptide complex (64); (2) Meta II rhodopsin in complex with an 11-amino-acid C-terminal fragment derived from G α (two residues mutated) (65); and (3) the β 2-AR*/G $\alpha_s\beta_1\gamma_2$ complex (32). In each of these structures, the shape of the extreme C-terminus is quite similar to the original NMR structure. In work presented here, this NMR structure was used to complete the G α_{i1} structure that was docked in CB₂ R*. The RMSD plot in Figure 9B shows that the shape of the last 10 residues in the C-terminal region has a low RMSD after the first 300 ns of production simulation for Trajectory 1 and 400 ns for Trajectory 2 when compared with the NMR structure.

We also report here that the insertion angle of the G α_{i1} α 5 helix changed from its starting angle (which mimicked the β 2-AR*/G $\alpha_s\beta_1\gamma_2$ complex (32)). Two reasons for this change are the position of the IC end of TMH5 in CB₂ R* and a key sequence

difference between $G\alpha_i$ and $G\alpha_s$ at the i-3 position on the $G\alpha_i$ $\alpha 5$ helix. One striking difference between the $\beta 2$ -AR and CB_2 sequences is that the $\beta 2$ -AR has the highly conserved P5.50, while CB_2 lacks this proline in TMH5 (L5.50 in CB_2). In the $\beta 2$ -AR*/ $G\alpha_s\beta_1\gamma_2$ complex (32)), TMH6 has moved away from the TMH bundle and broken the ionic lock (R3.50/E6.30), thus exemplifying an activated GPCR. The proline kink region of TMH5 flexes, but moves TMH5 towards the TMH bundle interior. When the $\alpha 5$ helix of $G\alpha_s$ inserts in this activated structure, it must insert in an opening formed by TMH6's outward movement. This region extends over to the elbow region of TMH7-Hx8. In the case of CB_2 , the C-terminal $\alpha 5$ helix of $G\alpha_{i1}$ can insert into a wider opening, one formed by the TMH5 and TMH6 outward movement. This in turn allows the angle of insertion to change in CB_2 .

R3.50 has been shown to be crucial for CB_2 signal transduction. Feng and Song reported no stimulation of agonist induced [35 S]GTP γ S binding for the R3.50A mutant in CB_2 (66). We show here that the change in the tilt angle of the $\alpha 5$ helix also permits formation of a salt bridge between R3.50 on CB_2 and D350 (i-4) on the $G\alpha_{i1}$ $\alpha 5$ helix. D350 (i-4) occupies a position in the C-terminus of $G\alpha_i$ that has an important divergence from $G\alpha_s$. For the $G\alpha_i$'s, this position is occupied by a negatively charged residue (D in $G\alpha_{i1}$ and $G\alpha_{i2}$; E in $G\alpha_{i3}$). For $G\alpha_s$, however, this position is an uncharged residue (Q390 (i-4)). Figure 10 illustrates the difference in the interaction of the extreme C-terminus of $G\alpha_{i1}$ with the receptor that occurs partly as a consequence of this sequence difference. In the $\beta 2$ -AR (see Figure 10A), R3.50 has an aromatic stacking interaction with Y391 (i-3)

on the $G\alpha_s$ $\alpha 5$ helix. Although our initial dock of $G\alpha_i$ with CB2 R* mimicked this (see Figure 10B), after 295 ns in Trajectory 1, the tilt of the $\alpha 5$ helix has changed such that $G\alpha_{i1}$ moves towards TMH5 – TMH6, allowing R3.50 to now interact with D350 (i-4) (see Figure 10C), while the hydrophobic part of R3.55 interacts with L353 (i-1). A similar change occurred in Trajectory 2.

Second Intracellular Loop Interaction with G α Protein

Interactions between GPCR IC-2 loops and G protein have been shown to be critical in GPCR/G protein coupling for numerous receptors. The IC-2 loop of the muscarinic M3 receptor has been shown to interact with the N terminal region of $G\alpha_q$ protein (67). IC-2 interactions also have been shown to be critical for coupling in the follicle-stimulating hormone receptor (FSH) with $G\alpha_s$ (68). In the $\beta 2$ -AR*/ $G\alpha_s\beta_1\gamma_2$ crystal structure, IC-2 loop residue, F139, inserts into an aromatic/hydrophobic pocket on $G\alpha_s$ comprised of H41, V217, F129, F376, R380 and I383 on the $G\alpha_s$ C terminal region and $G\alpha_s$, $\beta 2$ and $\beta 3$ sheets (see Figure 4c in ref (32)). The importance of this interaction is underscored by mutagenesis studies which demonstrate that a $\beta 2$ -AR F139A mutation significantly impairs $\beta 2$ -AR coupling to $G\alpha_s$ (69). We show here that $G\alpha_{i1}\beta_1\gamma_2$ rotation about the z-axis ceased once the IC-2 loop residue, P139 establishes a hydrophobic interaction with the hydrophobic pocket residues on $G\alpha_{i1}$ (Figures 6 and 7). The two proteins appear to be in “register” once this interaction occurs. Consistent with this idea, no further $G\alpha_{i1}\beta_1\gamma_2$ rotation occurs in either trajectory. In support of the importance of

this interaction, Zheng and colleagues have reported that a P139A mutation in CB₂ results in the loss of coupling with G α_i (70).

Third Intracellular Loop Interaction with the $\alpha_4\beta_6$ Region of Ga

Our chemical cross-linking strategy led to a DSS (Lys-Lys) crosslink between the TMH5 residue K5.64 (215) and K317 on the G α_{i1} $\alpha_4\beta_6$ loop. In the MD simulations reported here, this crosslink becomes possible only after G $\alpha_{i1}\beta_1\gamma_2$ rotation under CB₂ (see Figures 4, 5 and 11, 12). The importance of α_4/β_6 loop residues to GPCR/ G protein complex formation has been shown for multiple GPCRs. Slessareva *et al.* have shown that the G α_{i1} α_4 helix- α_4/β_6 loop are involved in 5-HT1a, 5-HT1b and muscarinic M2 receptor interactions (71). For the rhodopsin – transducin (G α_t) complex, residues in the G α_t $\alpha_4\beta_6$ loop (R310 to K313) were shown to crosslink with residues in the IC-3 loop of rhodopsin using a photoactivatable reagent, N-[(2-pyridyldithio)-ethyl], 4-azido salicylamide (72). For the rat M3 muscarinic acetylcholine receptor (M3R) – G α_q complex system, a crosslink has been reported between a D321C mutation on $\alpha_4\beta_6$ loop of G α_q and a K7.58(548)C mutation on M3R. Here the crosslinking agent was a short bi-functional, irreversible chemical crosslinker bis-maleimisoethane (BMOE) (67).

Conclusions

The result of this study is a CB₂ R*/ G $\alpha_{i1}\beta_1\gamma_2$ complex in which the proteins are in the correct register as indicated by chemical crosslinking studies. The next stage of this project will be the study of the changes that complex formation with CB₂ R* induces in

$G\alpha_i\beta_1\gamma_2$. Our ultimate goal will be the activated state of $G\alpha_i\beta_1\gamma_2$ in which GDP has been released.

CHAPTER II

ROLE OF THE INTRACELLULAR LOOPS OF THE CANNABINOID CB₂ RECEPTOR IN THE ACTIVATION OF THE G_i PROTEIN

Jagjeet Singh, Diane L. Lynch, Alan Grossfield, Dow P. Hurst, Michael C. Pitman and Patricia H. Reggio (To be published)

Abstract

Previously, we used molecular dynamics simulations to study the activation of the cannabinoid CB₂ receptor by its endogenous ligand, 2-arachidonoylglycerol (2-AG) via the lipid bilayer (17). We then reported the formation of the CB₂ / G $\alpha_{i1}\beta_1\gamma_2$ complex using our activated CB₂ receptor model (73). In the next step of our study of the G-protein signaling cascade, we are studying the activation of the G α_{i1} protein catalyzed by an activated CB₂ receptor that leads to guanosine di phosphate (GDP) release (32,74,75). Here we report the relationship between specific receptor interactions with the G α_{i1} protein and the resultant progression of GDP hydration. We propose that such hydration is likely required for GDP release from G α proteins.

Results from our 5 μ s MD simulations suggest that intracellular loop interactions contribute to the hydration of GDP, with the larger contribution from IC2 interaction, when P139 (IC2 loop of CB₂) interacts with a hydrophobic pocket on G α_{i1} (V34, L194, F196, F336, T340, I343 and I344) and a lesser contribution from the IC3 interaction, when R229 (IC3 loop of CB₂) reaches to the end of the α_4 helix to E297 and

E298. IC1 interactions (R66 on CB₂ interaction with E28 on N terminal helix of G α_{i1} protein) with G α_{i1} protein does not correlate with any increase in the GDP hydration. Taken together these findings suggest that IC2 and IC3 loops of CB₂ interact with ras-like (GTPase) domain on the G α_{i1} protein, resulting in an increase in GDP hydration.

Introduction

The cannabinoid CB₂ receptor is encoded by the *CNR2* gene and is mainly expressed in T cells of the immune system (13). It has been also shown to be weakly expressed in the gastrointestinal system (14,15). CB₂ has also been reported to play an important role in central immune responses during neuropathic pain in mice (16). CB₂ belongs to Class A of the GPCRs and has been shown experimentally to couple only to G α_i inhibitory protein (18-20).

G protein coupled receptors (GPCRs) catalyze the activation of G-proteins by the releasing tightly bound guanosine diphosphate (GDP). GDP is held in the unactivated G-protein between the ras-like (GTPase) and helical domains of the G α protein. However the molecular mechanism by which this happens is not completely understood (21,76,77). Earlier studies have shown the importance of the G α C-terminus and the α 4- β 6 loop of G α (63,71,72) in receptor coupling. F139A mutagenesis studies of the β 2-AR/Gs system have suggested that receptor IC-2 loop interaction with G-protein is critical (69). The only crystal structure of a GPCR/G-protein complex (β 2-AR/Gs) clearly shows the interaction between F139 and a hydrophobic pocket in the ras-like domain of Gs (32). Receptor IC-3 loop involvement with the α 4 helix (78,79) and the α 4- β 6 loop (71,72) of

the G-protein has also been shown important for G-protein activation. Taken together, the literature suggests the involvement of various regions on GPCRs with $G\alpha$ protein regions to be important for G-protein activation but the molecular mechanism by which such dynamic interactions in the complex lead to activation is also still unclear (21).

In the work reported here, we studied the role of CB_2 intracellular regions in $G\alpha_i$ protein activation by using microsecond-long molecular dynamics simulations. We tested the hypothesis that GDP release upon activation requires the hydration of GDP. Results from our 5 μ s MD simulations suggest that intracellular loop interactions do contribute to the hydration of GDP, with the larger contribution from IC-2 loop interaction and a lesser contribution from IC-3 loop interaction. In contrast, IC-1 loop interactions with $G\alpha_{i1}$ protein does not correlate with any increase in GDP hydration.

Methods

CB₂ Receptor Model

The $CB_2 R^*$ model used in this study was taken from our previously published microsecond-long simulation of the activation of the CB_2 receptor by the endogenous ligand, 2-AG, via the lipid bilayer (17).

G-Protein Modeling

For the current study, the crystal structure of $G\alpha_{i1}\beta_1\gamma_2$ (26) was used to dock with $CB_2 R^*$. Missing parts of the $G\alpha_{i1}\beta_1\gamma_2$ protein were completed as described in Chapter I. Briefly, to complete the missing extreme $G\alpha_{i1}$ C-terminus, the NMR structure of $G\alpha_t$ was used (27) and the missing C-terminus of $G\gamma_2$ was built using the NMR structure of $G\gamma_1$

(28). Lipidation sites (Palmitic acid, Myristic acid) were attached to the N-terminus of $G\alpha_{i1}$ at Cys3 (29) and Gly2 respectively (30) and a geranylgeranyl group was attached to Cys 68 in the $G\gamma_2$ C-terminus (31).

CB₂/G_i-Protein Complex

Our initial CB₂ R* / $G\alpha_{i1}\beta_1\gamma_2$ complex was based on the β_2 -AR / $G\alpha_s\beta_1\gamma_2$ complex crystal structure (32) as described in Chapter I.

Construction of CB₂/G $\alpha_{i1}\beta_1\gamma_2$ Complex in POPC Bilayer

The CB₂ R*/G protein complex was placed in the simulation cell size of 130.0Å x 130.0Å x 170.6 Å as described in the Chapter I. The CB₂/G $\alpha_{i1}\beta_1\gamma_2$ protein complex was centered at the middle of the POPC lipid bilayer using scripts derived from CHARMM-GUI (33). The CHARMM22 protein force field with CMAP corrections (35,80) and the CHARMM 36 lipid force field (36) were used in this study. Parameters for GDP and lipidation sites were obtained as described in Chapter I (73).

Molecular Dynamics Simulations

To relieve poor initial contacts, minimization and equilibration was performed using CHARMM (38), and NAMD (39) as previously published (73) For all production runs, NAMD (39) was used. Long range electrostatics were included using PME (40) (see Chapter I for details). Production dynamics was performed on the BSBC cluster at UNC Greensboro (<http://bsbc.uncg.edu/index.html>) and a Blue Gene supercomputer (41) located at the Thomas J. Watson Research Center, Yorktown Heights, New York. Results from the 5 μ s long trajectory are reported here. The trajectory analysis was performed

using visual molecular dynamics (42) and the Lightweight Object-Oriented Structure library (LOOS) (43).

Results

CB₂ R / G α_{i1} Protein Complex*

The CB₂ intracellular (IC) loops that directly interact with the G α_{i1} ras-like domain were in close proximity of the G α_{i1} ras-like domain in our initial CB₂ R* / G α_{i1} protein complex (Figure 14). The G α_{i1} C terminal $\alpha 5$ helix was pointing towards the CB₂ TMH7/Hx8 “elbow” region. The IC-3 loop was close to the G α_{i1} $\alpha 4\beta 6$ loop and $\alpha 4$ helix. The IC-2 loop was above the region between the G α_{i1} N-terminal helix and the G α_{i1} C terminal $\alpha 5$ helix. The IC-1 loop was away from the G α_{i1} N terminal helix (Figure 14).

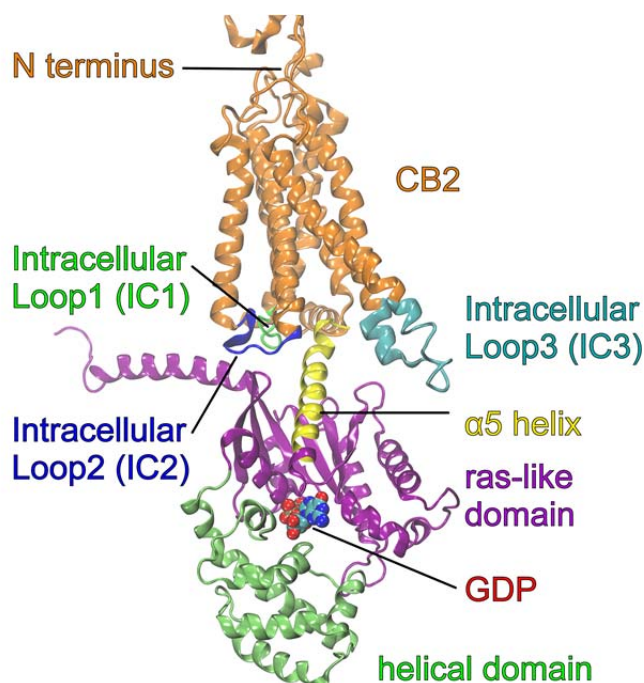


Figure 14. The Orientation of CB₂ Intracellular Loops Relative to G α_{i1} Protein

This figure shows the G α_{i1} protein underneath the CB₂ receptor. Here the CB₂ receptor is shown in orange. The G α_{i1} ras-like and helical domains are shown in purple and green respectively. The GDP bound between the G α_{i1} helical and ras-like domains is represented in VdW display with carbons, nitrogens and oxygens colored green, blue and red respectively. The CB₂ IC loops are colored green, blue and cyan for IC-1, IC-2 and IC-3 respectively.

During our 5 μ s long MD simulation of the CB₂ / G α_{i1} protein complex, the intracellular loops of the activated CB₂ receptor developed interactions with various parts of the ras-like domain of the G α_{i1} protein. These interactions are discussed in detail below.

IC-1 Loop Interactions with the G α_{i1} N-terminal Helix

An electrostatic interaction between the CB₂ IC-1 loop residue R66 and E28 on the G α_{i1} N-terminal helix was observed (Figure 15A). This interaction started between 600 ns to 750 ns for a short time, but between 1000 ns to 2800 ns these residues interacted with each other for a longer period. Then after losing their interaction for almost a microsecond, R66 and E28 regain their interaction from 3900 ns until the end of the trajectory (Figure 15B).

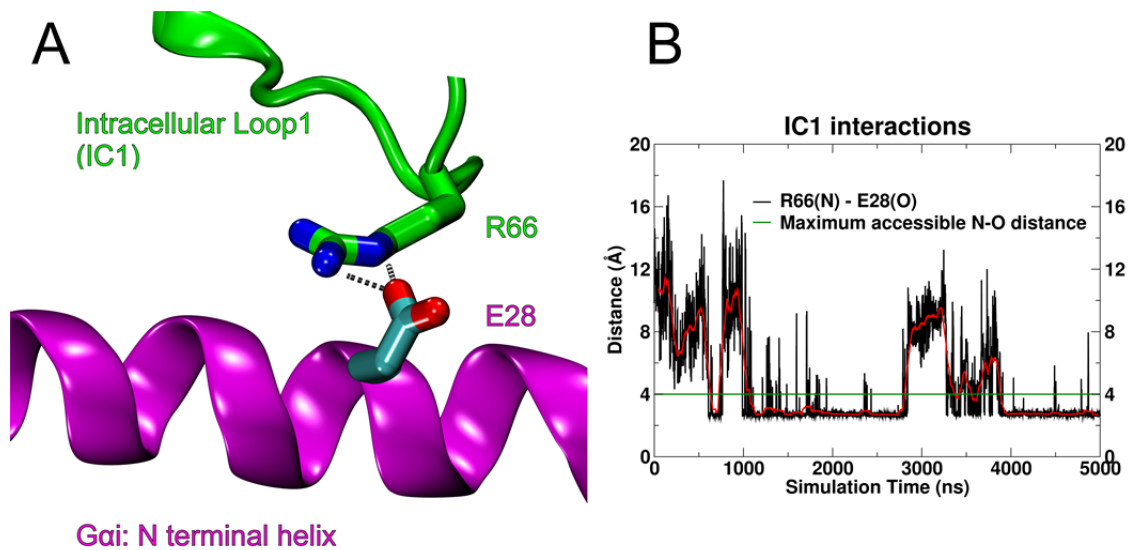


Figure 15. CB2 IC-1 Loop Interactions with the *Gai1* N-terminal Helix

(A) Figure 15A shows the interaction between R66 on the CB₂ IC-1 loop with E28 on the G α_{i1} N-terminal helix at t=2058 ns.

(B) The black line in this figure represents the N-O distance between R66 on the CB₂ IC-1 loop and E28 on the G α_{i1} N-terminal helix. The green line at 4.0 Å represents the maximum accessible distance between N and O (81). The red line represents the running average over a 100 ns frame.

IC-2 Loop Interaction with $G\alpha_i$ Protein

A hydrophobic interaction between Proline 139 on the IC-2 loop of CB₂ and a hydrophobic pocket on $G\alpha_{i1}$ protein was observed. This pocket includes residues from the $G\alpha_{i1}$ N-terminus (V34), $\beta 1$ and $\beta 2$ sheets (L194 and F196), and $\alpha 5$ helix (I344, I343, T340 and F336). This interaction was not present in our initial CB₂ R*/ $G\alpha_{i1}\beta 1\gamma 2$ dock (based on the $\beta 2$ -AR/ $G\alpha_s\beta 1\gamma 2$ crystal structure), but developed over the trajectory (Figure 16).

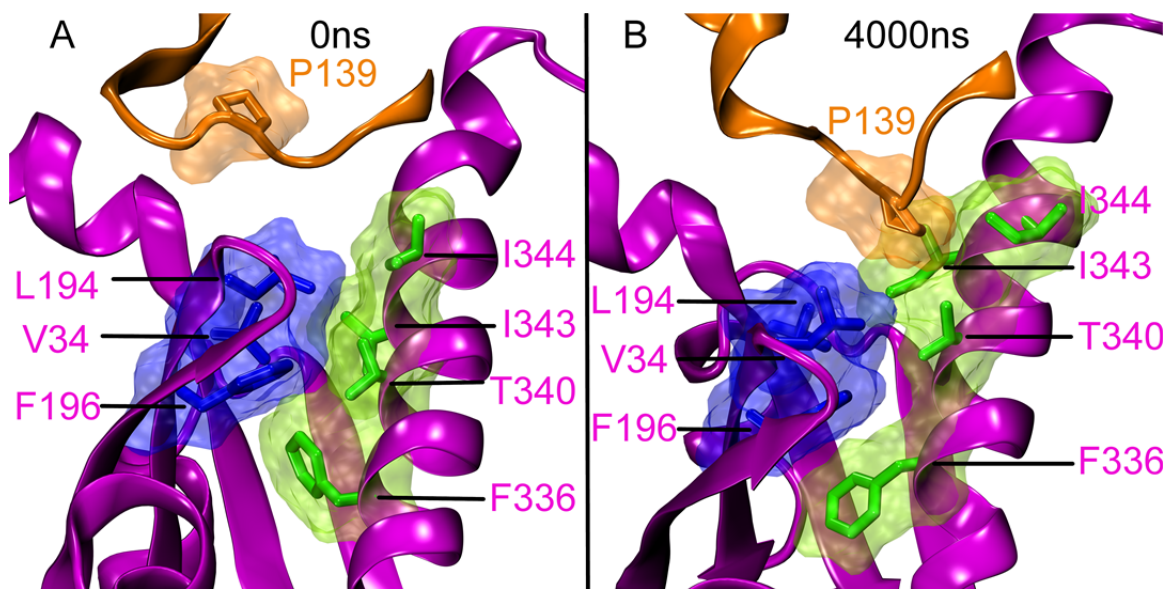


Figure 16. CB₂ IC-2 Loop / $G\alpha_{i1}\beta 1\gamma 2$ Interaction

This figure shows the interaction between the CB₂ IC-2 loop residue (P139, colored orange) and a hydrophobic pocket on $G\alpha_{i1}$. This hydrophobic pocket is composed of residue(s) immediately after the $G\alpha_{i1}$ N-terminus (V34, colored blue), residue(s) on the $G\alpha_{i1}$ $\beta 1$, and $\beta 2$ sheets (L194 and F196, colored blue), as well as residues on the $G\alpha_{i1}$ $\alpha 5$ helix (F336, T340, I343 and I344, colored green).

(A) This shows the starting structure ($t=0$ ns) in which P139 (orange) is in the proximity of the $G\alpha_{i1}$ hydrophobic pocket, but not pointing towards it.

(B) This shows the complex at a later time ($t= 4000$ ns) at which P139 (orange) is interacting with the hydrophobic pocket.

The P139 interaction with the $G\alpha_{i1}$ hydrophobic pocket was followed by monitoring the solvent accessible surface area (SASA) of P139 over the 5 μ s long trajectory. The SASA of P139 was 200 \AA^2 ($t=0$ ns), at the beginning of the trajectory, but decreased and reached its lowest SASA (80 \AA^2) during the period between 250 ns to 300 ns. After 3000 ns, the P139 SASA stayed at 120 \AA^2 . Over the 5000 ns long trajectory, P139 entered and exited the hydrophobic pocket multiple times; at 1000 ns and 2500 ns it is out of the hydrophobic pocket (black line in Figure 17A). A similar trend was shown by following the P139 interaction energy with the $G\alpha_{i1}$ hydrophobic pocket over the course of 5 μ s long trajectory. The interaction energy between P139 and the $G\alpha_{i1}$ hydrophobic pocket was close to zero at the start of trajectory, but dropped to a minimum of -7 kcal/mol between 250 ns to 300 ns. Then at 1000 ns and again at 2500 ns (black line in Figure 17B), the interaction energy was close to zero when the SASA was at a maximum (black line in Figure 17A). Between 3000 ns to 4000 ns the interaction energy remained at a value of -5 kcal/mol.

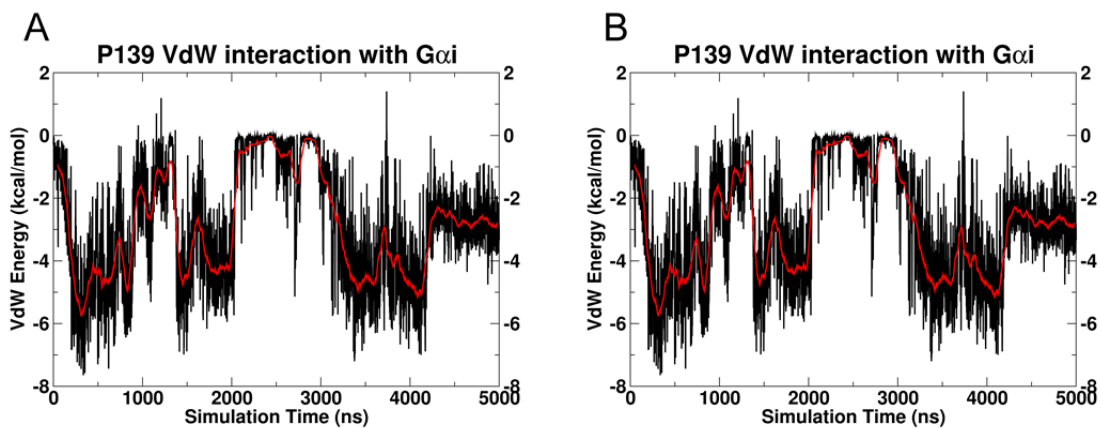


Figure 17. IC-2 Loop P139 Interaction with $G\alpha_i$ Protein

These plots show the change in the

(A) solvent accessible surface area (SASA) and

(B) the Van der Waals interaction energy for the P139 (CB₂ IC-2 loop) interaction with the $G\alpha_{i1}$ hydrophobic pocket. The red line represents the running average over 100 ns.

Over the 5 μ s trajectory, P139 entered and exited the hydrophobic pocket multiple times.

IC-3 Loop Interactions with the $G\alpha_i \alpha_4$ Helix

In the MD simulation starting structure, the CB₂ IC-3 loop residue R229 was close to the $G\alpha_i \alpha_4$ helix residue E308. A long lasting interaction between R229 and E308 was observed between 2000 – 4000 ns, where the R229 (N) – E308 (O) distance stays below 4 Å (Figure 18A). An IC-3 loop interaction with the other residues on the $G\alpha_i \alpha_4$ helix was observed from 1.4 to 1.6 μs, when the CB₂ IC-3 residue R229 “dove” down to interact with E297 and E298 (Figure 18B). After 2 μs, R229 interacted with Q304 and E308 on the $G\alpha_i \alpha_4$ helix favoring an E208 interaction.

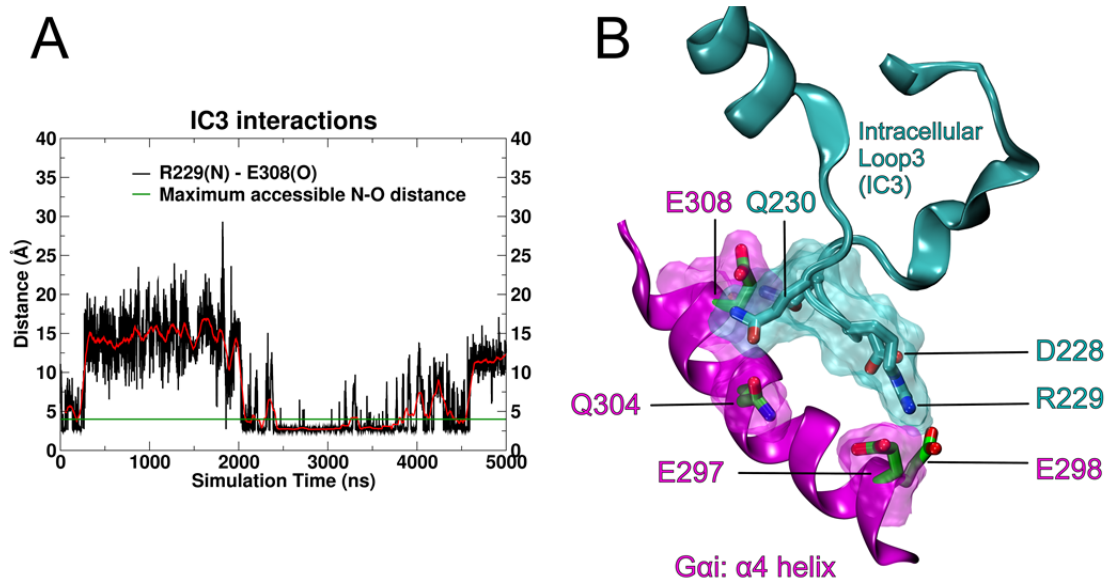


Figure 18. IC-3 Loop R229 Interaction with $G\alpha_i \alpha_4$ Helix Residue E308

(A) A plot of the N-O distance between CB₂ IC-3 loop residue R229 and $G\alpha_i \alpha_4$ helix residue E308 versus simulation time (black line) is presented here. The green line at 4.0 Å represents the maximum accessible distance between N and O (81). The red line represents the running average over 100 ns.

(B) This figure shows the $G\alpha_i \alpha_4$ helix in magenta and the CB₂ IC-3 loop in cyan color at $t=1533$ ns.

Interaction Between CB₂ TMH7/Hx8 Elbow Region and G α_i C-Terminus

At the start of the MD simulation, the CB₂ receptor elbow region (TMH7/Hx8) residue R7.56 (302) was not interacting with the G α_i C-terminal α 5 helix residue D350 (i-4), it was pointing towards lipid (Figure 19A). However, an interaction between these two residues developed after 3 μ s in the trajectory.

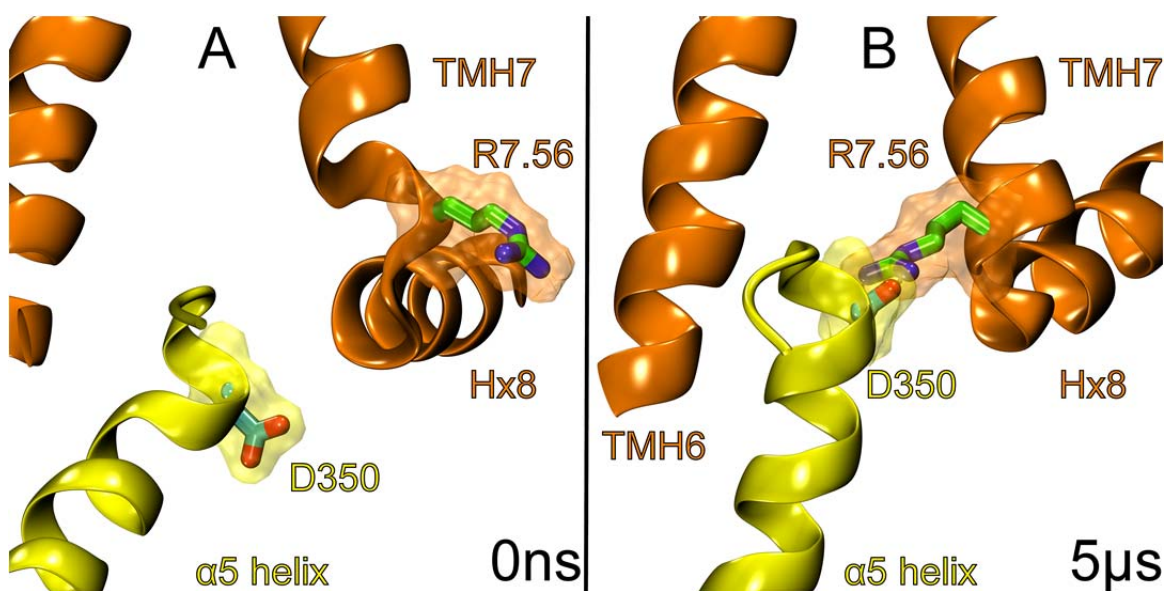


Figure 19. Interaction Between CB₂ TMH7/Hx8 Elbow Region and G α_i C-Terminus

This figure shows the interaction between the CB₂ elbow region residue (R7.56, green carbons and blue nitrogens) and the G α_i C-terminal residue (D350, cyan carbons and red oxygens).

(A) At t=0 ns R7.56 (orange) is pointing towards lipid, not towards D350 (i-4).

(B) At t= 5 μ s R7.56 is interacting with D350 (i-4).

This elbow region interaction with the G α_i C-terminal α 5 helix is followed by a slow decrease in the C α distance (black line in Figure 20) between R7.56 (302) and D350 (i-4) after the start of the trajectory. The long standing interaction between R7.56 (302) and

D350 (i-4) that is eventually established is reflected in the N - O distance between R7.56 – D350 which stays under 4 Å after 3 μs of the trajectory (blue line in Figure 20).

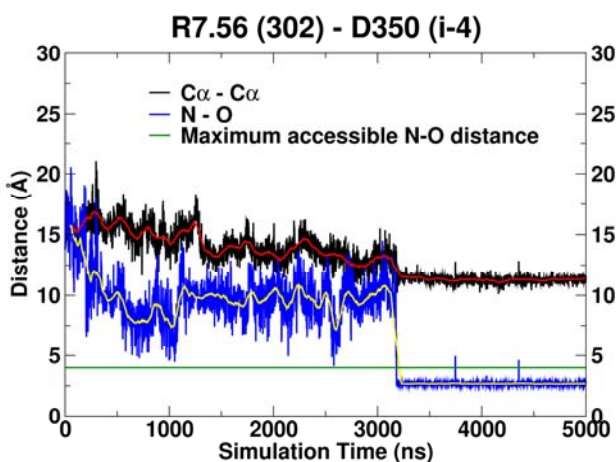


Figure 20. Plot of N – O Distance Between CB₂ TMH7/Hx8 Elbow Residue R7.56 and Gai C-Terminus Residue D350 (i-4) as a Function of Time

The black line in Figure 20 shows the decrease in the C α distance between R7.65 (302) and D350 (i-4) over the course of the trajectory. The blue line shows the decrease in the N-O distance between R7.65 (302) and D350 (i-4). The green line at 4.0 Å represents the maximum accessible distance

between N and O (81). The red and yellow lines represent the running average over 100 ns.

GDP Hydration

Over the 5 μs long MD simulation, a significant increase in the GDP hydration occurred. GDP is completely occluded by water at the end of 5 μs (Figure 21B and 21D) as compared to the beginning of the trajectory (Figure 21A and 21C). Only a small part of GDP is visible at the end of 5 μs (see Figures 21B and 21D).

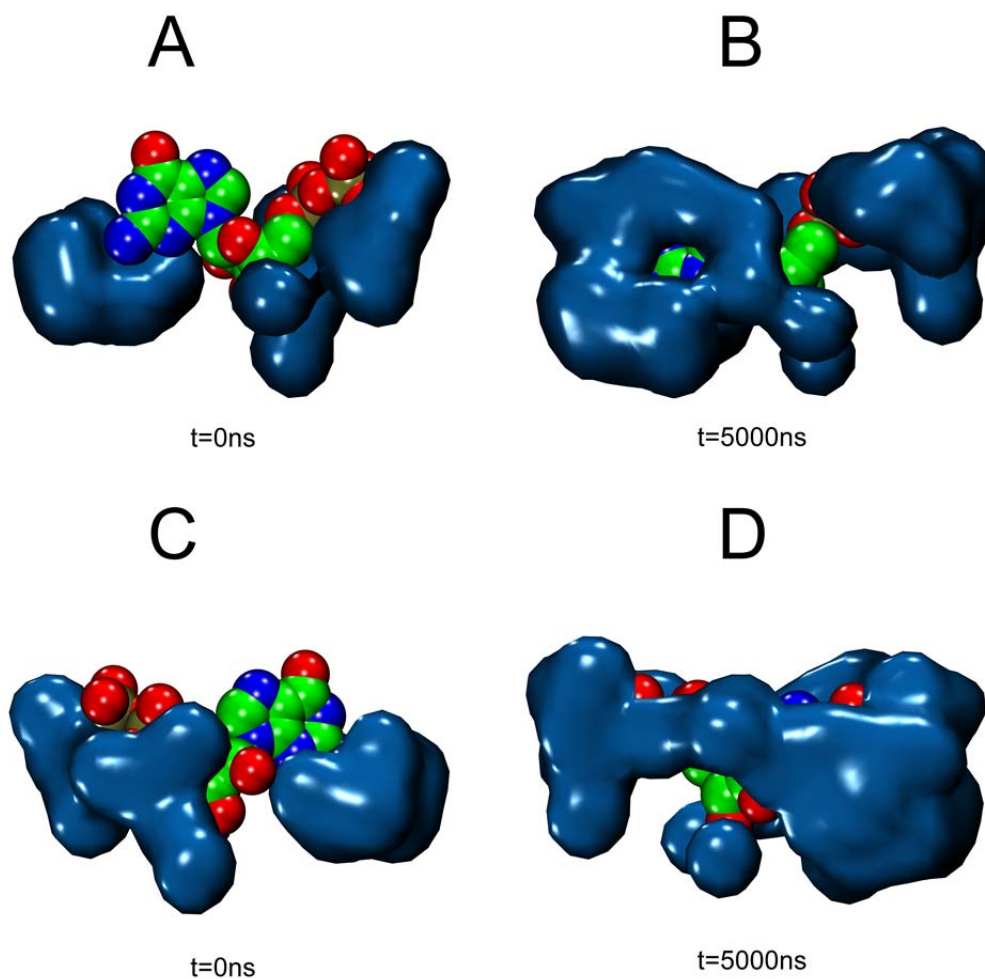


Figure 21. GDP Hydration

This figure shows GDP in VdW display with green carbons, blue nitrogens and red oxygens.

(A) Shown in blue surface display is the water within 4 Å of GDP at the start of the trajectory (t = 0 ns).

(B) Water within 4 Å of GDP at t = 5000 ns is shown in blue surface.

(C) and (D) In these figures GDP has been rotated 180° relative to the view shown in (A) and (B). Part C shows the water surrounding GDP at t=0 ns and D shows this at t = 5000 ns.

The hydration of GDP during the trajectory was monitored by counting the number of waters within 4 Å of GDP and also by following the solvent accessible surface area (SASA) of GDP.

For the first microsecond of our trajectory, a slow increase in the number of water molecules surrounding GDP (within 4 Å) was observed from 16 to 24 molecules (black line in Figure 22A). Between 1.5 – 3.5 μs of the trajectory there were 24 water molecules surrounding GDP, but there was an increase in the number of water molecules from 24 to 34 molecules after 3.5 μs (black line in Figure 22A). The initial increase in the number of water molecules surrounding GDP is also reflected in the increase in GDP SASA from 25 Å² to 125 Å² for the first microsecond. During 1.5 – 2.5 μs of the trajectory, GDP SASA remained close to 125 Å² (black line in Figure 22B). The second increase in the water influx after 3.5 μs is also reflected in the GDP SASA from 100 Å² to 170 Å² (Figures 22A and 22B).

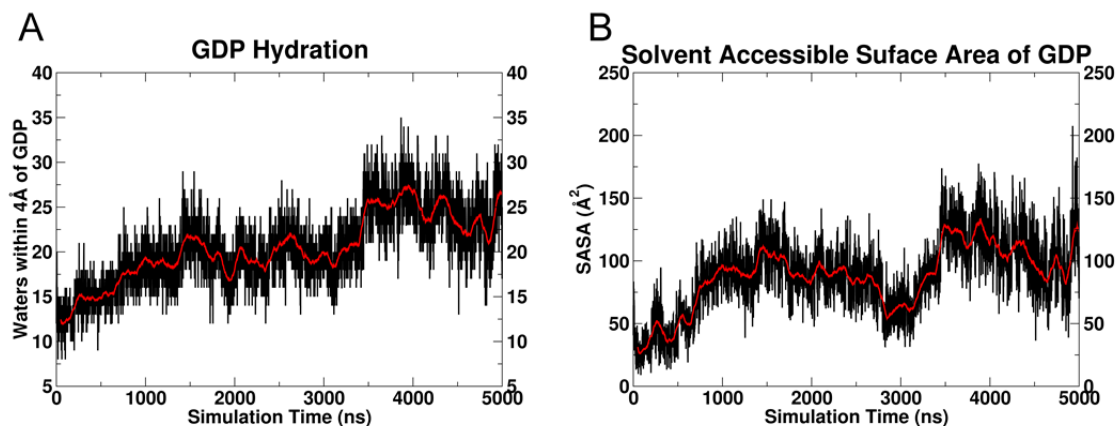


Figure 22. Solvent Accessible Surface Area of GDP

(A) The black line shows the increase in the number of water molecules within 4Å of GDP over the 5μs long trajectory.

(B) The black line shows the increase in the solvent accessible surface area of GDP from 25 Å² to 170 Å² over the 5μs long trajectory. The red line in both the figures represents the running average over 100 ns.

GDP Hydrogen Bonding

In the initial CB₂ / Gα_{i1} protein complex, there were 20 hydrogen bonds between GDP and surrounding Gα_{i1} residues and 10 hydrogen bonds between GDP and the water surrounding GDP. Over the 5 μs trajectory these numbers changed, with 10 hydrogen bonds between GDP and surrounding residues on the Gα_{i1} protein and 20 hydrogen bonds between GDP and the surrounding water by the end of the trajectory. A slow decrease in the number of hydrogen bonds between GDP and surrounding Gα_i residues was observed during first microsecond (black line in the Figure 23). A steady increase in the number of hydrogen bonds between GDP and surrounding water was observed during first microsecond (blue line in the Figure 23). This correlates well with increase in GDP SASA over the same time period (Figures 22A and 22B). After 3.5 μs, the number of

hydrogen bonds between GDP and water exceeds the number of hydrogen bonds with $G\alpha_i$. This correlates well with the increase in GDP SASA over the same time periods (Figures 22A and 22B).

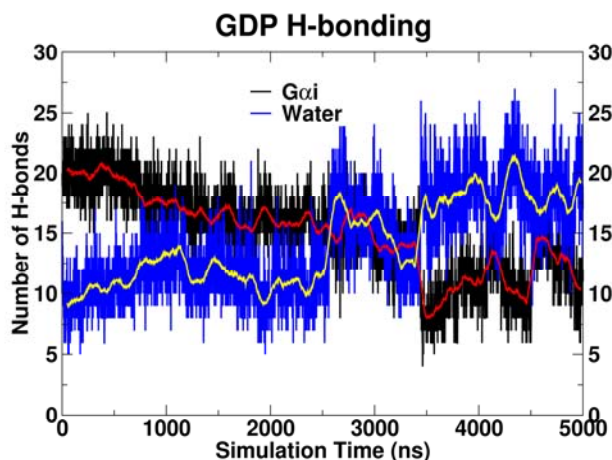


Figure 23. GDP Hydrogen Bonding

The black line here represents the number of hydrogen bonds between GDP and the $G\alpha_i$ protein and the blue line represents the number of hydrogen bonds between GDP and water over the 5 μ s long trajectory. The red and yellow lines represent the running averages over 100 ns.

Correlation Between GDP Hydration and Intracellular Loop Interactions

Over the 5 μ s of the trajectory, all three CB_2 intracellular loops interacted with the $G\alpha_i$ ras-like domain. As discussed above, a significant increase in GDP hydration was observed during the trajectory as well.

IC-2 Loop Interactions and GDP Hydration

During first microsecond of the simulation, P139 on IC-2 loop established an interaction with the $G\alpha_i$ hydrophobic pocket (Figures 17A and 17B), this was the result of the reorientation of the G protein under the CB_2 receptor (73). At the same time, a slow increase in the number of water molecules surrounding GDP and increase in GDP SASA was observed (Figures 22A, 22B and 23). These times correlate with periods in

which the IC-2 loop residue P139 was interacting with the $G\alpha_i$ hydrophobic pocket (Figures 17A and 17B).

IC-3 Loop Interactions and GDP Hydration

During the initial 200 ns of the simulation, the CB₂ IC-3 loop residue, R229 interacted with the $G\alpha_i$ $\alpha 4$ helix residue, E308. Later, this interaction was observed for a longer period of time (2000 – 4000 ns) (Figure 18A). However, it is the R229 interaction with other $G\alpha_i$ $\alpha 4$ helix residues (E297 and E298; see Figure 18B) from 1.4 to 1.6 μ s, that appears to be correlated with an increase in the number of waters within 4 Å of GDP and an increase in the SASA of GDP (Figures 22A and 22B).

IC-1 Loop Interactions and GDP Hydration

The CB₂ IC-1 loop residue, R66, interacted with the $G\alpha_i$ N-terminal helix residue, E28, between 1000 – 2800 ns and later after 3900 ns in the 5 μ s long trajectory (Figure 15B), but there was no significant increase in the hydration of GDP or increase in the SASA of GDP during these time periods of the simulation.

In summary (see Figure 24), our 5 μ s long MD simulations suggest that the initial increase in the hydration of GDP occurs during the time when the IC-2 loop establish contacts with $G\alpha_i$ ras-like domain during the first microsecond of the simulation. Later, when the IC-3 loop residue R229 extends to reach E297 and E298 on the $G\alpha_i$ $\alpha 4$ helix on the ras-like domain of $G\alpha_i$ protein, another increase in the GDP hydration occurs. The final period of GDP hydration increase occurs when the TMH7/Hx8 “elbow” region interacts with the $G\alpha_i$ C-terminal $\alpha 5$ helix.

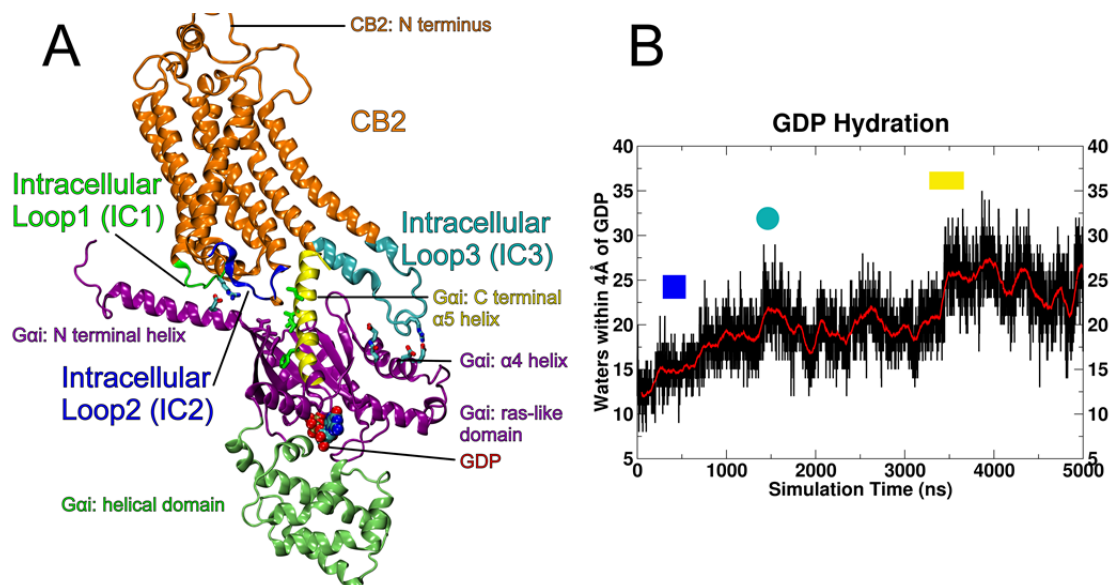


Figure 24. CB₂ Intracellular Loops Contacting G α_i Protein and GDP Hydration

(A) This figure shows the interactions of all the CB₂ intracellular loops with the G α_i protein. The helical domain of the G α_i protein is shown in green. The GDP bound between the helical and ras-like domains of G α_{i1} is represented in VdW display with carbons, nitrogens and oxygens colored green, blue and red respectively. The IC loops on the CB₂ receptor are colored green, blue and cyan for IC-1, IC-2 and IC-3 respectively. This snapshot is at t=1500 ns in the 5 μ s long trajectory.

(B) The blue, cyan and yellow points correspond to the increase in GDP hydration due to the initial IC-2 loop, IC-3 loop and elbow region interactions respectively with the G α_{i1} ras-like domain.

The interactions of all the three intracellular loops are shown in Figure 24 at 1500 ns of the trajectory. The IC-2 and IC-3 loop interactions of CB₂ receptor with the G α_i ras-like domain that correlated with GDP hydration increases were the results of the loop “tugging” on the G α_i ras-like domain (Blue and cyan points in Figure 24B). These “tugs” allowed more water molecules to move into the pocket containing GDP. It is our hypothesis that this increase in hydration will facilitate the dissociation of GDP from G α_i protein.

Discussion

During the last decade, a lot of high-resolution X-ray crystal structures for various GPCRs have been solved (5,6,48-55,82) including one lipid receptor (S1P1) (3), but most of these are either missing parts of the IC loops, specifically IC-3, or there are other proteins attached to these loops for crystallization like lysozymes, nanobodies etc. There are X-ray crystal structures available for the G protein heterotrimer ($G\alpha\beta\gamma$) (26,57,58) with an unresolved C-terminal on $G\alpha$ and $G\gamma$. There is only one crystal structure of a GPCR/G-protein complex ($\beta 2$ -AR/Gs) available so far, which is missing the IC-3 loop. Here, the G-protein heterotrimer is stabilized with a nanobody inserted between the $G\alpha$ and the $G\beta$ subunits. This GPCR/G-protein complex ($\beta 2$ -AR/Gs) represents the empty state where GDP has left the G protein heterotrimer

We have shown here that an activated GPCR can trigger changes in a G-protein leading to its activation. Biochemical and biophysical data suggests the importance of the C-terminus and $\alpha 4$ - $\beta 6$ loop of the $G\alpha$ proteins (63,71,72) in receptor coupling. The interaction between the IC-2 loop on the receptor with G-protein has been shown to be critical by F139A mutagenesis studies for $\beta 2$ -AR/Gs system (69). The only GPCR/G-protein complex ($\beta 2$ -AR/Gs) crystal structure showed the interaction between F139 and a hydrophobic pocket on the ras-like domain of Gs-protein (32). The involvement of the IC-3 loop with the $G\alpha$ $\alpha 4$ helix (78,79) and $\alpha 4$ - $\beta 6$ loop (71,72) has also been shown to be important for G-protein activation. However, the molecular mechanism by which the receptor catalyzes the G-protein activation is not completely understood.

In this work, we report the role of the IC loops of the CB₂ receptor in the activation of the G α_i protein. To understand the dynamic nature of these interactions we undertook multi-microsecond molecular dynamics simulations of the CB₂ / G α_{i1} $\beta_1\gamma_2$ protein complex, which was based on the empty state crystal structure of the β_2 -AR with G α_s protein after GDP dissociation (32). In this crystal structure the IC-3 loop has not been fully resolved and a nanobody is used to artificially stabilize the complex for crystallization. Our MD simulations are unbiased as there is no nanobody, T4-lysozyme or any other constraint being used.

Our 5 μ s long MD results suggest that the initial interactions between intracellular loops 2 and 3 of the CB₂ receptor and the ras-like domain of G α_i protein triggers increasing hydration of GDP by “tugging” on the G α_i ras-like domain from both sides, the IC-3 loop interact with the G α_i α_4 helix on one side of the ras-like domain and the IC-2 loop interact with the opposite side of on the G α_i ras-like domain, specifically with the hydrophobic pocket comprising the G α_i N-terminus (V34), β_1 and β_2 sheets (L194 and F196), and α_5 helix (I344, I343, T340 and F336) on the G α_i ras-like domain (Figure 24).

Role of IC-2 Loop in the Activation of G α_{i1} Protein

In our simulations, P139 showed a hydrophobic interaction with the G α_i protein. The importance of this interaction to G-protein activation is underscored by mutagenesis studies which demonstrate that a β_2 -AR F139A mutation significantly impairs β_2 -AR coupling to G α_s (69).

In our simulation, this is the main loop interaction that causes an increase in GDP hydration and SASA (Figures 17A, 17B and Figures 22A, 22B). For the $CB_2 / G\alpha_{i1}\beta_1\gamma_2$ protein complex, Zheng et al., have reported that a P139A mutation results in the loss of coupling with $G\alpha_i$ protein, thus supporting our simulations (70).

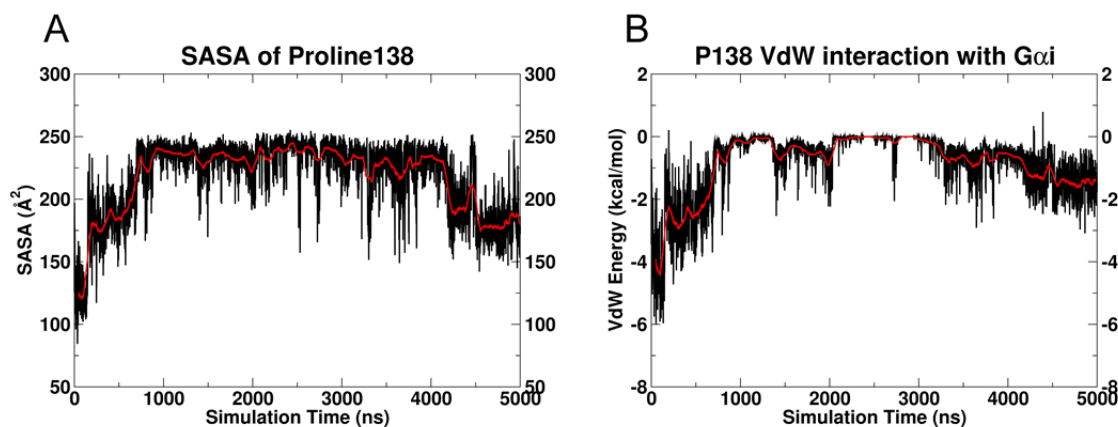


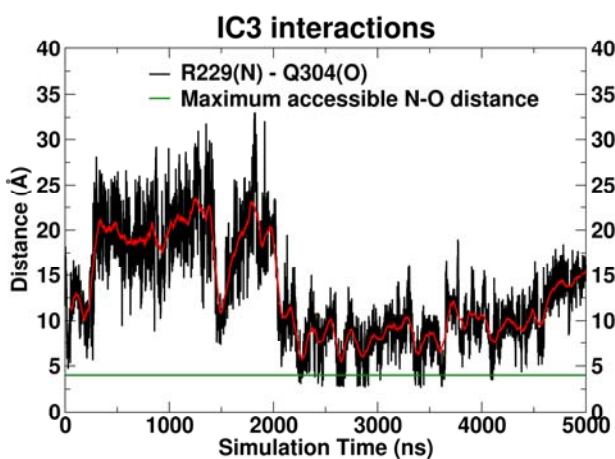
Figure 25. IC-2 Loop P138 Interaction with $G\alpha_i$ Protein

These plots show the change in the (A) solvent accessible surface area (SASA) and (B) the Van der Waals (VdW) interaction energy for the P138 (CB_2 IC-2 loop) interaction with the $G\alpha_{i1}$ hydrophobic pocket. The red line represents the running average over 100 ns.

There is another proline in the IC-2 loop, P138 that is adjacent to P139. Figure 25 illustrates that P138 does not contribute to the $CB_2 / G\alpha_{i1}\beta_1\gamma_2$ protein interactions (Figures 25A and 25B) despite the fact that P139 does not interact throughout the simulation with the $G\alpha_{i1}$ hydrophobic pocket, instead it enters and exits the $G\alpha_{i1}$ hydrophobic pocket multiple times during the simulation.

Role of IC-3 Loop in the Activation of $G\alpha_i$ Protein

The importance of the $G\alpha_i$ $\alpha 4$ helix residues, Q308 and E308, in $G\alpha_i$ protein activation has been shown by Hamm and co-workers in the 5-HT_{1B} / $G\alpha_i$ protein system (71,78,79). In our simulation, the CB₂ IC-3 loop residue, R229, interacts with the $\alpha 4$ helix residue E308 between 2000 – 4000 ns (Figure 18A). However a significant increase in the GDP hydration and SASA was observed during another IC-3 loop interaction when R229 interacted with the $\alpha 4$ helix residues E297 and E298 (Figures 18A and 18B). Although this interaction only lasted for 200ns, it suggested that the further down the $\alpha 4$ helix the IC-3 loop can reach, the more the influence on GDP hydration. In our simulation, R229, interacted with $G\alpha_i$ $\alpha 4$ helix residues E308 for more of the trajectory than with the $G\alpha_i$ $\alpha 4$ helix residue Q304 (Figure 26). Figure 26 shows that the N-O distance for this pair of residues rarely decreases below 4 Å, the threshold distance for a salt bridge (81).



Å, the threshold distance for a salt bridge.

Figure 26. IC-3 Loop Residue R229 Interaction with $G\alpha_i$ $\alpha 4$ Helix Residues Q304

The black line in the Figure represents the N-O distance between R229 on the IC3 loop of the CB₂ receptor and Q308 on the $\alpha 4$ helix of the $G\alpha_i$ protein. The green line at 4.0 Å represents the maximum accessible distance between N and O (81). The red line represents the running average over 100 ns. It is clear here that the N-O distance rarely decreases below 4

Interaction Between TMH7/Hx8 Elbow Region and C-Terminus of $G\alpha_i$ Protein

In our starting $CB_2 / G\alpha_{i1}\beta_1\gamma_2$ protein complex, the CB_2 receptor elbow region (TMH7/Hx8) residue R7.56 (302) was pointing towards lipid (Figure 19A), however from 3.5 μ s to 5 μ s in the trajectory, R7.56 (302) has developed a long lasting interaction with the $G\alpha_i$ C-terminal $\alpha 5$ helix residue D350 (i-4). This interaction also contributes to the increase in GDP hydration (yellow rectangle in Figure 24B) and an increase in GDP SASA.

In summary, the $G\alpha_{i1}$ ras –like domain experiences interactions from multiple domains of the CB_2 receptor. These include the CB_2 TMH7/Hx8 R7.56/ $G\alpha_{i1}$ C-terminal $\alpha 5$ helix residue D350 (i-4) interaction; the CB_2 IC-3 loop/ $G\alpha_i$ $\alpha 4$ helix interaction; the CB_2 IC-2 loop/ $G\alpha_{i1}$ hydrophobic pocket interaction; and the CB_2 IC-1 loop / $G\alpha_i$ N-terminal helix interaction. These cover all the $G\alpha_i$ ras –like domain regions exposed to the CB_2 receptor.

Conclusions

Our MD simulations shows the contribution that the intracellular regions of the CB_2 receptor make to the interaction with the $G\alpha_i$ protein. Many of these interactions lead to an increase in GDP hydration. These IC regions include all IC loops and the TMH7/Hx8 elbow region. Our ultimate goal is to achieve the activated state of $G\alpha_{i1}\beta_1\gamma_2$ in which GDP has been dissociated from $G\alpha_i$ protein. While there is significant progress in GDP hydration by 5 μ s, the simulations have not yet achieved 100% GDP hydration and activation has not yet occurred. At this writing, the simulation continues!

CHAPTER III

HOMODIMER FORMATION OF THE CANNABINOID CB₂ RECEPTOR

Jagjeet Singh, Zhuanhong Qiao, Diane L. Lynch, Alan Grossfield, Dow P. Hurst ,
Michael C. Pitman, Zhao-Hui Song and Patricia H. Reggio

Abbreviations: CB₂ R – Inactive Cannabinoid Receptor Sub-type 2, CB₂ R* - Activated Cannabinoid Receptor Sub-type 2, D2 – Dopamine Receptor, CXCR4 – Chemokine Receptor, EC – Extracellular, IC – Intracellular, TMH5 – Transmembrane Helix 5, TMH6 – Transmembrane Helix 6, MD – Molecular Dynamics, POPC– 1-palmitoyl-2-oleoyl-phosphatidylcholine, SCAM - Substituted Cysteine Accessibility Method

Abstract

Activation of CB₂ has been shown experimentally to produce coupling to G α_i inhibitory protein. This receptor is activated by an endogenous, membrane derived ligand, sn-2-arachidonoylglycerol (2-AG). In turn, the activated receptor activates the heterotrimeric G $_i$ protein. There is a growing body of literature which suggests that GPCRs can exist as dimers and higher order oligomers in the cellular membrane. Multiple dimer interfaces for these receptors have been proposed including the TMH4/TMH5 region and TMH1/TMH1 region for D2 receptor, and the TMH4/TMH5 region for rhodopsin. In addition, it has been shown that the optimum signaling complex for a homodimer is one that includes one receptor in the activated state dimerized with one in inactive state.

In this work, we studied the CB₂ active (R*)/ inactive (R) homodimer interface. Based on the unpublished data from our collaborator and using the chemokine CXCR4 crystal structure as a template, we built the CB₂ R/ R* homodimer. We then modeled the CB₂ R/R* homodimer as a singling complex with Gα_{i1}β₁γ₂ protein. To study the stability of the CB₂R R*/ Gα_{i1}β₁γ₂ complex, molecular dynamics simulations in a POPC bilayer were performed. Results from two independent trajectories of 500 ns each, suggest that on TMH6, A6.60 (270) and H6.57 (267) and on TMH5 L5.40 (191), L5.41 (192), L5.44 (195), L5.45 (196), F5.61 (202) are involved in the CB₂ R R* homodimer interface. However, we found that the complex formed between the CB₂ R R* homodimer and the Gα_{i1}β₁γ₂ protein was not stable. Work on this project was halted to focus on the CB₂ R*/ Gα_{i1}β₁γ₂ signaling complex described in Chapters 1 and 2.

Introduction

In early work on G-protein coupled receptors (GPCR), these receptors were assumed to act as monomers with each receptor signaling through its own G-protein. More recently, there has been a growing body of literature that has focused on the possibility that GPCRs may exist and act as dimers or higher order oligomers (83-86). If such species form and signal, there is likely a defined interface for dimerization. Early work on the dopamine D2 receptor identified the TMH4/TMH5 region of this receptor as its homodimer interface. A cysteine crosslinking study of the inverse agonist bound dopamine D2 receptor identified a symmetric TMH4-TMH5 homodimer interface (87) consistent with the atomic force microscopy (AFM) – based model of the dimer interface

of dark state rhodopsin (88). An additional TMH1/TMH1 interface was later found for D2 in its oligomeric state (89) and a different set of TMH4 residues was found to form the dimeric interface in activated D2 (90). The symmetric TMH4-TMH5 interface has been predicted computationally for numerous GPCRs (91,92).

Importance of GPCR Dimerization in GPCR Function

Do all GPCR dimers have a TMH4/TMH5 interface? Recent GPCR crystal structures suggest alternate interfaces such as TMH5/TMH6 and TMH7/TMH1, but are these physiologically relevant? The case against these crystallographic interfaces being physiologically relevant is that for crystallization, receptors are purified and detergent solubilized as monomers. The formation of parallel and anti-parallel dimers occurs during crystallogenesis and probably reflects differences in the most energetically favorable interactions under the crystallography conditions (54). In addition, modifications made to GPCR structure (such as the insertion of T4-lysozyme into the IC-3 loop to promote crystallization) may also favor certain interfaces. This may be the case for the μ -opioid (OPRM1) receptor with its close association of T4-lysozymes (5). On the other hand, the case for these interfaces being physiologically relevant is that the interfaces that are emerging from crystallographic data of unrelated GPCRs do suggest the propensity for certain interfaces to form dimers. For example, the TMH5-TMH6 interface found in the OPRM1 has also been found in five crystal structures of the CXCR4 receptor complexed with small molecule and cyclic peptide antagonists (52).

In the absence of experimental information, there are methods that have been developed to predict dimer interfaces. Weinstein and co-workers, for example, have proposed a hydrophobic mismatch approach for prediction of dimer interfaces for GPCRs (93). This method is based on the calculation of free energy cost for protein-bilayer hydrophobic mismatch. The work shown here benefits from preliminary crosslinking data from the Zhao-Hui Song lab. This data suggests that the CB₂ homodimer interface involves residues on the EC end of TMH6.

Functional Relevance of Dimerization

Functional studies of GPCR heteromers have shown that activating one receptor in the presence of a second receptor can modulate the activity of second receptor alone (94-96). Javitch and co-workers have shown for the dopamine D2 receptor homodimer, that for a signaling unit, consisting of a dopamine D2 homodimer of an inactive (R) and activated (R*) receptor in complex with a single heterotrimeric G protein, the unit appears to be maximally activated by agonist binding to a single protomer. Agonist binding to both the protomers actually reduced signaling (97).

The cannabinoid CB₁ receptor has been shown to form homodimers and heterodimers with dopamine D1 receptor and opioid receptors (98). No dimers of the cannabinoid CB₂ receptor (which belongs to GPCR Class A) have yet been reported. In the current work, we studied the formation of a CB₂R*/ R homodimer and then CB₂R R*/ G $\alpha_1\beta_1\gamma_2$ complex as a signaling unit.

Methods

Crosslinking and Immunoblotting

The CB₂ receptor has been shown to exhibit high constitutive activity (19). For this reason, crosslinking experiments (performed by our collaborator, Dr. Zhao-Hui Song) were conducted in the absence of exogenous agonist. The crosslinker HgCl₂ was applied to intact adherent cells stably expressing the indicated cysteine mutants as described (99). The crosslinking reaction was stopped by addition of 10 mM *N*-ethylmaleimide, and the cells were harvested. The extracted proteins were resolved by SDS/PAGE and immunoblotting was conducted using an anti-CB₂ antibody (unpublished work).

Molecular Modeling: CB₂ Active and Inactive Receptor Models

The inactive (R) and active (R*) CB₂ model employed in this study were taken from our previously published microsecond-long simulation of the activation of the CB₂ receptor by the endogenous ligand, 2-AG, via the lipid bilayer (17). To represent the inactive state of the CB₂ receptor, we chose frame 288 from trajectory A in which the salt bridge between TMH3 and TMH6 is intact. The α -carbon distance between R3.55 (136) and D6.30 (240) was 11.3 Å and the heteroatom distance N (R3.55 (136)) – O (D6.30 (240)) was 3.4 Å. To represent the activated state of the CB₂ receptor, we chose frame 322 from trajectory E in which the salt bridge between TMH3 and TMH6 is broken. The α -carbon distance between R3.55 (136) and D6.30 (240) was 15.2 Å and the heteroatom distance N (R3.55 (136)) – O (D6.30 (240)) was 12.7 Å (17).

Construction of the CB₂ R/R* Homodimer Interface

CB₂ R/R* homodimer was built using the X-ray crystal structure of chemokine CXCR4 receptor as a template (52). Both CB₂ R and CB₂ R* were palmitoylated at C320 and were truncated at G232. Experimental information from our collaborator, Dr. Zhao-Hui Song, suggested that residues at the EC and of TMH6 were involved in the CB₂ homodimer interface. We constructed the initial CB₂ homodimer model with a TMH5/TMH6 interface. For the TMH5/TMH6 dimer interface, both CB₂ R and CB₂ R* receptors were placed in relative orientations such that A6.60 on both receptors were close to each other. To relieve steric clashes between CB₂ R and R* both the receptors were optimized in the x-y-z directions. The intracellular and extracellular loops on the CB₂ R and CB₂ R* were detached during the relative placement of both the CB₂ receptors and reattached using the Maestro module from Schrodinger, LLC, New York, NY after the final placement of CB₂ receptors. The CB₂ R/ R* homodimer was minimized following a two step protocol. In the first step, a minimization was performed using a Polak-Ribier conjugate gradient and the OPLS2005 all atom force field in the Macromodel module from Schrodinger, LLC, New York, NY. The transmembrane regions and helices 8 of CB₂R and CB₂ R* were frozen and a minimization was performed for 20000 steps or until the system reached the 0.05 kJ/mol gradient in a distance-dependent dielectric of 80 ($\epsilon = 80$). In the second step, both CB₂R and CB₂ R* were frozen except for the sidechains of the residues L5.40 (191), L5.41 (192), L5.44 (195), L5.45 (196), F5.61 (202) on TMH5 and the minimization was performed for

10000 steps or until the system reached the 0.05 kJ/mol gradient in a distance-dependent dielectric of 1 ($\epsilon = 1$).

Calculation of Dimer Interface Interaction Energy

The interaction energies for the dimer interfaces of the initial CB₂ R/ R* homodimer model and X-ray crystal structure of chemokine CXCR4 homodimer were calculated using the OPLS2005 all atom force field in Macromodel module from Schrodinger, LLC, New York, NY using the component interactions script.

G Protein Modeling

As the crystal structure of G $\alpha_{i1}\beta_1\gamma_2$ heterotrimer (26) is missing the G α_{i1} C-terminus and G γ_2 C-terminus, NMR structures (27,28) were used to complete the structure as published (100). Lipidation sites were attached to G $\alpha_{i1}\beta_1\gamma_2$ heterotrimer, a palmitic acid was attached to the N-terminus of G α_{i1} at Cys3 (29), a myristic acid was attached to Gly2 of G α_{i1} (30) and a geranylgeranyl group was attached to Cys 68 in the G γ_2 C-terminus (31).

CB₂ R/R* / 2-AG/ Gi Protein Complex

The relative orientations of G $\alpha_{i1}\beta_1\gamma_2$ under the CB₂ R/R* homodimer was based on the orientation proposed by Han et al. (97). The C terminal α_5 helix was inserted into the active CB₂ R* receptor and the N terminal helix of G α_i was placed under the inactive CB₂ R receptor by rotation and translation in the x- y- z directions of the G $\alpha_{i1}\beta_1\gamma_2$ heterotrimer using the Maestro module from Schrodinger, LLC, New York, NY.

Molecular Dynamics Simulation of the CB₂ Homodimer /Gα_{i1}β₁γ₂ Complex in lipid

Bilayer

In the CB₂ R/R* /Gα_{i1}β₁γ₂ protein complex, the CB₂ R (inactive) receptor residue E1.49 was protonated and the CB₂ R* (active) receptor residues E1.49, D6.30 and D3.49 were protonated as published previously (17). The CB₂ R/R* /Gα_{i1}β₁γ₂ protein complex was oriented such that the amphipathic helix 8 was approximately parallel to the plane of the phospholipid membrane at the water/phospholipid interface. The simulation cell system was constructed with the replacement method, using scripts derived from CHARMM-GUI (33). The final size of the simulation cell was 130.0Å x 130.0Å x 170.6 Å and contained 423 lipid molecules for a total of 279647 atoms. The system was neutralized with NaCl added such that the ionic strength was approximately 0.1M. The system was minimized using CHARMM (38) for 500 steps of steepest decent to eliminate the initial poor contacts with no restraints applied to the protein. The system was then minimized for 20,000 steps of conjugate gradient minimization using NAMD (39). The minimized system was heated in 10K increments to 310K with restraints on the protein (using a force constant of 10 kcal/mol/Å² for the backbone and 5.0 kcal/mol/Å² for the sidechains), and on the POPC phosphates (using force constant of 5.0 kcal/mol/rad²) and a harmonic dihedral restraint on the POPC cis double bond and the glycerol C2 chiral center (using force constant of 500 kcal/mol/rad²). At each increment, 500 steps of minimization were performed followed by 10ps of dynamics at the higher temperature. Equilibration was performed for 25 ps for the first 3 steps and 200 ps for the

next 3 steps of molecular dynamics and then the restraints were released in 6 steps.

Production dynamics was performed on a Blue Gene supercomputer (41) located at the Thomas J. Watson Research Center. Two independent trajectories of 500 ns each were run for this complex. All analysis was performed using visual molecular dynamics (42).

Results

Identification of CB₂ Crosslinks (unpublished data)

Substituted cysteine accessibility method (SCAM) performed on the CB₂ receptor at the Song laboratory identified that a CB₂ A6.60C mutant formed a spontaneous CB₂ homodimer. Upon treatment of HgCl₂, H6.57C and A6.60C expressing cells had immunoreactive bands of about double the size of the bands of the wild-type CB₂ expressing cells. In the presence of dithiothreitol (DTT), the higher molecular weight immunoreactive bands disappeared, indicating the higher sized bands are crosslinked monomers of CB₂ receptor (Unpublished data).

CB₂ R/R* Homodimer

The initial CB₂ R/R* homodimer was based on the crystallographic TMH5-TMH6 dimer interface reported in the X-ray crystal structure of chemokine CXCR4 receptor bound to a cyclic peptide CVX15 and a small molecule IT1t (52). In the CB₂ R/ R* homodimer, the extracellular end of CB₂ R* TMH6 is close to extracellular end of CB₂ R TMH6 (white surface in the Figure 27 and A6.60 (red tubes) in Figure 28). The C α distance between A6.60 (270) on CB₂ R and CB₂ R* was 6 Å. The extracellular ends of TMH6 (A6.60) on CB₂ R and R* together also positioned transmembrane regions of

TMH5 on CB₂ R and R* crossing each other bringing together the hydrophobic residues L5.40 (191), L5.41 (192), L5.44 (195), L5.45 (196) and F5.61 (202) (Figure 28). L5.40 (191) on the CB₂ R was facing L5.41 (192) on the CB₂ R* and L5.41 (192), L5.44 (195) were facing L5.44 (195) on the CB₂ R* making an asymmetric TMH5-TMH5 dimer interface.

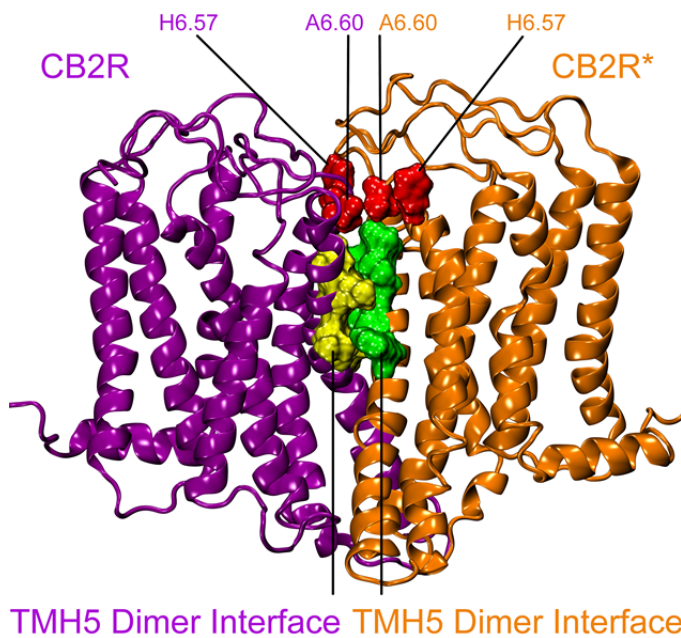


Figure 27. CB₂ R/ R* Homodimer

This figure shows the CB₂ R* receptor in orange and the CB₂ R in purple. The dimer interface on TMH5 CB₂ R is in yellow surface and the dimer interface on TMH5 CB₂ R* is in green surface. The dimer interface on the extracellular ends of TMH6 CB₂ R and R* is shown in red surface (A6.60 and H6.57).

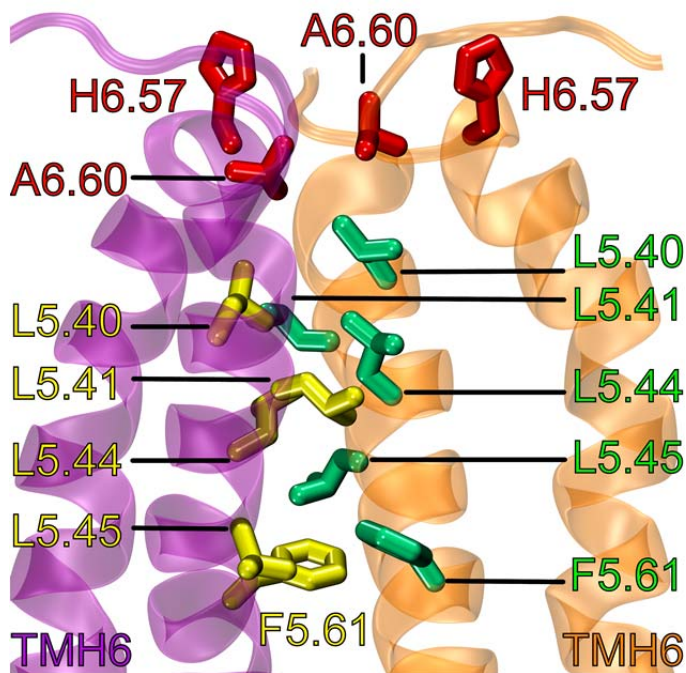


Figure 28. TMH5-TMH6 Dimer Interface Residues

In this figure part of the CB₂ R* receptor is shown in orange and part of the CB₂ R receptor is shown in purple. The residues on TMH5 that are part of the dimer interface on CB₂ R are labeled yellow (L5.40 (191), L5.41 (192), L5.44 (195), L5.45 (196), F5.61 (202)) and the residues on TMH5 that are part of the dimer interface on CB₂ R* are labeled green (L5.40 (191), L5.41 (192), L5.44 (195), L5.45 (196), F5.61 (202)). A6.60 and H6.57 on TMH6, which is part of the TMH6 dimer interface on CB₂ R and CB₂ R* are colored and labeled red.

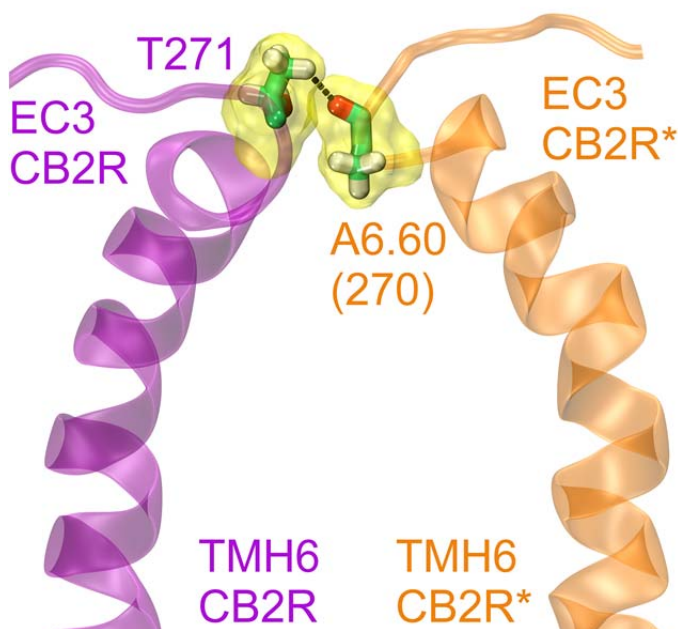


Figure 29. Hydrogen Bond Between A6.60 - T271

This figure shows TMH6 and the EC3 loop on CB₂ R in purple and TMH6 and the EC3 loop on CB₂ R* in orange. The hydrogen bond between A6.60(270) on TMH6 CB₂ R* and T271 (EC3) on CB₂ R is shown by the black dotted line.

Interaction Energies of the Homodimer Interface

The total interaction energy for the TMH5-TMH6 CB₂ R/R* homodimer interface was 17.8 kcal/mol. The hydrogen bond between A6.60 (270) of CB₂ R* and T271 on EC3 loop (Figure 29) of CB₂R TMH6 contributed 7.8 kcal/mol and the VdW interaction energy between TMH5 residues L5.40 (191), L5.41 (192), L5.44 (195), L5.45 (196), A5.48 (199), F5.61 (202) on both CB₂ R and R* contributed the rest of the dimer interface interaction energy (see Table 1).

Table 1. Interaction Energy of CB2 Homodimer

CB₂ R* (Active)	CB₂ R (Inactive)	Interaction Energy (kcal/mol)
L5.41(192)	L5.44(195)	-2.5
L5.44(195)	L5.44(195)	-1.2
	L5.45(196)	-3.1
L5.45(196)	A5.48(199)	-1.2
	F5.51(202)	-1.1
A6.60(270)	A6.60(270)	-1.9
	T271(EC3)	-7.8
	Total	-17.8

The total computed VdW energy of interaction for the X-ray crystal structure of chemokine CXCR4 receptor was -18.4 kcal/mol with the major contribution coming from the interaction between W5.34 (195) and L267 on EC3 loop and rest from TMH5 residues L5.33 (194), V5.36 (197), V5.37 (198), F5.40 (201), M5.44 (205) of CXCR4 receptors (Table 2).

Table 2. Interaction Energy of CXCR4 Homodimer

CXCR4 A	CXCR4 B	Interaction Energy (kcal/mol)
L5.33(194)	L267(EC3)	-1.2
W5.34(195)	L267(EC3)	-11.7
V5.36(197)	V5.36(197)	-1.5
V5.37(198)	V5.36(197)	-1.0
	F5.40(201)	-1.9
M5.44(205)	M5.44(205)	-1.1
	Total	-18.4

Orientation of $G\alpha_{i1}\beta_1\gamma_2$ Protein Relative to CB_2 Homodimer in the CB_2 R R* / $G\alpha_{i1}\beta_1\gamma_2$ Protein Dock

The initial heterotrimer $G\alpha_{i1}\beta_1\gamma_2$ protein dock with the CB_2 R/R* homodimer (Figure 30) was based on the orientation of G protein with the GPCR homodimer proposed by Javitch and Weinstein for the dopamine D2 receptor/ Gq protein complex system (97). In this complex, the $G\alpha$ protein interacts with the active (R*) receptor by inserting its C terminal α_5 helix between the TMH3-TMH5-TMH6 opening on the GPCR and the $G\alpha$ N terminus was placed under the inactive (R) receptor (Figures 5c and 5d in reference 18). In the CB_2 R R* / $G\alpha_{i1}\beta_1\gamma_2$ complex, the C terminal α_5 helix of the $G\alpha_{i1}$ protein (yellow helix in Figure 30) was placed between the opening made by TMH3-

TMH5-TMH6-TMH7 region on the active CB₂ R* receptor and the N terminus of the G α_{i1} protein was placed under the inactive CB₂ R receptor (Figure 30). This orientation of G $\alpha_{i1}\beta_1\gamma_2$ protein placed the G β_1 and G γ_2 subunit of the heterotrimer under the inactive CB₂ receptor. Figure 30 illustrates the initial CB₂ R R* homodimer bound to 2-AG / G $\alpha_{i1}\beta_1\gamma_2$ complex model.

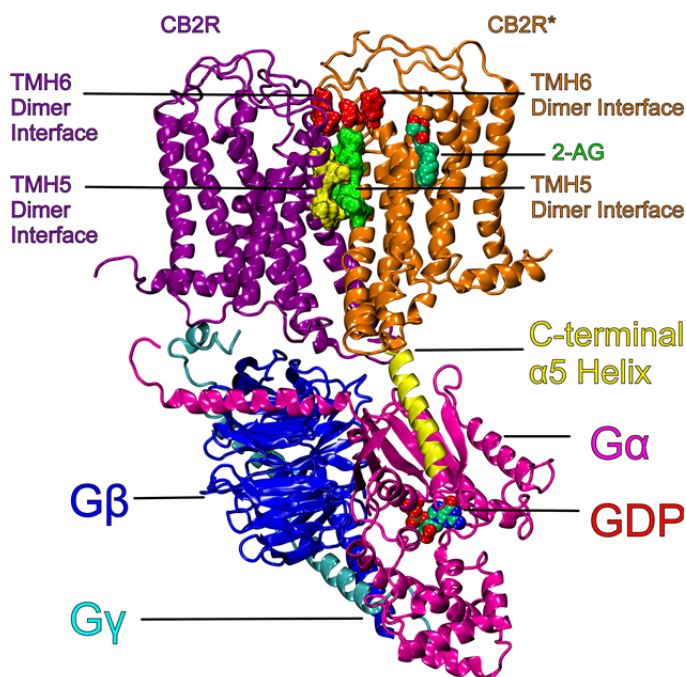


Figure 30. CB₂ Homodimer/ G $\alpha_{i1}\beta_1\gamma_2$ Complex

The initial 2-AG/CB₂ R R*/ G $\alpha_{i1}\beta_1\gamma_2$ complex is presented here. The CB₂ R* receptor is shown in orange bound to 2-AG (VdW green carbons and red oxygens) and the CB₂ R receptor is shown in purple. The CB₂ R/R* dimer interface is shown in green and yellow surfaces on TMH5 of CB₂ R* and CB₂ R respectively. CB₂ R/R* dimer interface on TMH6 is shown in red surface. The G α subunit of the G protein heterotrimer is in magenta with its C terminal helix in yellow, G β is in blue and G γ is in cyan. GDP is bound between the helical and ras-like domains of G α and is

shown in VdW display with carbons, nitrogens and oxygens colored green, blue and red respectively.

Molecular Dynamics Simulations

To study the dynamics of the CB₂ R R*/ Gα_{i1}β₁γ₂ complex in physiological conditions, all atom, fully hydrated POPC lipid bilayer molecular dynamics (MD) simulations were performed on this complex system. Results from two independent 500 ns trajectories are discussed below.

Extracellular End of TMH6 in the TMH5-TMH6 Dimer Interface of CB₂ R/ R*

Homodimer

In the starting structure of the CB₂ R R* homodimer in complex with Gα_{i1}β₁γ₂ protein, the extracellular ends of the TMH6s of CB₂ R and CB₂ R* were close to each other (Figures 31A and 31C). The Cα distance between A6.60 (270) CB₂ R and A6.60 (270) CB₂ R* was 7.7 Å for Trajectory 1 and 5.7 Å for Trajectory 2 in the starting structure. During the initial 50 ns this distance stayed under 10 Å for both the trajectories but after 50 ns the distance increased above 10 Å for Trajectory 1. In Trajectory 2, this distance stayed around 12 Å, but decreased below 10 Å at 65 and 150 ns (Figure 33A). After 500ns of production dynamics, A6.60 (270) CB₂ R and A6.60 (270) CB₂ R* were 14.7 Å apart in Trajectory 1 and 10.9 Å apart in Trajectory 2 (Figures 31B and 31D).

SCAM results provided by our collaborator, Dr. Zhao-Hui Song also suggested involvement of H6.57(267) in the CB₂ homodimer interface. The Cα distance between H6.57(267) CB₂ R and H6.57(267) CB₂ R* was monitored for both the trajectories in the 500 ns long MD simulations. This distance was 13.6 Å and 13.4 Å for Trajectory 1 and

Trajectory 2 respectively at the start of CB₂ R R* homodimer /Gαi1β1γ2 protein complex trajectory (Figure 32A and 32C).

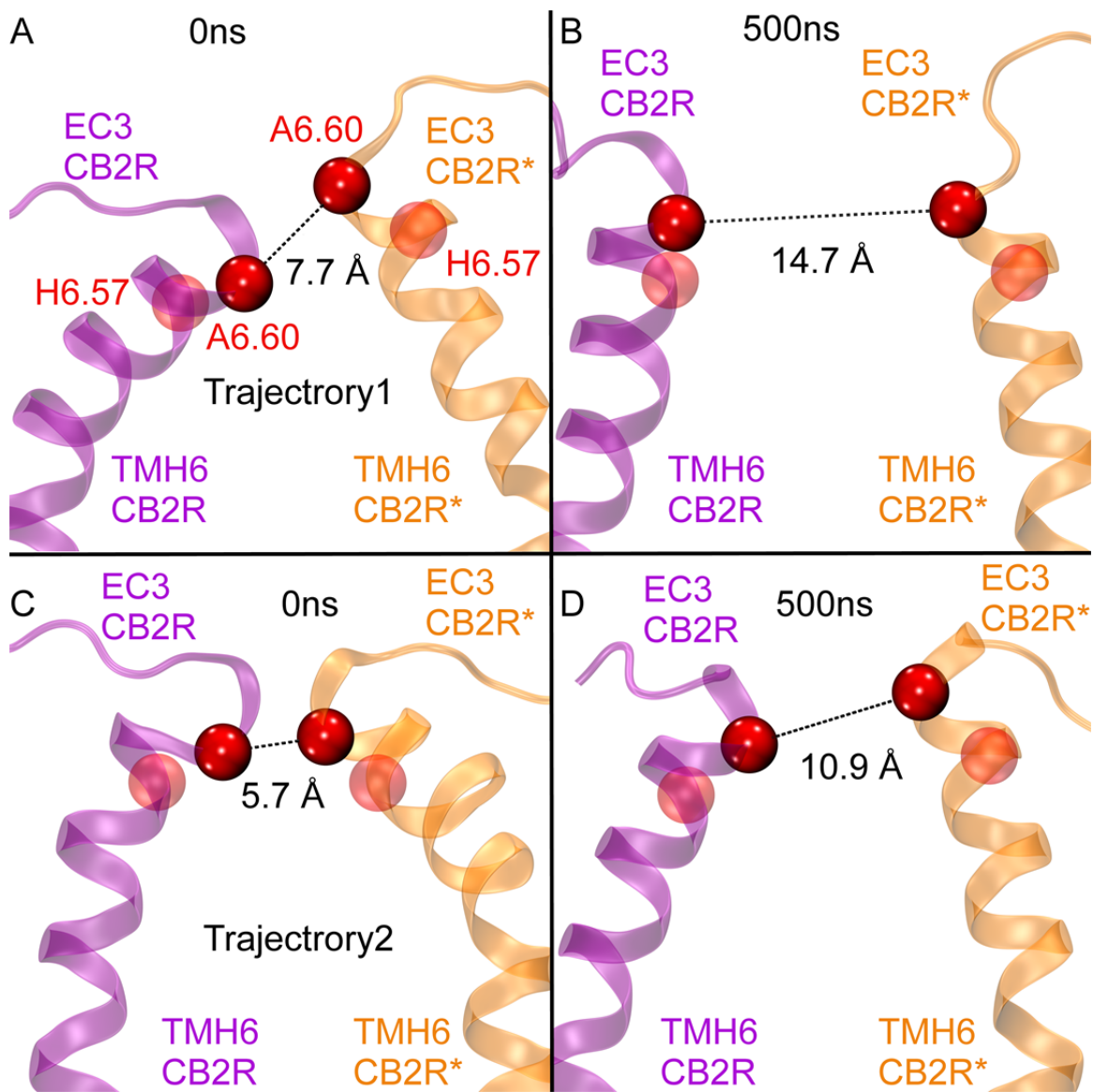


Figure 31. Relative Location of TMH6 Residue A6.60 in CB₂ R/ R* Homodimer

Figures A and C show the C α - C α distances between A6.60(270) on CB₂ R and CB₂ R* at the beginning t=0 ns of Trajectory 1 and Trajectory 2 respectively. Figures B and D show the C α - C α distances between A6.60 (270) on CB₂ R and CB₂ R* at the end t=500 ns of Trajectory 1 and Trajectory 2 respectively. Here, only TMH6 from each protomer is illustrated. TMH6 in CB₂ R is shown in purple, while CB₂ R* is shown in orange. The C α of A6.60 (270) on each helix is colored red.

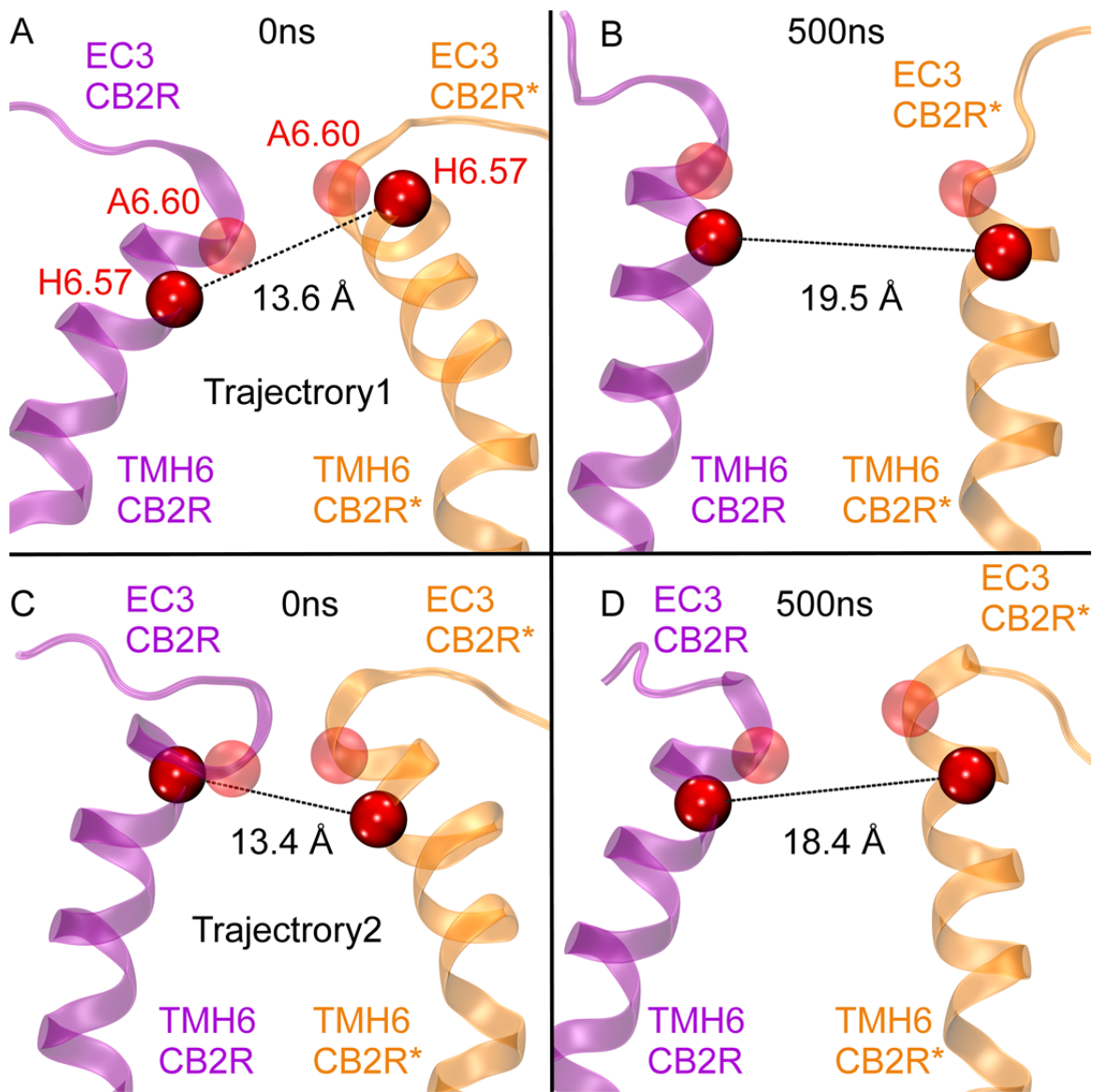


Figure 32. Relative Location of TMH6 Residue H6.57 in CB₂ R/ R* Homodimer

Figures A and C show the $C\alpha$ - $C\alpha$ distances between H6.57(267) on CB₂ R and CB₂ R* at the beginning $t=0$ ns of Trajectory 1 and Trajectory 2 respectively.

Figures B and D show the $C\alpha$ - $C\alpha$ distances between H6.57(267) on CB₂ R and CB₂ R* at the end $t=500$ ns of Trajectory 1 and Trajectory 2 respectively.

Here, only TMH6 from each protomer is illustrated. TMH6 in CB₂ R is shown in purple, while CB₂ R* is shown in orange. The $C\alpha$ of H6.57(267) on each helix is colored red.

For the first 20 ns of Trajectory 1, the $C\alpha - C\alpha$ distance between H6.57 – H6.57 decreased to below 10 Å and then remained above 10 Å. In the case of Trajectory 2, this distance never decreased below 10 Å, remaining instead 18 Å throughout the trajectory (Figure 33B). At the end of 500ns in the MD simulations, the $C\alpha$ distance between H6.57(267) CB_2 R and H6.57 (267) CB_2 R* was 19.5 Å in Trajectory 1 and 18.4 Å in Trajectory 2 (Figures 32B and 32D).

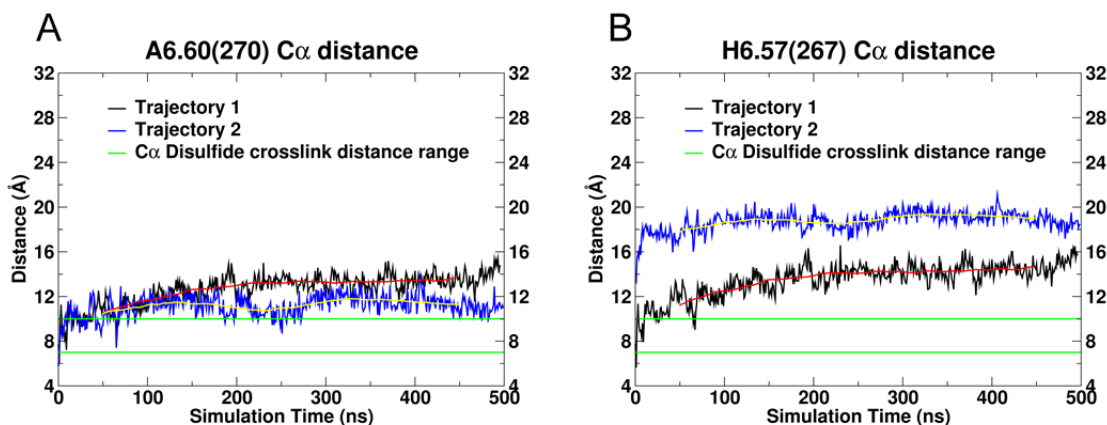


Figure 33. Plots of Distance versus Simulation Time for the TMH6 Dimer Interface
A plot of $C\alpha - C\alpha$ distance as a function of simulation time is shown here for the A6.60 (270) and H6.57(267). Trajectory 1 results are shown in black and Trajectory 2 results are in blue with the running averages over 100 ns represented by the red and magenta lines respectively. The green lines at 7 Å and 10 Å correspond to the distance range for crosslink formation between two cysteines using $HgCl_2$. These results indicate that the residues were only occasionally within the correct distance range for crosslinking.

Transmembrane Helix 5 (TMH5) Dimer Interface Interaction Energy

In the CB₂R R* homodimer model TMH5 hydrophobic residues L5.40 (191), L5.41 (192), L5.44 (195), L5.45 (196) and F5.61 (202) on CB₂R were facing the corresponding residues on CB₂R* (Figure 28) with nearly half of the dimer interface interaction energy (8.9 kcal/mol from total of 17.8 kcal/mol) coming from these interactions. The VdW interaction energy between these hydrophobic pairs was followed over the 500 ns long trajectories. For both the trajectories the VdW interaction energy between the hydrophobic residues on TMH5 on CB₂R and CB₂R* remained close to -14 kcal/mol (Figure 34).

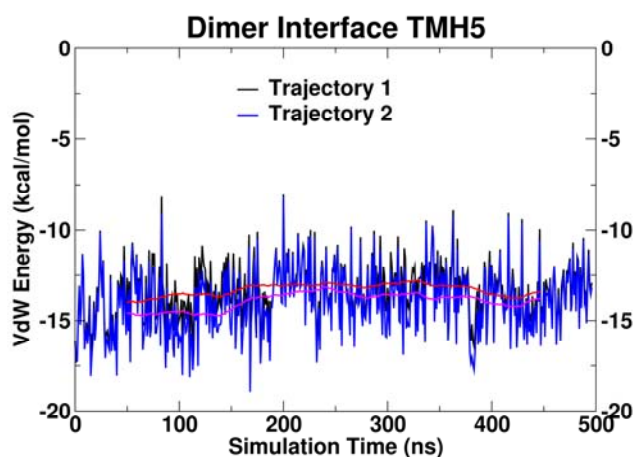


Figure 34. TMH5 Dimer Interface Interaction Energy

This plot shows the change in the Van der Waals interaction energy for the TMH5 residues (L5.40 (191), L5.41 (192), L5.44 (195), L5.45 (196) and F5.61 (202)) between CB₂R and CB₂R* for Trajectory 1 (black line) and for Trajectory 2 (blue line). The red and magenta lines represent the running average over 100 ns for Trajectory 1 and Trajectory 2 respectively.

The Orientation of the $G\alpha_{i1}\beta_1\gamma_2$ Heterotrimer Relative to the $CB_2 R/R^*$ Homodimer

In our initial $CB_2 R/R^*/G\alpha_{i1}\beta_1\gamma_2$ complex, the C terminal α_5 helix of $G\alpha_{i1}$ protein was placed in the opening in the TMH3-5-6-7 region on the active $CB_2 R^*$ receptor and the N terminus of the $G\alpha_{i1}$ protein was placed under the inactive $CB_2 R$ receptor (Figure 29). This placement of G protein was based on the dopamine D2 receptor work performed by Javitch, Weinstein and co-workers (97).

We monitored the changes in the $CB_2 R/R^*/G\alpha_{i1}\beta_1\gamma_2$ complex over the 500 ns long MD simulations. In the initial orientation of $G\alpha_{i1}\beta_1\gamma_2$ protein, the C terminal α_5 helix of $G\alpha_{i1}$ was placed close to the plane of the lipid membrane (green helix in Figures 35A and 35C) in the opening made by the TMH3-5-6-7 region on the active $CB_2 R^*$ receptor. During 500 ns of MD the $G\alpha_{i1}\beta_1\gamma_2$ heterotrimer changed its orientation under the $CB_2 R/R^*$ homodimer. The C terminal α_5 helix of $G\alpha_{i1}$ left the $CB_2 R^*$ receptor opening by rolling with the $G\alpha_{i1}\beta_1\gamma_2$ in such a way that the helical domain of $G\alpha_{i1}$ moved close to the membrane (Figures 35B and 35D). This change in the orientation of $G\alpha_{i1}\beta_1\gamma_2$ heterotrimer under the $CB_2 R/R^*$ homodimer was observed for Trajectory 1, as well as Trajectory 2.

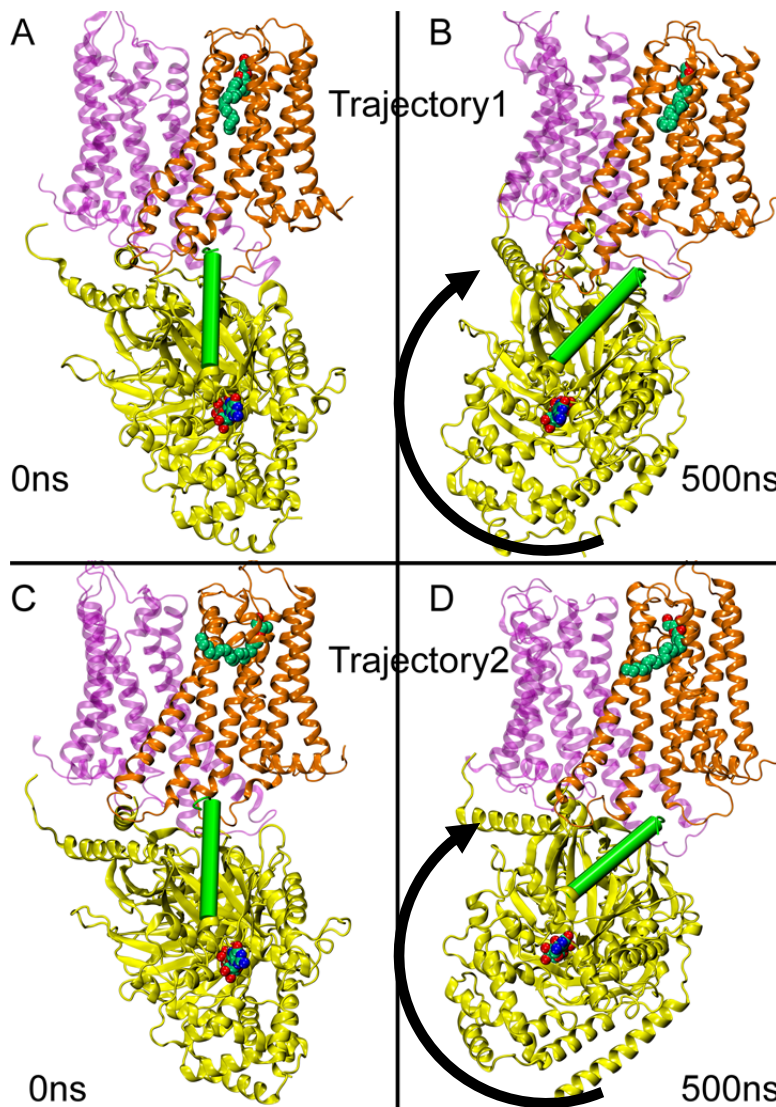


Figure 35. Change in the Orientation of $G\alpha_{i1}\beta_1\gamma_2$ Protein

This figure illustrates the change in the orientation of $G\alpha_{i1}\beta_1\gamma_2$ protein relative to the CB_2 R/ R* homodimer. CB_2 R is shown in purple, CB_2 R* in orange and $G\alpha_{i1}\beta_1\gamma_2$ protein in green with C-terminal α_5 helix of $G\alpha_{i1}$ protein in green cylinder.

Figures A and C show the position of the $G\alpha_{i1}\beta_1\gamma_2$ protein relative to CB_2 R/ R* homodimer at the start ($t=0$ ns) of Trajectory 1 and Trajectory 2 respectively. Figures B and D show the rotation in the $G\alpha_{i1}\beta_1\gamma_2$ protein at the end ($t=500$ ns) of Trajectory 1 and Trajectory 2 respectively. A rolling motion in the $G\alpha_{i1}\beta_1\gamma_2$ protein is observed under the CB_2 R R* homodimer at the end of 500 ns in both the trajectories.

Discussion

The involvement of TMH4 and TMH5 in the dimer interface of GPCRs has been reported by various groups (86,87,89,90). The X-ray crystal structures of chemokine receptor showed TMH5/TMH6 as crystallographic dimer interface for CXCR4 receptor

(52). The μ -opioid receptor was crystalized with two different dimer interfaces, TMH5/TMH6 and TMH1-TMH2-Hx8 (5).

In our work we modeled the CB₂ R R* homodimer G $\alpha_{i1}\beta_1\gamma_2$ protein signaling complex based on the work of Javitch and Weinstein which showed that an inactive (R) and activated (R*) receptor in complex with a single heterotrimeric G protein is the maximally activated signaling unit for dopamine D₂ dimers (97). Furthermore we performed all-atom, fully hydrated lipid bilayer molecular dynamics simulations on this complex to study the stability of this signaling unit.

Role of Extracellular End of TMH6 in CB₂ R/ R* Homodimer Interface

The C α – C α distance range for two cysteines to be crosslinked using HgCl₂ as crosslinker is 7 – 10 Å (44,45). Our MD results suggest that the A6.60 (CB₂ R) – A6.60 (CB₂ R*) C α distance stays below 10 Å for first 50 ns in Trajectory 1 and Trajectory2 suggesting that A6.60 on the extracellular end of TMH6 is part of the CB₂ dimer interface. The C α – C α distance between H6.57 (CB₂ R) – H6.57 (CB₂ R*) was observed below 10 Å for only 20 ns in Trajectory 1, also suggesting involvement of H6.57 in the CB₂ dimer interface. However, the fact that these distances do not spend a significant part of the entire trajectory in correct proximity suggests that the dimer interface is less likely to occur. A6.60 and H6.57 are two amino acids apart and thus not on the same face of TMH6 (Figures 31 and 32), therefore A6.60 on CB₂ R faces A6.60 on CB₂ R*, but H6.57 on CB₂ R does not face H6.57 on CB₂ R* (Figure 28). For H6.57 on CB₂ R to face H6.57 on CB₂ R*, a rearrangement in the faces of TMH6 would be needed as proposed by Guo

et al. for the dopamine D₂ receptor TMH4-TMH5 dimer interface. The rearrangement in the dimer interface would be very challenging to capture by MD.

Role of TMH5 in CB₂ R/R* Homodimer Interface

On TMH5 residues L5.40 (191), L5.41 (192), L5.44 (195), L5.45 (196), F5.61 (202) were packed on both CB₂ receptors contributing nearly half of the interaction energy in our CB₂ R/R* homodimer model (Table 1). This is in agreement with the crystallographic dimer interface as seen in the CXCR4 crystal structure (Table 2). The energy of interaction between TMH5 residues L5.40 (191), L5.41 (192), L5.44 (195), L5.45 (196), and F5.61 (202) on both CB₂ receptors was -14 kcal/mol during the 500 ns of MD run in both the trajectories. These results suggest that this hydrophobic patch on the TMH5 in the CB₂ R/R* homodimer is a stable feature of the homodimer. Further experimental mutation studies need to be designed to verify that these TMH5 residues form part of the CB₂ R/R* homodimer interface.

The Orientation of G $\alpha_i\beta_1\gamma_2$ Heterotrimer Relative to CB₂ R/R* Homodimer

There is only one GPCR/ G protein complex (β_2 AR / G $\alpha_s\beta_1\gamma_1$ complex) that has been crystalized to date (32). In addition there is no crystal structure available for any GPCR homodimer in complex with their partner heterotrimeric G protein. It is very challenging both experimentally and computationally to predict precise orientations of the proteins in the GPCR dimer/ G protein complex in a first attempt.

In the initial CB₂ R/R* / G $\alpha_i\beta_1\gamma_2$ complex model, G $\alpha_i\beta_1\gamma_2$ was placed under the CB₂ R/R* homodimer, but during 500 ns simulations, the G-protein changed its

orientation in both the trajectories and pulled away from the dimer. This suggests that our initial orientation of $G\alpha_{i1}\beta_1\gamma_2$ protein relative to CB_2 R/R* homodimer was not correct. We abandoned this homodimer project when monomeric β_2 -adrenergic receptor/Gs crystal structure became available (32). We reasoned that this structure provided a better starting structure for a receptor-G-protein complex. As discussed in Chapter I, this initial interface changed in our simulation of the CB_2 R*/ $G\alpha_{i1}\beta_1\gamma_2$ complex as well, however the proteins remained in complex. This was in contrast to what was seen for the CB_2 R R* homodimer / $G\alpha_{i1}\beta_1\gamma_2$ protein complex. As discussed in Chapter I, the change in the orientation of $G\alpha_{i1}\beta_1\gamma_2$ heterotrimer protein relative to the monomer CB_2 in our later simulations may better reflect the complex geometry for G_i coupled GPCRs (100).

Conclusions

Result suggested that the extracellular end of TMH6 and hydrophobic patch on TMH5 may be involved in the CB_2 R R* homodimer interface. The next stage of this project will be the experimental verification of the importance of TMH5 residues to the dimer interface and additional study of the formation of the CB_2 R R* / $G\alpha_{i1}\beta_1\gamma_2$ signaling complex with a different orientation of $G\alpha_{i1}\beta_1\gamma_2$ protein under the CB_2 R/ R* homodimer.

REFERENCES

1. Pierce, K. L., Premont, R. T., and Lefkowitz, R. J. (2002) Seven-transmembrane receptors. *Nat Rev Mol Cell Biol* 3, 639-650
2. Regard, J. B., Sato, I. T., and Coughlin, S. R. (2008) Anatomical profiling of G protein-coupled receptor expression. *Cell* 135, 561-571
3. Hanson, M. A., Roth, C. B., Jo, E., Griffith, M. T., Scott, F. L., Reinhart, G., Desale, H., Clemons, B., Cahalan, S. M., Schuerer, S. C., Sanna, M. G., Han, G. W., Kuhn, P., Rosen, H., and Stevens, R. C. (2012) Crystal structure of a lipid G protein-coupled receptor. *Science (New York, N.Y)* 335, 851-855
4. Wu, H., Wacker, D., Mileni, M., Katritch, V., Han, G. W., Vardy, E., Liu, W., Thompson, A. A., Huang, X. P., Carroll, F. I., Mascarella, S. W., Westkaemper, R. B., Mosier, P. D., Roth, B. L., Cherezov, V., and Stevens, R. C. (2012) Structure of the human kappa-opioid receptor in complex with JDTic. *Nature* 485, 327-332
5. Manglik, A., Kruse, A. C., Kobilka, T. S., Thian, F. S., Mathiesen, J. M., Sunahara, R. K., Pardo, L., Weis, W. I., Kobilka, B. K., and Granier, S. (2012) Crystal structure of the micro-opioid receptor bound to a morphinan antagonist. *Nature* 485, 321-326
6. Wang, C., Jiang, Y., Ma, J., Wu, H., Wacker, D., Katritch, V., Han, G. W., Liu, W., Huang, X. P., Vardy, E., McCorvy, J. D., Gao, X., Zhou, X. E., Melcher, K., Zhang, C., Bai, F., Yang, H., Yang, L., Jiang, H., Roth, B. L., Cherezov, V., Stevens, R. C., and Xu, H. E. (2013) Structural basis for molecular recognition at serotonin receptors. *Science (New York, N.Y)* 340, 610-614
7. Lefkowitz, R. J., and Shenoy, S. K. (2005) Transduction of receptor signals by beta-arrestins. *Science* 308, 512-517
8. Weis, W. I., and Kobilka, B. K. (2008) Structural insights into G-protein-coupled receptor activation. *Curr Opin Struct Biol* 18, 734-740
9. Clapham, D. E., and Neer, E. J. (1997) G protein beta gamma subunits. *Annual review of pharmacology and toxicology* 37, 167-203

10. Smrcka, A. V. (2008) G protein betagamma subunits: central mediators of G protein-coupled receptor signaling. *Cellular and molecular life sciences : CMLS* 65, 2191-2214
11. Lin, Y., and Smrcka, A. V. (2011) Understanding molecular recognition by G protein betagamma subunits on the path to pharmacological targeting. *Molecular pharmacology* 80, 551-557
12. Hamm, H. E. (1998) The many faces of G protein signaling. *J Biol Chem* 273, 669-672
13. Galiegue, S., Mary, S., Marchand, J., Dussossoy, D., Carriere, D., Carayon, P., Bouaboula, M., Shire, D., Le Fur, G., and Casellas, P. (1995) Expression of central and peripheral cannabinoid receptors in human immune tissues and leukocyte subpopulations. *Eur J Biochem* 232, 54-61
14. Storr, M., Gaffal, E., Saur, D., Schusdziarra, V., and Allescher, H. D. (2002) Effect of cannabinoids on neural transmission in rat gastric fundus. *Can J Physiol Pharmacol* 80, 67-76
15. Wright, K. L., Duncan, M., and Sharkey, K. A. (2008) Cannabinoid CB2 receptors in the gastrointestinal tract: a regulatory system in states of inflammation. *Br J Pharmacol* 153, 263-270
16. Racz, I., Nadal, X., Alferink, J., Banos, J. E., Rehnelt, J., Martin, M., Pintado, B., Gutierrez-Adan, A., Sanguino, E., Manzanares, J., Zimmer, A., and Maldonado, R. (2008) Crucial role of CB(2) cannabinoid receptor in the regulation of central immune responses during neuropathic pain. *J Neurosci* 28, 12125-12135
17. Hurst, D. P., Grossfield, A., Lynch, D. L., Feller, S., Romo, T. D., Gawrisch, K., Pitman, M. C., and Reggio, P. H. (2010) A lipid pathway for ligand binding is necessary for a cannabinoid G protein-coupled receptor. *The Journal of biological chemistry* 285, 17954-17964
18. Demuth, D. G., and Molleman, A. (2006) Cannabinoid signalling. *Life Sci* 78, 549-563
19. Bouaboula, M., Desnoyer, N., Carayon, P., Combes, T., and Casellas, P. (1999) Gi protein modulation induced by a selective inverse agonist for the peripheral cannabinoid receptor CB2: implication for intracellular signalization cross-regulation. *Mol Pharmacol* 55, 473-480

20. Bouaboula, M., Poinot-Chazel, C., Marchand, J., Canat, X., Bourrie, B., Rinaldi-Carmona, M., Calandra, B., Le Fur, G., and Casellas, P. (1996) Signaling pathway associated with stimulation of CB2 peripheral cannabinoid receptor. Involvement of both mitogen-activated protein kinase and induction of Krox-24 expression. *Eur J Biochem* 237, 704-711
21. Preininger, A. M., Meiler, J., and Hamm, H. E. (2013) Conformational flexibility and structural dynamics in GPCR-mediated G protein activation: a perspective. *Journal of molecular biology* 425, 2288-2298
22. Zhang, R., Kim, T. K., Qiao, Z. H., Cai, J., Pierce, W. M., Jr., and Song, Z. H. (2007) Biochemical and mass spectrometric characterization of the human CB2 cannabinoid receptor expressed in *Pichia pastoris*--importance of correct processing of the N-terminus. *Protein expression and purification* 55, 225-235
23. Jensen, O. N., Wilm, M., Shevchenko, A., and Mann, M. (1999) Sample preparation methods for mass spectrometric peptide mapping directly from 2-DE gels. *Methods in molecular biology* 112, 513-530
24. Yu, E. T., Hawkins, A., Kuntz, I. D., Rahn, L. A., Rothfuss, A., Sale, K., Young, M. M., Yang, C. L., Pancerella, C. M., and Fabris, D. (2008) The collaboratory for MS3D: a new cyberinfrastructure for the structural elucidation of biological macromolecules and their assemblies using mass spectrometry-based approaches. *Journal of proteome research* 7, 4848-4857
25. Schilling, B., Row, R. H., Gibson, B. W., Guo, X., and Young, M. M. (2003) MS2Assign, automated assignment and nomenclature of tandem mass spectra of chemically crosslinked peptides. *Journal of the American Society for Mass Spectrometry* 14, 834-850
26. Wall, M. A., Coleman, D. E., Lee, E., Iniguez-Lluhi, J. A., Posner, B. A., Gilman, A. G., and Sprang, S. R. (1995) The structure of the G protein heterotrimer Gi alpha 1 beta 1 gamma 2. *Cell* 83, 1047-1058
27. Kisselev, O. G., Kao, J., Ponder, J. W., Fann, Y. C., Gautam, N., and Marshall, G. R. (1998) Light-activated rhodopsin induces structural binding motif in G protein alpha subunit. *Proceedings of the National Academy of Sciences of the United States of America* 95, 4270-4275
28. Kisselev, O. G., and Downs, M. A. (2003) Rhodopsin controls a conformational switch on the transducin gamma subunit. *Structure* 11, 367-373

29. Parenti, M., Vigano, M. A., Newman, C. M., Milligan, G., and Magee, A. I. (1993) A novel N-terminal motif for palmitoylation of G-protein alpha subunits. *The Biochemical journal* 291 (Pt 2), 349-353
30. Preininger, A. M., Van Eps, N., Yu, N. J., Medkova, M., Hubbell, W. L., and Hamm, H. E. (2003) The myristoylated amino terminus of Galpha(i)(1) plays a critical role in the structure and function of Galpha(i)(1) subunits in solution. *Biochemistry* 42, 7931-7941
31. Sanford, J., Codina, J., and Birnbaumer, L. (1991) Gamma-subunits of G proteins, but not their alpha- or beta-subunits, are polyisoprenylated. Studies on post-translational modifications using in vitro translation with rabbit reticulocyte lysates. *The Journal of biological chemistry* 266, 9570-9579
32. Rasmussen, S. G., DeVree, B. T., Zou, Y., Kruse, A. C., Chung, K. Y., Kobilka, T. S., Thian, F. S., Chae, P. S., Pardon, E., Calinski, D., Mathiesen, J. M., Shah, S. T., Lyons, J. A., Caffrey, M., Gellman, S. H., Steyaert, J., Skiniotis, G., Weis, W. I., Sunahara, R. K., and Kobilka, B. K. (2011) Crystal structure of the beta2 adrenergic receptor-Gs protein complex. *Nature* 477, 549-555
33. Jo, S., Kim, T., Iyer, V. G., and Im, W. (2008) CHARMM-GUI: a web-based graphical user interface for CHARMM. *Journal of computational chemistry* 29, 1859-1865
34. MacKerell, A. D., Jr., Bashford, D., Bellott, M., Dunbrack, R. L., Jr, Evanseck, J. D., Field, M. J., Fischer, S., Gao, J., Guo, H., Ha, S., Joseph-McCarthy, D., Kuchnir, L., Kuczera, K., Lau, F. T. K., Mattos, C., Michnick, S., Ngo, T., Nguyen, D. T., Prodhom, B., Reiher III, W. E., Roux, B., Schlenkrich, M., Smith, J. C., Stote, R., Straub, J., Watanabe, M., Wiorkiewicz-Kuczera, J., Yin, D., and Karplus, M. (1998) All-Atom Empirical Potential for Molecular Modeling and Dynamics Studies of Proteins. *J. Phys. Chem. B* 102, 3586-3616
35. Mackerell, A. D., Jr., Feig, M., and Brooks, C. L., 3rd. (2004) Extending the treatment of backbone energetics in protein force fields: limitations of gas-phase quantum mechanics in reproducing protein conformational distributions in molecular dynamics simulations. *Journal of computational chemistry* 25, 1400-1415
36. Klauda, J. B., Venable, R. M., Freites, J. A., O'Connor, J. W., Tobias, D. J., Mondragon-Ramirez, C., Vorobyov, I., MacKerell, A. D., Jr., and Pastor, R. W. (2010) Update of the CHARMM all-atom additive force field for lipids: validation on six lipid types. *The journal of physical chemistry. B* 114, 7830-7843

37. Foloppe, N., and MacKerell, A. D., Jr. (2000) All-atom empirical force field for nucleic acids: I. Parameter optimization based on small molecule and condensed phase macromolecular target data. *Journal of computational chemistry* 21, 86-104
38. Brooks, B. R., Brooks, C. L., 3rd, Mackerell, A. D., Jr., Nilsson, L., Petrella, R. J., Roux, B., Won, Y., Archontis, G., Bartels, C., Boresch, S., Caflisch, A., Caves, L., Cui, Q., Dinner, A. R., Feig, M., Fischer, S., Gao, J., Hodoseck, M., Im, W., Kuczera, K., Lazaridis, T., Ma, J., Ovchinnikov, V., Paci, E., Pastor, R. W., Post, C. B., Pu, J. Z., Schaefer, M., Tidor, B., Venable, R. M., Woodcock, H. L., Wu, X., Yang, W., York, D. M., and Karplus, M. (2009) CHARMM: the biomolecular simulation program. *Journal of computational chemistry* 30, 1545-1614
39. Phillips, J. C., Braun, R., Wang, W., Gumbart, J., Tajkhorshid, E., Villa, E., Chipot, C., Skeel, R. D., Kale, L., and Schulten, K. (2005) Scalable molecular dynamics with NAMD. *Journal of computational chemistry* 26, 1781-1802
40. Essmann, U., Perera, L., Berkowitz, M. L., Darden, T. A., Lee, J., and Pedersen, L. G. (1995) A smooth particle mesh Ewald method. *J Chem Phys* 103
41. Gara, A., Blumrich, M. A., Chen, D., Chiu, G. L., Coteus, P., Giampapa, M. E., Haring, R. A., Heidelberger, P., Hoenicke, D., Kopcsay, G. V., Liebsch, T. A., Ohmacht, M., Steinmacher-Burow, B. D., Takken, T., and Vranas, P. (2005) Overview of the Blue Gene/L system architecture. *IBM Journal of Res. and Dev.* 49, 195-212
42. Humphrey, W., Dalke, A., and Schulten, K. (1996) VMD: visual molecular dynamics. *J Mol Graph* 14, 33-38
43. Romo, T. D., and Grossfield, A. (2009) LOOS: An Extensible Platform for Structural Analysis of Simulations. in *31st Annual International Conference of the IEEE EMBS*, Springer-Verlag, Minneapolis, MN
44. Soskine, M., Steiner-Mordoch, S., and Schuldiner, S. (2002) Crosslinking of membrane-embedded cysteines reveals contact points in the EmrE oligomer. *Proc Natl Acad Sci U S A* 99, 12043-12048
45. Fass, D. (2012) Disulfide bonding in protein biophysics. *Annual review of biophysics* 41, 63-79
46. Green, N. S., Reisler, E., and Houk, K. N. (2001) Quantitative evaluation of the lengths of homobifunctional protein cross-linking reagents used as molecular rulers. *Protein science : a publication of the Protein Society* 10, 1293-1304

47. Banks, J. L., Beard, H. S., Cao, Y., Cho, A. E., Damm, W., Farid, R., Felts, A. K., Halgren, T. A., Mainz, D. T., Maple, J. R., Murphy, R., Philipp, D. M., Repasky, M. P., Zhang, L. Y., Berne, B. J., Friesner, R. A., Gallicchio, E., and Levy, R. M. (2005) Integrated Modeling Program, Applied Chemical Theory (IMPACT). *Journal of computational chemistry* 26, 1752-1780
48. Palczewski, K., Kumasaka, T., Hori, T., Behnke, C. A., Motoshima, H., Fox, B. A., Le Trong, I., Teller, D. C., Okada, T., Stenkamp, R. E., Yamamoto, M., and Miyano, M. (2000) Crystal structure of rhodopsin: A G protein-coupled receptor. *Science (New York, N.Y)* 289, 739-745
49. Rasmussen, S. G., Choi, H. J., Rosenbaum, D. M., Kobilka, T. S., Thian, F. S., Edwards, P. C., Burghammer, M., Ratnala, V. R., Sanishvili, R., Fischetti, R. F., Schertler, G. F., Weis, W. I., and Kobilka, B. K. (2007) Crystal structure of the human beta2 adrenergic G-protein-coupled receptor. *Nature* 450, 383-387
50. Jaakola, V. P., Griffith, M. T., Hanson, M. A., Cherezov, V., Chien, E. Y., Lane, J. R., Ijzerman, A. P., and Stevens, R. C. (2008) The 2.6 angstrom crystal structure of a human A2A adenosine receptor bound to an antagonist. *Science (New York, N.Y)* 322, 1211-1217
51. Warne, T., Serrano-Vega, M. J., Baker, J. G., Moukhametzianov, R., Edwards, P. C., Henderson, R., Leslie, A. G., Tate, C. G., and Schertler, G. F. (2008) Structure of a beta1-adrenergic G-protein-coupled receptor. *Nature* 454, 486-491
52. Wu, B., Chien, E. Y., Mol, C. D., Fenalti, G., Liu, W., Katritch, V., Abagyan, R., Brooun, A., Wells, P., Bi, F. C., Hamel, D. J., Kuhn, P., Handel, T. M., Cherezov, V., and Stevens, R. C. (2010) Structures of the CXCR4 chemokine GPCR with small-molecule and cyclic peptide antagonists. *Science (New York, N.Y)* 330, 1066-1071
53. Haga, K., Kruse, A. C., Asada, H., Yurugi-Kobayashi, T., Shiroishi, M., Zhang, C., Weis, W. I., Okada, T., Kobilka, B. K., Haga, T., and Kobayashi, T. (2012) Structure of the human M2 muscarinic acetylcholine receptor bound to an antagonist. *Nature* 482, 547-551
54. Granier, S., Manglik, A., Kruse, A. C., Kobilka, T. S., Thian, F. S., Weis, W. I., and Kobilka, B. K. (2012) Structure of the delta-opioid receptor bound to naltrindole. *Nature* 485, 400-404
55. Kruse, A. C., Hu, J., Pan, A. C., Arlow, D. H., Rosenbaum, D. M., Rosemond, E., Green, H. F., Liu, T., Chae, P. S., Dror, R. O., Shaw, D. E., Weis, W. I., Wess, J.,

- and Kobilka, B. K. (2012) Structure and dynamics of the M3 muscarinic acetylcholine receptor. *Nature* 482, 552-556
56. White, J. F., Noinaj, N., Shibata, Y., Love, J., Kloss, B., Xu, F., Gvozdenovic-Jeremic, J., Shah, P., Shiloach, J., Tate, C. G., and Grisshammer, R. (2012) Structure of the agonist-bound neurotensin receptor. *Nature* 490, 508-513
 57. Lambright, D. G., Sondek, J., Bohm, A., Skiba, N. P., Hamm, H. E., and Sigler, P. B. (1996) The 2.0 Å crystal structure of a heterotrimeric G protein. *Nature* 379, 311-319
 58. Nishimura, A., Kitano, K., Takasaki, J., Taniguchi, M., Mizuno, N., Tago, K., Hakoshima, T., and Itoh, H. (2010) Structural basis for the specific inhibition of heterotrimeric Gq protein by a small molecule. *Proceedings of the National Academy of Sciences of the United States of America* 107, 13666-13671
 59. Coleman, D. E., and Sprang, S. R. (1998) Crystal structures of the G protein Gi alpha 1 complexed with GDP and Mg²⁺: a crystallographic titration experiment. *Biochemistry* 37, 14376-14385
 60. Tesmer, J. J., Sunahara, R. K., Gilman, A. G., and Sprang, S. R. (1997) Crystal structure of the catalytic domains of adenylyl cyclase in a complex with Galpha.GTPgammaS. *Science* 278, 1907-1916
 61. Lambright, D. G., Noel, J. P., Hamm, H. E., and Sigler, P. B. (1994) Structural determinants for activation of the alpha-subunit of a heterotrimeric G protein. *Nature* 369, 621-628
 62. Hamm, H. E., Deretic, D., Arendt, A., Hargrave, P. A., Koenig, B., and Hofmann, K. P. (1988) Site of G protein binding to rhodopsin mapped with synthetic peptides from the alpha subunit. *Science* 241, 832-835
 63. Onrust, R., Herzmark, P., Chi, P., Garcia, P. D., Lichtarge, O., Kingsley, C., and Bourne, H. R. (1997) Receptor and betagamma binding sites in the alpha subunit of the retinal G protein transducin. *Science (New York, N.Y)* 275, 381-384
 64. Scheerer, P., Park, J. H., Hildebrand, P. W., Kim, Y. J., Krauss, N., Choe, H. W., Hofmann, K. P., and Ernst, O. P. (2008) Crystal structure of opsin in its G-protein-interacting conformation. *Nature* 455, 497-502

65. Choe, H. W., Kim, Y. J., Park, J. H., Morizumi, T., Pai, E. F., Krauss, N., Hofmann, K. P., Scheerer, P., and Ernst, O. P. (2011) Crystal structure of metarhodopsin II. *Nature* 471, 651-655
66. Feng, W., and Song, Z. H. (2003) Effects of D3.49A, R3.50A, and A6.34E mutations on ligand binding and activation of the cannabinoid-2 (CB2) receptor. *Biochem Pharmacol* 65, 1077-1085
67. Hu, J., Wang, Y., Zhang, X., Lloyd, J. R., Li, J. H., Karpiak, J., Costanzi, S., and Wess, J. (2010) Structural basis of G protein-coupled receptor-G protein interactions. *Nature chemical biology* 6, 541-548
68. Ulloa-Aguirre, A., Uribe, A., Zarinan, T., Bustos-Jaimes, I., Perez-Solis, M. A., and Dias, J. A. (2007) Role of the intracellular domains of the human FSH receptor in G(alphaS) protein coupling and receptor expression. *Molecular and cellular endocrinology* 260-262, 153-162
69. Moro, O., Lamah, J., Hogger, P., and Sadee, W. (1993) Hydrophobic amino acid in the i2 loop plays a key role in receptor-G protein coupling. *The Journal of biological chemistry* 268, 22273-22276
70. Zheng, C., Chen, L., Chen, X., He, X., Yang, J., Shi, Y., and Zhou, N. (2013) The second intracellular loop of the human cannabinoid CB2 receptor governs G protein coupling in coordination with the carboxyl terminal domain. *PloS one* 8, e63262
71. Slessareva, J. E., Ma, H., Depree, K. M., Flood, L. A., Bae, H., Cabrera-Vera, T. M., Hamm, H. E., and Graber, S. G. (2003) Closely related G-protein-coupled receptors use multiple and distinct domains on G-protein alpha-subunits for selective coupling. *The Journal of biological chemistry* 278, 50530-50536
72. Cai, K., Itoh, Y., and Khorana, H. G. (2001) Mapping of contact sites in complex formation between transducin and light-activated rhodopsin by covalent crosslinking: use of a photoactivatable reagent. *Proceedings of the National Academy of Sciences of the United States of America* 98, 4877-4882
73. Mnpotra, J., Qiao, Z., Cai, J., Lynch, D. L., Grossfield, A., Leioatts, N., Hurst, D. P., Pitman, M. C., Song, Z., and Reggio, P. H. (2014) Structural Basis of G Protein Coupled Receptor-Gi Protein Interaction: Formation of the Cannabinoid CB2 Receptor / Gi Protein Complex. *The Journal of biological chemistry*

74. Van Eps, N., Preininger, A. M., Alexander, N., Kaya, A. I., Meier, S., Meiler, J., Hamm, H. E., and Hubbell, W. L. (2011) Interaction of a G protein with an activated receptor opens the interdomain interface in the alpha subunit. *Proceedings of the National Academy of Sciences of the United States of America* 108, 9420-9424
75. Alexander, N. S., Preininger, A. M., Kaya, A. I., Stein, R. A., Hamm, H. E., and Meiler, J. (2014) Energetic analysis of the rhodopsin-G-protein complex links the alpha5 helix to GDP release. *Nature structural & molecular biology* 21, 56-63
76. Oldham, W. M., and Hamm, H. E. (2008) Heterotrimeric G protein activation by G-protein-coupled receptors. *Nature reviews. Molecular cell biology* 9, 60-71
77. Johnston, C. A., and Siderovski, D. P. (2007) Receptor-mediated activation of heterotrimeric G-proteins: current structural insights. *Mol Pharmacol* 72, 219-230
78. Bae, H., Anderson, K., Flood, L. A., Skiba, N. P., Hamm, H. E., and Graber, S. G. (1997) Molecular determinants of selectivity in 5-hydroxytryptamine1B receptor-G protein interactions. *The Journal of biological chemistry* 272, 32071-32077
79. Bae, H., Cabrera-Vera, T. M., Depree, K. M., Graber, S. G., and Hamm, H. E. (1999) Two amino acids within the alpha4 helix of Galpha11 mediate coupling with 5-hydroxytryptamine1B receptors. *The Journal of biological chemistry* 274, 14963-14971
80. MacKerell, A. D., Jr., and Bashford, D. (1998) All-Atom Empirical Potential for Molecular Modeling and Dynamics Studies of Proteins. *J. Phys. Chem. B* 108 3586-3616
81. Musafia, B., Buchner, V., and Arad, D. (1995) Complex salt bridges in proteins: statistical analysis of structure and function. *Journal of molecular biology* 254, 761-770
82. Zhang, K., Zhang, J., Gao, Z. G., Zhang, D., Zhu, L., Han, G. W., Moss, S. M., Paoletta, S., Kiselev, E., Lu, W., Fenalti, G., Zhang, W., Muller, C. E., Yang, H., Jiang, H., Cherezov, V., Katritch, V., Jacobson, K. A., Stevens, R. C., Wu, B., and Zhao, Q. (2014) Structure of the human P2Y12 receptor in complex with an antithrombotic drug. *Nature* 509, 115-118
83. Milligan, G. (2004) G protein-coupled receptor dimerization: function and ligand pharmacology. *Molecular pharmacology* 66, 1-7

84. Milligan, G. (2007) G protein-coupled receptor dimerisation: molecular basis and relevance to function. *Biochimica et biophysica acta* 1768, 825-835
85. Gurevich, V. V., and Gurevich, E. V. (2008) How and why do GPCRs dimerize? *Trends in pharmacological sciences* 29, 234-240
86. Palczewski, K. (2010) Oligomeric forms of G protein-coupled receptors (GPCRs). *Trends in biochemical sciences* 35, 595-600
87. Guo, W., Shi, L., and Javitch, J. A. (2003) The fourth transmembrane segment forms the interface of the dopamine D2 receptor homodimer. *J Biol Chem* 278, 4385-4388
88. Liang, Y., Fotiadis, D., Filipek, S., Saperstein, D. A., Palczewski, K., and Engel, A. (2003) Organization of the G protein-coupled receptors rhodopsin and opsin in native membranes. *J Biol Chem* 278, 21655-21662
89. Guo, W., Urizar, E., Kralikova, M., Mobarec, J. C., Shi, L., Filizola, M., and Javitch, J. A. (2008) Dopamine D2 receptors form higher order oligomers at physiological expression levels. *The EMBO journal* 27, 2293-2304
90. Guo, W., Shi, L., Filizola, M., Weinstein, H., and Javitch, J. A. (2005) From The Cover: Crosstalk in G protein-coupled receptors: Changes at the transmembrane homodimer interface determine activation. *Proc Natl Acad Sci U S A* 102, 17495-17500
91. Filizola, M. (2009) Increasingly accurate dynamic molecular models of G-protein coupled receptor oligomers: Panacea or Pandora's box for novel drug discovery? *Life Sci* 86, 590-597
92. Filizola, M., and Weinstein, H. (2002) Structural models for dimerization of G-protein coupled receptors: The opioid receptor homodimers. *Biopolymers* 66, 317-325
93. Mondal, S., Khelashvili, G., Shan, J., Andersen, O. S., and Weinstein, H. (2011) Quantitative modeling of membrane deformations by multihelical membrane proteins: application to G-protein coupled receptors. *Biophysical journal* 101, 2092-2101
94. Vilardaga, J. P., Nikolaev, V. O., Lorenz, K., Ferrandon, S., Zhuang, Z., and Lohse, M. J. (2008) Conformational cross-talk between alpha2A-adrenergic and mu-opioid receptors controls cell signaling. *Nature chemical biology* 4, 126-131

95. Sartania, N., Appelbe, S., Pediani, J. D., and Milligan, G. (2007) Agonist occupancy of a single monomeric element is sufficient to cause internalization of the dimeric beta2-adrenoceptor. *Cellular signalling* 19, 1928-1938
96. Parenty, G., Appelbe, S., and Milligan, G. (2008) CXCR2 chemokine receptor antagonism enhances DOP opioid receptor function via allosteric regulation of the CXCR2-DOP receptor heterodimer. *The Biochemical journal* 412, 245-256
97. Han, Y., Moreira, I. S., Urizar, E., Weinstein, H., and Javitch, J. A. (2009) Allosteric communication between protomers of dopamine class A GPCR dimers modulates activation. *Nature chemical biology* 5, 688-695
98. Mackie, K. (2005) Cannabinoid receptor homo- and heterodimerization. *Life Sci* 77, 1667-1673
99. Hastrup, H., Sen, N., and Javitch, J. A. (2003) The human dopamine transporter forms a tetramer in the plasma membrane: cross-linking of a cysteine in the fourth transmembrane segment is sensitive to cocaine analogs. *J Biol Chem* 278, 45045-45048
100. Mnpotra, J. S., Qiao, Z., Cai, J., Lynch, D. L., Grossfield, A., Leioatts, N., Hurst, D. P., Pitman, M. C., Song, Z. H., and Reggio, P. H. (2014) Structural Basis of G Protein-Coupled Receptor- Gi Protein Interaction: Formation of the Cannabinoid CB2 Receptor / Gi Protein Complex. *J Biol Chem* 289, 20259-20272